

Ragnhild Skjoldli

Transient temperature estimations to facilitate dynamic current rating of power cables

Master's thesis in Energy and Environmental Engineering

Supervisor: Erling Ildstad

June 2020

Ragnhild Skjoldli

Transient temperature estimations to facilitate dynamic current rating of power cables

Master's thesis in Energy and Environmental Engineering
Supervisor: Erling Ildstad
June 2020

Norwegian University of Science and Technology

Preface

This thesis concludes my M.Sc. degree in Electric Power Engineering at the Norwegian University of Science and Technology (NTNU).

Special thanks to my supervisor Erling Ildstad for supporting me through the last year of my study. I am very grateful that you have provided me with guidance, extensive knowledge, and for always being available at the office when needed. I also wish to thank Tony Lucignano from Statnett for an exciting visit to see the high-voltage cable installation investigated and for being such helpful with providing me with data and information when necessitated.

Trondheim, June 2020

Ragnhild Skjoldli

Abstract

Today, the maximum current load capacity of power cables is normally not fully utilized. However, the increasing demand for electric energy causes the desire for more efficient use of the installed reserve in the power grid. Dynamic cable rating is thus becoming a key aspect of optimizing today's system. The maximum current load capacity of a cable system is limited by the maximum allowed temperature of the insulation, meaning that knowledge of temperature behavior is essential for better use of the underutilized cable system.

The main purpose of this thesis is to establish a simple thermal model based on analytical methods according to IEC standards for power cable rating aiming to simulate transient temperature calculations. The results determined from computer simulations are compared with measured data from a laboratory experiment conducted. Additionally, a case-study has been completed for an installed high voltage XLPE power cable with the main focus of predicting the conductor temperature. The principle of superposition plays a vital role considering the effect of variable loads.

The results obtained concludes that the simulation made has a very positive correlation with the measured temperature response from both experiments in the lab and data provided by Statnett from the high voltage cable. Additionally, the simulation considering the principle of superposition also turns out to correlates well with the real measured responses. Simulations of an overloading case example found that the cable installation in the lab could handle an overload of 30% above maximum permissible current for 24 minutes under normal operation without exceeding the thermal limit. Furthermore, aiming to study the load history impact, the ambient cable temperature was reached after 2 hours and 45 minutes after switching off a load of 150 A. Considering the maximum load of 800 A for April 2019 for the case-study investigated, the cable could handle 150% of the maximum load for 6 and 8 hours under respectively normal and emergency operation for both laying conditions in air and culvert. Comparing a week in January with a week in June reveals that an overload of 150% to the cable located in a duct may be applied for 1 and 2 hours longer for respectively normal and emergency operation for the week in January.

Sammendrag

I dag er den maksimale strømbelastningen for en strømkabel vanligvis ikke fullt utnyttet. Den økende etterspørselen for elektrisk energi fører til et ønske om en mer effektiv bruk av den ubrukte kapasiteten i dagens strømmnett. Beregning av dynamisk belastningsevne for strømkabler er derfor blitt sentralt for å optimalisere dagens system. Maksimal strømbelastning i et kabelsystem er begrenset av den tillatte temperaturen på isolasjonen, noe som betyr at kunnskap rundt temperaturer i kabelen er viktig for å vurdere kabelens belastningsevne.

Et viktig formål med denne masteroppgaven er å etablere en enkel termisk modell basert på analysemetoder i henhold til IEC standarder for vurdering av kraftkablens belastning. Dette gjøres for å kunne gjennomføre transiente beregninger av kabelens temperatur. Resultater fra datasimuleringer sammenlignes med målte data fra laboratorieeksperiment. I tillegg er et case-studie gjennomført for en installert XLPE høyspenningskabel, med fokus på å beregne ledertemperaturen til kabelen. Prinsippet superposisjon spiller en viktig rolle når det gjelder effekten av en variabel belastning i en slik situasjon.

Resultatene oppnådd konkluderer med at simuleringen etablert har en svært positiv korrelasjon til de målte verdiene fra både lab-eksperimentet og dataen målt av Statnett. I tillegg korrelerer simuleringen godt med eksperimentet ved lastvariasjoner der superposisjonsprinsippet er gjeldende. Ved å simulere overbelastning av kabelinstallasjonen i lab, ble det funnet ut at kabelen kunne håndtere en overbelastning på 30% over tillatte maksimale temperatur i 24 minutter. Ved å studere lasthistorikkens innvirkning på kabelen ble det funnet ut at omgivelsestemperaturen ble nådd etter 2 timer og 45 minutter forutsatt at en strøm på 150 A var slått av. Case-studiet i denne masteren fokuserer på å forutsi kabelens ledertemperatur. 800 A er brukt som referanse for studiet ettersom det var den observerte maksimale belastningen i april 2019, og i følge simuleringen kan høyspenningskabelen håndtere en strøm på 150% av belastningen for 6 og 8 timer under henholdsvis normal drift og i nødsituasjon for både kabel i luft og i kulverten. Ved å gjennomføre en sammenligning mellom en uke i januar og en uke i juni 2019, avslører simuleringen at en overbelastning på 150% kan påtrykkes i henholdsvis 1 time og 2 timer lenger for normal og i nødsituasjon for uken i januar.

Table of Contents

Preface	1
Abstract	i
Summary	i
Table of Contents	vi
List of Tables	viii
List of Figures	xiii
Abbreviations	xiv
1 Introduction	1
1.1 Background and motivation	1
1.2 Dynamic rating principle	2
1.3 Project description and scope	3
2 Literature Review on Dynamic Rating	5
2.1 Dynamic rating of different grid components	5
2.2 Utilization of dynamic cable rating principle in a power grid	6
2.2.1 Temperature measurements of power cables	7
2.2.2 Motivation for installing and utilizing cable temperature measurement	10
3 Theoretical Background	13
3.1 Heat transfer mechanisms	13

3.1.1	Conduction	13
3.1.2	Transient heat conduction	14
3.1.3	Convection	15
3.1.4	Radiation	15
3.2	Ampacity calculations of power cables	15
3.2.1	IEC standards concerning cable rating	16
3.3	Transient thermal modeling	16
3.3.1	Analytical and numerical method for transient thermal modeling of power cables	17
3.3.2	Superposition principle to examine a system's transient response	18
4	Thermal Modelling - Calculation Methodology	23
4.1	Circuit theory for thermal modeling	23
4.1.1	Van Wormer coefficient	25
4.2	Heat sources causing cable losses	26
4.3	Steady-state temperature: IEC 60287	27
4.3.1	Thermal equivalent circuit	27
4.3.2	Thermal resistance	29
4.4	Transient temperature: IEC 60853	32
4.4.1	Transient thermal equivalent circuit	32
4.4.2	Thermal capacitance	32
4.4.3	Reduction to a two-loop circuit	33
4.4.4	Transient temperature rise of cable installation	35
4.4.5	Calculating several load changes utilizing the principle of superposition	36
5	Experimental methodology	39
5.1	General explanation of the laboratory setup	39
5.1.1	Material list	40
5.1.2	Cable installation	40
5.1.3	Laying conditions of the laboratory setup	41
5.2	Methods of measuring the relevant parameters of the experiment	42
5.2.1	Temperatures of different cable layers	42
5.2.2	Conductor current	43
5.2.3	Ambient temperature	43
6	Results and Discussion	45
6.1	Analytical modeling based on IEC standards for cable installation utilized in the laboratory setup	46
6.2	Results from the experimental methodology carried out in the lab	48

6.2.1	Test 1: 100 A current increase	49
6.2.2	Test 2: A current step of 150 A	51
6.3	Verification of calculation methodology through comparison with experimental methodology	53
6.3.1	Comparison of Test 1 from the experiment with the calculation methodology	53
6.3.2	Comparison of Test 2 from the experiment with the calculation methodology	59
6.4	Studying the effect of superposition principle considering the cable installation from laboratory setup	62
6.5	Overloading case example of cable installation from laboratory setup	66
6.6	Load history impact on power cable systems in air	67
7	Case-Study Utilizing Data Provided by Statnett	71
7.1	General explanation of the cable installation	72
7.1.1	Laying conditions	73
7.1.2	Method for measuring values	75
7.2	A comparison between the simulated sheath temperature and the logged sheath temperature	75
7.2.1	Cable in free air	78
7.2.2	Cable in culvert	79
7.3	Case-study predicting conductor temperatures	81
7.3.1	Case 1: Temperature rise due to a current increase	81
7.3.2	Case 2: Temperature response due to several current changes discussing the effect of superposition principle	82
7.3.3	Case 3: Overloading example of the cable installation	85
7.3.4	Case 4: Seasonal changes impact on conductor temperature response	88
8	Conclusion	93
9	Further Work	95
	Bibliography	97
	Appendix A: Determining $\Delta\theta_s$ for cable installations in free air	102
	Appendix B: Conversion between circular and rectangular duct	104
	Appendix C: Ladder network for thermal model	105
	Appendix D: Conductor and sheath temperature rise calculations	106

Appendix E: Large scaled figures of the results from Chapter 6	110
Appendix F: Figures illustrating the overloading case for Statnett cable	123
Appendix G: Results from detailed simulation regarding overloading cable installation	125
Appendix H: Simulation codes utilized for predicting the temperature responses	126

List of Tables

4.1	Analogy between thermal and electrical circuits including quantities, symbols and unit comparisons.	24
4.2	Values for constants Z , E and g for cables in free air [4].	31
6.1	Cable parameters for cable installation in the experiment.	46
6.2	Thermal resistances calculated for both laying conditions.	46
6.3	Thermal capacitance calculated for both laying conditions.	47
6.4	Parameters P_1 , P_2 , N_0 and M_0 obtained from the two-loop network for both laying conditions.	47
6.5	Thermal resistance of the conductor temperature rise and sheath temperature rise for both cable laying methods.	47
6.6	Comparison of the ratio dy/dx for conductor temperature simulation and lab-exercise for Position 2-4.	55
6.7	Comparison of the ratio dy/dx for sheath temperature simulation and lab-exercise for Position 1 – 4.	58
6.8	Overview of type of operation with maximum permissible conductor temperature including an explanation of the operation [3].	62
6.9	Overview of current applied and time of current changed investigating the principle of superposition.	63
6.10	Overview of current applied and time of current changed in a short time period.	65
6.11	Results from overloading the cable installation from experimental methodology in air.	67
6.12	Time for conductor and sheath to reach ambient temperature after the current is switched to 0 A. Assuming temperature margin of 0.05 °C.	68

6.13	Time for conductor to reach ambient temperature after the current is switched to 0 A. Assuming temperature margin of 0.01 °C. . . .	68
7.1	Overview of current applied and time elapsed from 23/05.	82
7.2	Results for testing the superposition principle through one current increase of 1000 A.	84
7.3	Results for testing the superposition principle through two current increases of 500 A.	84
7.4	Overview of applied currents and time before reaching normal operation limit and emergency operation limit for both laying conditions considering ambient temperature of 10 °C.	86
7.5	Overview of applied currents and time before reaching short circuit limit for both laying conditions considering ambient temperature of 10 °C.	87
7.6	Overview of the results comparing overloading cases for cable installation in culverts for a week in respectively January and June.	90
7.7	Overview of the results comparing overloading cases for cable installations in free air for a week in respectively January and June.	90
9.1	Overview of applied currents and time before reaching normal operation limit and emergency operation limit for both laying conditions.	125

List of Figures

2.1	Temperature profile of a 230 kV cable surface, indentifying three hot spots [15].	8
2.2	A cross section of an XLPE cable with installed sensing fiber [13].	9
2.3	Schematic of an RTTR system [13].	10
2.4	An overview on how the information provided by the dynamic rating system used today.	11
3.1	Physical illustration of conduction heat transfer [18].	14
3.2	Comparison of numerical and analytical method [27].	18
3.3	Example of an simplified power system model with three heat sources and five temperature measurement points [29].	19
3.4	Temperature rise due to one step of current and applying of superposition principle.	21
4.1	Model of the cable system before equivalence (left figure) and after equivalent π -circuit (right figure), including Van Wormer's coefficient [33].	25
4.2	Thermal equivalent circuit for single power cable.	28
4.3	Reduction from ladder circuit to a two-loop thermal circuit.	33
5.1	Overview of the laboratory setup. (Not drawn to scale)	40
5.2	Rated cable data for 50/16 mm ² cable (24 kV) and illustration of the power cable used for experimental method in laboratory [44]. .	41
5.3	Overview of the measurement points on the cable construction. . .	42
6.1	The current pattern for Test 1 performed in experimental methodology.	48

6.2	The current pattern for Test 2 performed in experimental methodology.	49
6.3	Temperature responses for the four measurements applying a current of 100 A for Position 1 – 4.	50
6.4	Temperatures for the four measurements applying a step current of 150 A for Position 1 - 4.	52
6.5	Comparison between conductor temperature obtained from laboratory setup and simulation provided in MATLAB for the four positions with an applied current of 100 A.	54
6.6	Comparison of conductor temperature in Position 2 for lab-exercise and simulation with corresponding slopes illustrating the steep of the starting temperature.	55
6.7	Zoomed in figure of the conductor temperature for Position 2 showing only the time span of 1.5 – 1.6 hours.	56
6.8	Comparison between sheath temperature obtained from laboratory setup and simulation provided in MATLAB for all four positions with an applied current of 100 A.	57
6.9	Zoomed in figure of the sheath temperature for Position 2 showing only the time span of 1.5 – 1.6 hours.	58
6.10	Comparison between conductor temperature obtained from laboratory setup and simulation provided in MATLAB for the four positions with an applied step current of 150 A.	59
6.11	Comparison between the conductor temperature simulated and the one obtained from lab-experiment.	60
6.12	Comparison between sheath temperature obtained from laboratory setup and simulation provided in MATLAB for the four positions with an applied step current of 150 A.	61
6.13	Several current loads applied every second hour to the cable located in free air.	63
6.14	Several current load applied every hour to the cable in free air. . .	64
6.15	Conductor and sheath temperature of a complex example consisting of several different current changes during a short time period.	65
6.16	Simulated conductor and sheath temperature in order to verify the permissible load of the cable system.	66
7.1	Simplified illustration of cable construction. Not drawn to scale. . .	72
7.2	Transition between the overhead power lines and the cables that are entering the culverts.	73
7.3	Average, maximum and minimum sheath temperature of the cable route from Brenntangen to Solbergstøa.	74

7.4	Standard deviation of maximum and minimum temperature difference on the route from Brenntangen to Solbergstøa.	74
7.5	Current loads of April 2019	76
7.6	Ambient temperature detected by the DTS-system logging the temperature of the FO-cable before entering the HV-cable.	76
7.7	Current step logged from April 14 th to April 16 th	77
7.8	Comparison of simulated and logged sheath temperature for cable in free air from April 14 th to April 16 th	78
7.9	Comparison of simulated and logged sheath temperature for cable in free air from April 15 th to April 16 th	78
7.10	Comparison of simulated and logged sheath temperature for cable in free air from April 14 th to April 16 th	79
7.11	Comparison of simulated and logged sheath temperature for cable in free air from April 15 th to April 16 th	80
7.12	Simulated conductor and sheath temperature from April 14 th to April 16 th applying a current increase of 750 A.	81
7.13	Logged current loads from May 23 th to May 25 th	82
7.14	Simulated conductor and sheath temperature for the time period from May 23 th to May 25 th	83
7.15	Overview of two cases applying where current is switched off after 15 hours.	85
7.16	Logged ambient temperature during a week in January 2019.	88
7.17	Logged ambient temperature during a week in June 2019.	88
7.18	Simulated conductor temperature of a week of respectively January and June 2019 including the normal operation limit for cable installation in culvert.	89
9.1	Relationship between ratio of y/x and the function f	104
9.2	Ladder network for thermal model	105
9.3	Temperature responses for the four measurements applying a current of 100 A for Position 1.	110
9.4	Temperature responses for the four measurements applying a current of 100 A for Position 2.	111
9.5	Temperature responses for the four measurements applying a current of 100 A for Position 3.	111
9.6	Temperature responses for the four measurements applying a current of 100 A for Position 4.	112
9.7	Temperatures for the four measurements applying a step current of 150 A for position 1.	112

9.8	Temperatures for the four measurements applying a step current of 150 A for position 2.	113
9.9	Temperatures for the four measurements applying a step current of 150 A for position 3.	113
9.10	Temperatures for the four measurements applying a step current of 150 A for position 4.	114
9.11	Comparison between conductor temperature from laboratory setup and simulation for Position 1 with a load of 100 A.	114
9.12	Comparison between conductor temperature from laboratory setup and simulation for Position 2 with a load of 100 A.	115
9.13	Comparison between conductor temperature from laboratory setup and simulation for Position 3 with a load of 100 A.	115
9.14	Comparison between conductor temperature from laboratory setup and simulation for Position 4 with a load of 100 A.	116
9.15	Comparison between sheath temperature obtained from laboratory setup and simulation for Position 1 with a load of 100 A.	116
9.16	Comparison between sheath temperature obtained from laboratory setup and simulation for Position 2 with a load of 100 A.	117
9.17	Comparison between sheath temperature obtained from laboratory setup and simulation for Position 3 with a load of 100 A.	117
9.18	Comparison between sheath temperature obtained from laboratory setup and simulation for Position 4 with a load of 100 A.	118
9.19	Comparison between conductor temperature from laboratory setup and simulation for Position 1 with a step current of 150 A.	118
9.20	Comparison between conductor temperature from laboratory setup and simulation for Position 2 with a step current of 150 A.	119
9.21	Comparison between conductor temperature from laboratory setup and simulation for Position 3 with a step current of 150 A.	119
9.22	Comparison between conductor temperature from laboratory setup and simulation for Position 4 with a step current of 150 A.	120
9.23	Comparison between sheath temperature from laboratory setup and simulation for Position 1 with a step current of 150 A.	120
9.24	Comparison between sheath temperature from laboratory setup and simulation for Position 2 with a step current of 150 A.	121
9.25	Comparison between sheath temperature from laboratory setup and simulation for Position 3 with a step current of 150 A.	121
9.26	Comparison between sheath temperature from laboratory setup and simulation for Position 4 with a step current of 150 A.	122
9.27	Simulated conductor temperature due to overloading currents of 1000 A, 1200 A and 1400 A.	123

9.28 Simulated conductor temperature due to overloading currents of 1600 A, 1700 A and 1800 A.	123
9.29 Simulated conductor temperature due to overloading currents of 1900 A, 2000 A and 2100 A.	124

List of symbols and abbreviations

A	=	Conductor area [mm ⁻⁶]
$a_{n-1}i$	=	Numerator equation coefficient
b_n	=	Denominator equation first coefficient
c	=	Volumetric thermal capacity [J/Km ³]
c_{cond}	=	Specific heat of conductor [J/Km ³]
c_i	=	Specific heat of material i [J/Km ³]
c_{ins}	=	Specific heat of XLPE insulation [J/Km ³]
c_{screen}	=	Specific heat of screen layer [J/Km ³]
c_{sheath}	=	Specific heat of sheath layer [J/Km ³]
D_e	=	External diameter of sheath [mm]
D_o	=	Outside diameter of duct [mm]
D_i	=	Inside diameter of duct [mm]
D_{ext}	=	External diameter of cable [mm]
D_i	=	Diameter of layer i [mm]
D_{ins}	=	Diameter of insulation [mm]
D_{int}	=	Internal diameter of cable [mm]
D_{cable}	=	Diameter of outer cable [mm]
D_{cond}	=	Diameter of cable conductor [mm]
D_s	=	Internal diameter of sheath [mm]
DLR	=	Dynamic line rating
DTR	=	Dynamic transformer rating
DTS	=	Distributed temperature sensing
E	=	Constant depending on installation mode of cable
EMS	=	Energy Management System
FEM	=	Finite Element Method
FO	=	Fiber optic
g	=	Constant depending on installation mode of cable
H	=	Solar radiation intensity [W/m ²]
$H(s)$	=	Transfer function
h	=	Heat transfer coefficient
IEC	=	International Electrotechnical Commission
j	=	Index from 1 to n
k	=	Thermal conductivity of material [W/mK]
L	=	Burial depth of cable installation [m]
M_0	=	Variable used to simplify calculations
n	=	Total number of loops in network

P_1	=	Time constant of simplified circuit
P_2	=	Time constant of simplified circuit
P_j	=	Poles of transfer function
$P(s)$	=	Polynomials of poles
q_1	=	Field-effect transistor 1
q_2	=	Field-effect transistor 2
q_3	=	An example coil
Q_A	=	Two-loop circuit thermal capacitance A [J/K]
Q_B	=	Two-loop circuit thermal capacitance B [J/K]
Q_c	=	Thermal capacitance of conductor [J/K]
Q_i	=	Thermal capacitance of insulation [J/K]
Q_{scr}	=	Thermal capacitance of screen [J/K]
Q_{sheath}	=	Thermal capacitance of sheath [J/K]
$Q(s)$	=	Polynomials of zeroes
\dot{q}	=	Rate at which heat is produced per unit volume [W/m ³]
R_{ac}	=	Conductor resistance at 20°C [Ω]
R_θ	=	Temperature dependent conductor resistance [Ω]
RTTR	=	Real-Time Temperature Rating
SCADA	=	Supervisory Control And Data Acquisition
T	=	Temperature [K]
T_A	=	Two-loop circuit thermal resistance A [K/W]
T_B	=	Two-loop circuit thermal resistance B [K/W]
T_1	=	Thermal resistance of insulation [K/W]
T_2	=	Thermal resistance between sheath and armour [K/W]
T_3	=	Thermal resistance of sheath [K/W]
$T_{4,1}$	=	Thermal resistance between cable surface and duct [K/W]
$T_{4,2}$	=	Thermal resistance of duct itself [K/W]
$T_{4,3}$	=	External thermal resistance of duct [K/W]
T_{ij}	=	Coefficient
T_{J1}	=	Temperature point at field-effect transistor 1
T_{J2}	=	Temperature point at field-effect transistor 2
T_{LEAD1}	=	Temperature point at ground pin in small-outline
T_{BOARD}	=	Temperature point between two field-effect transistors
T_x	=	Temperature point at axial-leaded device
t_i	=	Thickness of layer I [mm]
t	=	Starting time of the temperature step
t_{ins}	=	Thickness of insulation layer [mm]
t_{sheath}	=	Thickness of sheath layer [mm]
U, V, Y	=	Material constants defined

V_b	=	Volume of a objects body [m ³]
W_t	=	Conductor heat loss [W/m]
W_d	=	Dielectric losses per unit length [W/m]
W_{scr}	=	Screen losses per unit length [W/m]
W_{cond}	=	Conductor losses per unit length [W/m]
W_{sol}	=	Solar radiation losses [W/m]
W_{conv}	=	Convection losses [W/m]
W_{rad}	=	Radiation losses [W/m]
XLPE	=	Cross-linked polyethylene
Z	=	Constant depending on installation mode of cable
Z_{ki}	=	Zeros of transfer function
α	=	Temperature coefficient
α_{cu}	=	Temperature coefficient of copper
α_e	=	Attachment factor
ρ	=	Density of medium [kg/m ³]
ρ_i	=	Thermal resistivity of layer i [Km/W]
ρ_{20}	=	Specific resistivity of conductor at 20C [Km/W]
ρ_{ins}	=	Thermal resistivity of XLPE insulation [Km/W]
ρ_{sheath}	=	Thermal resistivity of sheath layer [Km/W]
ρ_{soil}	=	Thermal resistivity of soil [Km/W]
θ	=	Temperature coefficient
θ_{amb}	=	Ambient temperature [K]
$\theta_{rise,i}$	=	Conductor temperature rise at node i [K]
θ_i	=	Temperature rise of cable layer i [K]
θ_{cond}	=	Temperature rise of conductor [K]
θ_m	=	Mean temperature of the filling medium between cable and duct [K]
θ_{tot}	=	Total temperature rise [K]
$\Delta\theta_s$	=	Cable surface temperature rise above ambient [K]
Ψ_{ij}	=	Thermal coefficient giving rise at i due to heat in j
p	=	Van Wormer coefficient regarding insulation layer
p^*	=	Van Wormer coefficient regarding sheath layer
σ	=	Solar absorption coefficient
σ_B	=	Stefan-Boltzmann coefficient
ϵ	=	Cable external covering emissivity
λ_1	=	Sheath loss factor
λ_2	=	Armour loss factor

Introduction

This chapter provides an introduction that includes background and motivation for the problem investigated, followed by an explanation of the dynamic rating principle. Finally, the project description and the scope of the thesis is presented.

1.1 Background and motivation

In recent years, there has been an increasing interest in using renewable resources in the power grids. The increase is consequently changing the production pattern of electricity consumption. Thus, questions have been raised about the operation, and investment planning as the renewable energy produced is unpredictable. Subsequently, structural refurbishments are required in the power systems in order to fulfill the future requirements [1].

A requirement for higher power transmission capacity is applicable, observing the changes in the electricity consumption pattern. The maximum current load capacity of a cable system is limited by the maximum allowed temperature of the insulation. The study of cable current carrying capability is, therefore, of importance to the power system owners. The study allows the system owners to examine how much a cable conductor can carry continuously under certain conditions without exceeding the limit temperature [2]. One of the greatest challenges when it comes to power cable rating is understanding the heat dissipation that the cables undergo in several layers. In order to avoid exceeding the thermal limits of the power cable, correct ampacity rating calculations are significant. The ther-

mal limit differs depending on the cable insulation medium, and for cross-linked polyethylene (XLPE) cable installation, the thermal limit during normal operation is usually set to 90 °C [3]. The aim of ampacity calculations is to maximize the permissible current flow through a cable considering a given maximum operating temperature.

Earlier studies of power cable rating highlight the important relationship between electrical current applied to the system and the heat flow that occurs on account of the temperature difference between the cable conductor and the surrounding medium [4]. Studying daily variations where the current load is fluctuating, the transient temperature behavior plays a vital role in ampacity calculations. Additionally, the transient temperature is important to examine in order to investigate overloading conditions of the cable installation where the steady-state temperature is not reached. Accordingly, the relationship between electrical current applied and transient temperature behavior is essential to interpret in order to carry out the mathematical calculation of the transient response for a given cable system [5].

1.2 Dynamic rating principle

The conventional power grids are generally deciding the power cable capacity with simulations of worst-case scenarios. This means that a static limit is a basis for how much capacity the cable can handle at all times [6]. A problem with this procedure is that a great discrepancy may be observed between actual capacity and utilized capacity of the power cable. In such cases, the thermal capacity can be adjusted and optimized for better utilization of the capacity that is available in the system. Longer periods of current overload can thus be allowed during certain service conditions if the expected maximum temperatures of the cable system can be estimated. For this reason, awareness of the temperature behavior to facilitate the current rating is important.

Dynamic rating is a term adopted when observing the underutilized capacity of the cable in a power grid [7]. Dynamic rating means that the cable capacity can be adjusted based upon factors such as real-time cable loading, cable surface temperature, ambient temperature, and weather conditions instead of worst-case scenarios. The dynamic rating is typically higher than the static rating [8]. As the capacity can be changed dynamically, studying the transient temperature is relevant due to frequent changes in the current load applied. Overheating cables and increasing the aging process of the cables are typical hazards when considering dynamic cable

rating. As the conductor temperature is considered as the limiting parameter, the analysis of this specific layer is essential. Although overheating due to dynamic rating may be a reality, developments of communications and sensing technology provide support to be able to successfully perform dynamic rating in power grids today without remarkable system deterioration [9].

1.3 Project description and scope

This thesis aims to analyze the transient temperature response in order to facilitate the dynamic current rating of power cables. A literature survey is extracted, including the theory that is forming the base for the suggested method of estimating the temperatures of installed power cables. A calculation methodology is presented based on the thermal modeling of power cables. The calculation methodology is conducted based on analytical methods according to the IEC standards for power cable rating. This method strives to produce a data simulation in MATLAB that can examine both the conductor and sheath temperature of specified cable installations. An important question is how the conductor temperature, as the limiting factor of the ampacity calculations, is found. The calculation method includes calculations of the temperature response for cable lifted from the floor, cable placed on the floor, and cable located in ducts/culverts. All the cases investigated have air as the surrounding medium.

Furthermore, an experimental methodology is represented by establishing a laboratory setup that logs the current applied with the temperature at different layers. The method aims to utilize results from the calculation methodology and, if possible, verify these results with results from the experiment. By utilizing the calculation method on the cable installation found in the lab, discussions on the effect of the superposition principle can be made. Additionally, an overloading case example has been completed for the laboratory setup using the data simulation, as well as studying the load history impact on such cable installations.

Moreover, a case-study including four cases based upon interdependent measured data of current load, environment, and cable sheath temperatures of a high voltage cable provided by Statnett is completed. The high voltage cable studied has an installed distributed temperature sensing (DTS) system that is logging the sheath temperature of the cable installation. The logged sheath temperature has also been compared with the simulated sheath temperature to verify further and analyze the calculation method. A critical target of this case-study is to predict the conductor temperature and hence analyzing the cable ampacity with varying dynamical

loads. Included in the case-study is a discussion on the effect of the superposition principle, an overloading example of the high-voltage cable, and seasonal changes impact on the conductor temperature response.

Literature Review on Dynamic Rating

This chapter begins with a short introduction of dynamic ratings for different grid operators. Furthermore, the utilization of a dynamic rating principle in a power grid is discussed, which is the main focus of this chapter. A significant part of the following discussion involves the installation principle of the Distributed Temperature Sensing (DTS) system and the use of Real-Time Thermal Rating (RTTR) and how these systems are working.

2.1 Dynamic rating of different grid components

The principle of dynamic rating can be implemented on several different components in power transmission, aiming to assess the real-time capacity. Three components that are typically suitable for such a rating system are transmission lines, power transformers, and power cables. The use of the dynamic rating of these three components is shortly presented in this section.

One of the most typical distribution devices that can use the technology of dynamic rating is overhead transmission lines. Multiple studies have analyzed the approach of dynamic line rating (DLR), where many of the studies are focusing on how to utilize the already constructed lines to optimize the capacity [10],[11]. DLR is highly relevant as the overhead lines are exposed to significant weather changes. The conductor temperature will depend on different parameters, such as

ambient temperature, wind speed, the direction of the wind, solar radiation, humidity, location, and height above the sea level [12]. Because the conductors of an overhead line system are located in free air, the changes in the listed factors do have a considerable effect on the conductor temperature.

In recent years, dynamic rating for power cables, as the main focus in this thesis, has become a widely studied approach. Power cables are rarely exposed to the most serious weather conditions as they typically are sheltered from the greatest weather changes. Thus, the external parameters are typically more predictable for power cables than for overhead lines. Because of this, immense potential is seen for dynamic cable rating.

Dynamic transformer rating (DTR) is a technology that is currently emerging in which both industry and academia recently have shown more significant interest in [12]. The technology of DTR focuses on examining hot spots of the transformer windings. By gaining information about the hot spots, the capacity can be determined and optimized.

2.2 Utilization of dynamic cable rating principle in a power grid

As already stated, knowledge of a cable temperature profile gives the power system owners possibilities to figure out the current that the cable system can handle. Knowledge of this can lead to better control of both efficiency and maintenance of the overall system. Additionally, the temperature profile can support grid operators examining important parameters included in the system through information about the cable ampacity.

In order to utilize the dynamic cable rating principle in a smarter grid, the grid operators need to be aware of how to examine the conductor temperature response of the cable system due to a load applied. However, direct measurements of the conductor temperature in a power cable are rather advanced and challenging. Accordingly, the conductor temperature needs to be predicted by utilizing other parameters in the system. The main challenge faced by researchers is the ability to maximize asset utilization while still obtain a reliable cable system. Today, there are different existing methods for predicting the conductor temperature in a safe and effective matter. The usage of a Distributed Temperature Sensing (DTS) system in combination with a Real-Time Thermal Rating (RTTR) system has become

very popular and much used for these purposes. DTS and RTTR are discussed in the following sections.

2.2.1 Temperature measurements of power cables

The most common technology for thermal measurements on power cables is called distributed temperature sensing (DTS) [13]. A DTS system is often utilized in combination with an RTTR system. The DTS system allows system owners to measure temperatures along a cable through optical fibers acting as linear sensors. The usage of fiber-optic (FO) sensors are currently growing as it can measure temperatures in different grid equipment. Additionally, the system can decide the size of applied loads from heat sources in the system. The research of FO sensors has been constructed for many years, and the first construction on this theme was enabled in the early 1970s [14].

A DTS system installed in a power cable will measure and log the temperatures along the cable as a continuous profile with high accuracy, providing the user with temperature information in the fiber. Cigre [13] provides a list of reasons why the users are installing a DTS technology. Some of the bullet points of the list are rendered below:

- *The need to increase (or optimize) the power transfer through a cable corridor without incurring the significant expense to replace the cable system(s)*
- *The need to identify hot spots along cable corridors*
- *Lack of proper information about historical circuit classical “book” ratings and the need to establish operating power transfer limits*
- *The need to verify thermal calculation models*
- *To monitor the submarine cables and sudden changes in temperature caused by any potential exposure post-installation of buried cable due to scouring of the sea-bottom*

In order to optimize the grid with a DTS system, one needs to have accurate calculations of the conductor temperature. Real-Time Thermal Rating (RTTR) can be a solution as it can be used to determine the conductor temperature from the thermal model installed. One of the reasons why RTTR is widely used is that it may achieve higher reliability and deliver more distributed generation [13]. Measurements carried out can provide important data to the grid operators, such as whether to remove a hot spot detected to increase the capacity or manage the hot spot with

an RTTR system [13]. Besides, as the RTTR system can detect the temperatures in the hot spots, it allows the system operators to gain information on maximum ampacity for chosen zones.

Li, Tan, and Su are showing the value of installing a DTS system to power cables through identifying hot spots and introduce real-time rating to the cable [15]. Figure 2.1 shows the result obtained. By examining the temperature profile of a 230 kV underground cable, three hot spots were detected (A, B, and C in Figure 2.1). The illustration addresses the ability to decide the whole cable rating by solely consider the hot spots in the cable.

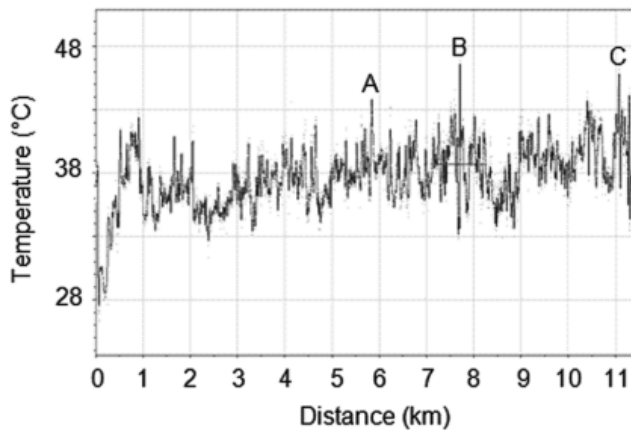


Figure 2.1: Temperature profile of a 230 kV cable surface, identifying three hot spots [15].

Installing a DTS system can be done in different ways, and the way of the installation may affect the accuracy of the calculations. The mathematical relationship between the measured temperatures from DTS and the conductor temperature is getting more complicated when the fiber optic sensors are placed far from the conductor. The closer to the conductor the sensors are, the fewer errors are normally present [13]. One common way is to install the DTS system as a part of the cable installation. In these situations, the fiber optic sensors are placed under the metallic sheath of the power cable. An example of a cable installation with integrated optical fibres are shown in Figure 2.2.

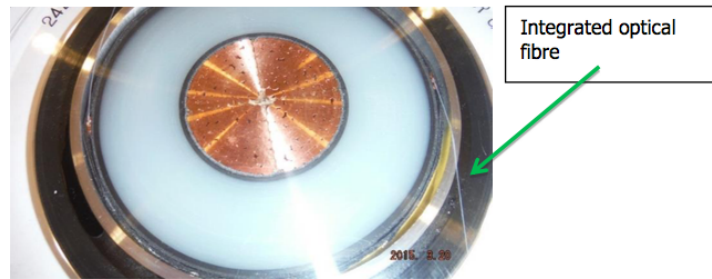


Figure 2.2: A cross section of an XLPE cable with installed sensing fiber [13].

Application and principle of a DTS and RTTR for rating calculations

The temperature profile that are given from temperature measurements with the DTS system provides data that can be transferred into the RTTR system. The RTTR system is using different calculation methods in combinations with thermal models of the cable installation in order to achieve the conductor temperature over the whole cable length, meaning one can examine the maximum conductor temperature for different sections of the cable route.

A schematic presented in Figure 2.3 is showing the working principle of an RTTR system. As the figure reveals, RTTR is taking advantage of the IEC standards (IEC 60287 and IEC 60853-2). The use of FEM is also commonly used; however, this thesis is utilizing the IEC standards, as shown in Figure 2.3.

The RTTR system is typically communicating with a SCADA (Supervisory Control And Data Acquisition) system offering a link between the RTTR and the energy management system (EMS) [13]. As Figure 2.3 shows, the RTTR system are using parameters of the cable installation and measurements from SCADA to calculate the temperatures. The results need to be verified, and then the unknown parameters are adjusted by utilizing the DTS temperature as well. Note that the schematic shown is represented for a cable buried in the soil. However, the same procedure also holds for different laying conditions. The working principle of SCADA and EMS hereafter not discussed in more detail.

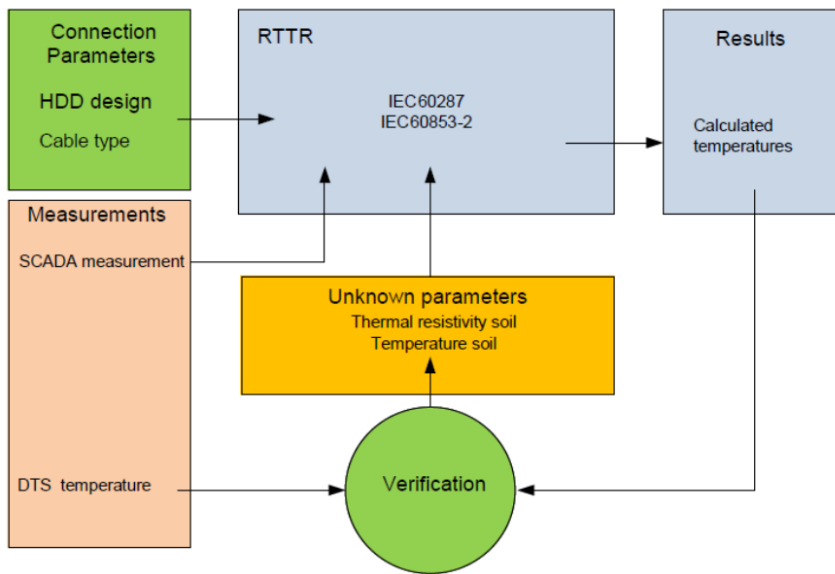


Figure 2.3: Schematic of an RTTR system [13].

2.2.2 Motivation for installing and utilizing cable temperature measurement

The number of cable installations with DTS systems is growing. As much as 66% of all users apply the DTS system in combination with RTTR. However, less than 3% are using the RTTR output for grid operation [13]. A survey carried out by Cigre [13] revealed that almost all information collected by DTS systems as of 2019 is used for learning purposes, as can be seen in Figure 2.4 for the total distribution. However, among the main applications for those that implement DTS and RTTR installations are dynamic rating or research on the topic. Figure 2.4 exposes that there still are a large potential when of utilizing the DTS installation. The survey highlights the importance of knowledge and study of the temperature behavior of power cables.

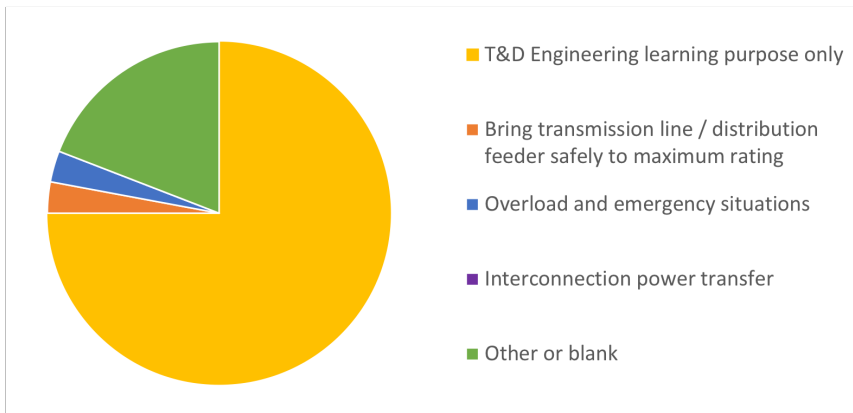


Figure 2.4: An overview on how the information provided by the dynamic rating system used today.

Despite the result revealed in Figure 2.4, there are examples of power system owners that have installed DTS in their systems today for purposes of optimizing the grid operation. The national electrical transmission and distribution company in Singapore, SP PowerGrid Ltd, is one such example. SP PowerGrid Ltd has installed DTS on all their underground cables since 1997, striving to optimize their system by dynamic loading [16].

Theoretical Background

This chapter is presenting the theoretical background relevant to the thesis. The first theory given in this chapter is the heat transfer mechanisms. Furthermore, ampacity calculations for power cables are discussed, including a representation of the IEC standards concerning cable rating. Finally, the chapter examines transient thermal modeling, which is the main focus of the calculations handled. Topics included are the difference between analytical and numerical methods and an explanation of the superposition principle to examine the transient response of the system due to step changes in input power.

3.1 Heat transfer mechanisms

Heat transfer mechanisms are described as transferring thermal energy between different objects to obtain equal energy states of heat or kinetic energy [17]. Three different mechanisms are relevant considering heat transfer, namely conduction, convection, and radiation. A theoretical introduction of the three heat mechanisms is given in this section. More emphasis is, however, placed on conduction as this is most significant for power cables installations.

3.1.1 Conduction

Heat conduction is known as the only heat transfer mechanism that is present for opaque solid materials. The motion of kinetic energy explains the process of heat

conduction through materials with non-uniform temperature distributions. The motion of heat takes place from the areas of higher temperature to the areas of lower temperature in the substances [17]. The action of heat motion happens until a balance between the solids is reached.

Conduction can be explained physically by considering a gas, including a temperature gradient between two material surfaces. The spacing separating the materials examined are held at different temperature levels and might be filled with a gas, as can be seen in Figure 3.1. Higher temperatures are related to higher molecular energies. When two adjacent molecules collide, the molecules consisting of less energetic molecules get energy from the more energetic molecules. As a consequence, energy transfer is transpiring by conduction in the decreasing direction illustrated in Figure 3.1 [18].

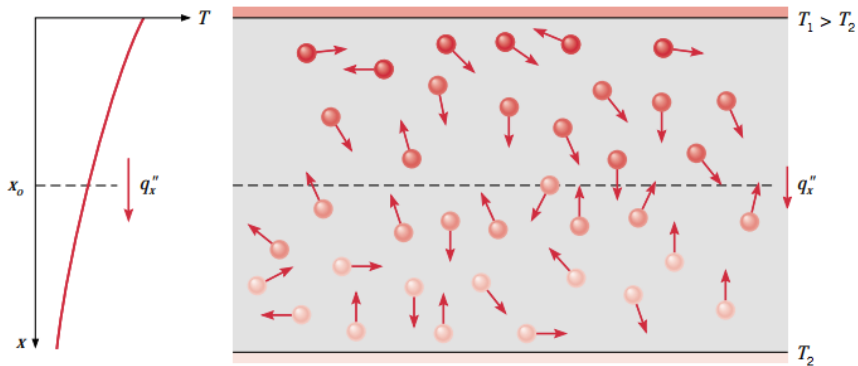


Figure 3.1: Physical illustration of conduction heat transfer [18].

Heat conduction for power cables is an essential aspect as both the heat generated in the conductor and the dielectric heat that is generated in the cable insulation should be transferred to the surroundings [19].

3.1.2 Transient heat conduction

As one of the main goals is to study the transient temperature responses of a cable system, transient heat conduction of power cables is discussed as a basis for the theoretical background. Unlike steady-state conditions, the transient conditions of heat flow are related to a time constant reviewing either periods of heating or cooling. Transient heat conduction that is relevant for the transient calculations is shown in Equation (3.1).

$$\frac{\partial}{\partial x} \left(k \frac{\partial T}{\partial x} \right) + \frac{\partial}{\partial y} \left(k \frac{\partial T}{\partial y} \right) + \frac{\partial}{\partial z} \left(k \frac{\partial T}{\partial z} \right) + \dot{q} = \rho c_i \frac{\partial T}{\partial t} \quad (3.1)$$

Where:

k = Thermal conductivity of material [W/mK]

T = Temperature [K]

\dot{q} = Rate at which heat is produced per unit volume [W/m^3]

ρ = Density of medium [kg/m^3]

c_i = Specific heat capacity of the material [J/kgK]

3.1.3 Convection

When the transporting heat from the cable surface into the surroundings, it may be carried out by heat conduction. However, considering that the surrounding medium is a gas, a more prominent heat mechanism is convection. This mechanism's basis is that hot gas or liquid flow is moving towards the areas with colder temperatures [20].

3.1.4 Radiation

Radiation is known as the action of heat transfer from one body to another body by electromagnetic waves [21]. An object that is warmer than its surroundings, which may be the case for a power cable that is applied a load, will release more considerable radiant energy than it absorbs from the surroundings [20].

3.2 Ampacity calculations of power cables

The term *ampacity* for power cables indicates the maximum amount of current that a cable can securely carry [22]. When applying a current to the power cable, the conductor is the first part to heat up, followed by the enclosing layers and mediums. The quantity of current that a cable can carry is dependent on how much the insulation layer can suffer [23]. Because of this, the insulation is defining the maximum operating temperature of the cable. Accordingly, ampacity calculations are important when rating a cable to avoid drastic temperature rises from applied currents.

Ampacity calculations usually consider two aspects. First of all, one has to consider the potential of the installation to remove the heat produced in the conductor. Secondly, currents applied to the cable lead to losses produced in the conductor. So the losses need to be dissipated to the surrounding medium to avoid overheating the various cable materials [23]. Consequently, one often says that a limiting factor regarding ampacity calculations is the heat dissipation of the cable. If the heat dissipation is managed effectively, the current-carrying capacity of the cable may increase. The ability to dissipate the heat depends on several elements, such as conductivity of the cable insulation and the surroundings [24]. Besides, the temperature of the cable depends on different factors, such as loss size, laying conditions, ambient temperature, and influence from neighboring cables.

There are three standardized ampacity ratings, namely steady-state, transient, and short-circuit. Depending on the duration of the applied current, the maximum continuous operating temperature varies as one can allow higher temperatures for a shorter duration, such as short-circuits. One typically say that XLPE cables can have a maximum conductor temperature of 90°C under normal operation, 105°C for emergency operations and 250°C for operations of short circuit [3].

3.2.1 IEC standards concerning cable rating

Different international and national standards evaluate the maximum current-carrying capacity or ampacity of power cables, which are the basis for several studies [23]. One renowned international standard when it comes to analytical methods for ampacity calculations is the IEC standards. Two different IEC standards are used in this thesis, depending on whether steady-state or transient ampacity calculations are implemented: IEC-60853 'Calculation of the cyclic and emergency current rating of cables' are used for transient temperature calculations, while IEC-60287 'Calculation of the continuous current rating of cables (100 % Load factor) for steady-state temperature calculations.

3.3 Transient thermal modeling

This section presents the theoretical background with transient considerations, including methods for transient thermal modeling and the principle of superposition utilized for load variations.

Cable currents cycle through a day varies typically in conjunction with the different power use. Accordingly, the temperature is diverse as well, corresponding to the heat loss cycle from the cable conductor [25]. In situations where the current cycle fluctuates for relatively short periods, the transient temperature calculations play an essential role in cable ampacity calculations. In case of emergencies where one cable in a system fails, the system owners do not necessarily need to shut down the entire system. A solution may be to continue the power service by switching the current loads to other cables. In such circumstances, knowledge of transient temperature behavior of the cable installation is of high importance due to preventing critical occasions such as overheating and cable failure.

3.3.1 Analytical and numerical method for transient thermal modeling of power cables

There are typically two different approaches discussed when studying the thermal behavior of power cables, namely analytical and numerical methods. Both methods may calculate the transient temperature rise of a specific power cable when the current load changes. In this thesis, the analytical approach, according to IEC standards for ampacity calculations, is used. However, this section provides a short overview of the different methods, including a comparison.

The analytical approach is a well-known and broadly used method as many historical engineers, such as Neher and McGrant [26], has enhanced and developed the method for a long time. Nevertheless, the calculations required in engineering problems related to transient temperature estimation are often too complex to solve with analytical methods without making simplified assumptions. Consequently, analytical approaches are often based on intuitive calculations with simplifying some assumptions such as laying conditions as well as cable constructions.

Using numerical methods for solving heat transfer problems, on the other hand, has become a popular method as computers are being more intelligent and advanced. The advantages of these methods include its ability to obtain accurate simulations of the temperature distributions and the ability of high-level handling of the different parameters, including mutual heating effects and more precise regions' boundaries [4]. Consequently, numerical methods lead to more flexibility for changing parameters and investigating system differences. A drawback is, however, that numerical methods require advanced computers for iterative formulations, which is associated with time-consuming workloads. Two numerical approaches broadly used is called the finite-element method and finite-difference method, which both

are suited when neighboring cables impact the system.

Various researches have studied whether to use analytical or numerical approaches when assessing the heat transfer equations. It turns out that it depends on factors such as the availability of equipment present, the purpose of the study, and the time limits of the survey.

Earlier studies show that the results from temperature response calculations with an analytical method according to IEC standards and numerical approaches gives a quite similar outcome. Millar [27] did such study, and the result can be seen in Figure 3.2. The slight differences in the results may be considered insignificant compared to other factors included in a thermal model. Factors that may ensure errors between calculated temperature and measured temperature are system cooling effects, laying conditions, and environmental impacts. Parameters of the surrounding medium are particularly proven to be unsure.

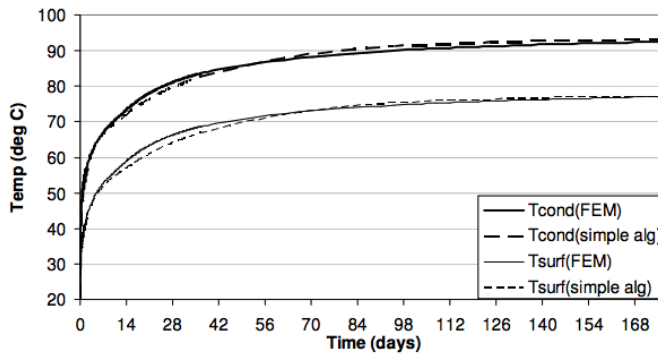


Figure 3.2: Comparison of numerical and analytical method [27].

3.3.2 Superposition principle to examine a system’s transient response

Superposition for a thermally linear system can be applied to predict the cable transient response due to changes in the load [28]. As the term implies, linear superposition may be used when investigating a linear system. A thermal network is considered as a linear network, just like an electric circuit consisting of solely resistors, capacitors, and inductance are called a linear network. Superposition is suitable for such linear networks.

Thermal linear superposition is summarizing individual effects produced when all components in a system are turned on at the same time [29]. The principle of linear superposition may better be understood by including an example of a power system model, as illustrated in Figure 3.3. The example is taken from reference [29]. Note that the example is concentrating on teaching the general situation of linear superposition and shows a steady-state analysis of multiple heat-sources.

As can be seen in Figure 3.3, the example includes three heat sources: Two field-effect transistors (q_1, q_2) and one coil (q_3). Moreover, it contains five temperature points of interest to measure: At the two field-effect transistors (T_{J1}, T_{J2}), at the axial-led device (T_x), at the ground pin on the small-outline (T_{LEAD1}) and between the two field-effect transistors (T_{BOARD}).

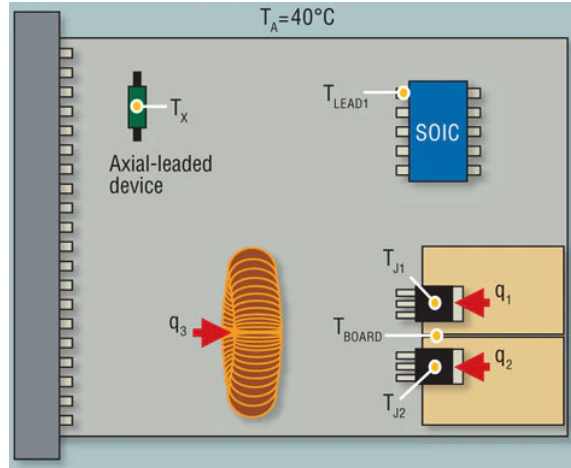


Figure 3.3: Example of an simplified power system model with three heat sources and five temperature measurement points [29].

A mathematical expression is developed from the setup in Figure 3.3, and can be explained by describing the situation in a matrix form as shown in Equation (3.2). The matrix represents five separate equations to make a relationship between the points of temperature measurements and the heat sources through a theta-matrix consisting of 15 coefficients.

$$\begin{bmatrix} \Delta T_{J1} \\ \Delta T_{J2} \\ \Delta T_x \\ \Delta T_{LEAD1} \\ \Delta T_{BOARD} \end{bmatrix} = \begin{bmatrix} \theta_{J1A} & \Psi_{12} & \Psi_{13} \\ \Psi_{21} & \theta_{J2A} & \Psi_{23} \\ \Psi_{x1} & \Psi_{x2} & \Psi_{x3} \\ \Psi_{L11} & \Psi_{L12} & \Psi_{L13} \\ \Psi_{B1A} & \Psi_{B2A} & \Psi_{B3A} \end{bmatrix} \begin{bmatrix} q_1 \\ q_2 \\ q_3 \end{bmatrix} \quad (3.2)$$

The matrix shown in Equation (3.2) makes it possible to write the different equations separately as well. As an example, consider the first equation which can be written separately as shown in Equation (3.3).

$$\Delta T_{J1} = \theta_{J1A}q_1 + \Psi_{12}q_2 + \Psi_{13}q_3 \quad (3.3)$$

Where the θ coefficients represent self-heating terms, while the Ψ coefficients are the interaction terms. Thus:

- ΔT_{J1} = Temperature rise of FET no. 1 for given power vector and theta-coefficients
- θ_{J1A} = Thermal resistance from junction to the ambient of FET no. 1
- Ψ_{12} = Thermal coefficient giving rise at FET no. 1 due to heat at FET no. 2 (q_2)
- Ψ_{13} = Thermal coefficient giving rise at FET no. 1 due to heat in coil (q_3)

Equation (3.3) is in fact a direct expression of the concept linear superposition as it reveals that a linear association of three single terms makes the overall temperature rise at junction 1. The three individual terms in Equation (3.3) are representing the total temperature rise imagining the only heat source present is the heat source considered here [29]. For instance, if q_1 was the only heat source of the system, the temperature rise of FET no. 1 would be $\Delta T_{J1} = \theta_{J1A}q_1$.

As already stated, the above example shows the principle of linear superposition through a steady-state analysis. Nevertheless, the principle is suitable for transient analysis as well by changing the parameters to time-varying parts and by describing the heat sources as step changes instead of established values. In doing so, the heat sources can be varying values. Linear superposition in case of transient temperature rises due to changing current loads can be seen in Figure 3.4.

Figure 3.4a manages a step current, which is switched off after some time, where a square-edge approximation describes the current. Typically for a real current step applied to a cable system, the time-varying power input does not have a rectangular pulse like the one in this illustration. However, one often neglects the temperature details. Furthermore, the lower part of Figure 3.4a divides the two individual actions from the square power pulse (when switching on the current and when turning off the current, respectively), resulting in one positive contribution and one negative contribution.

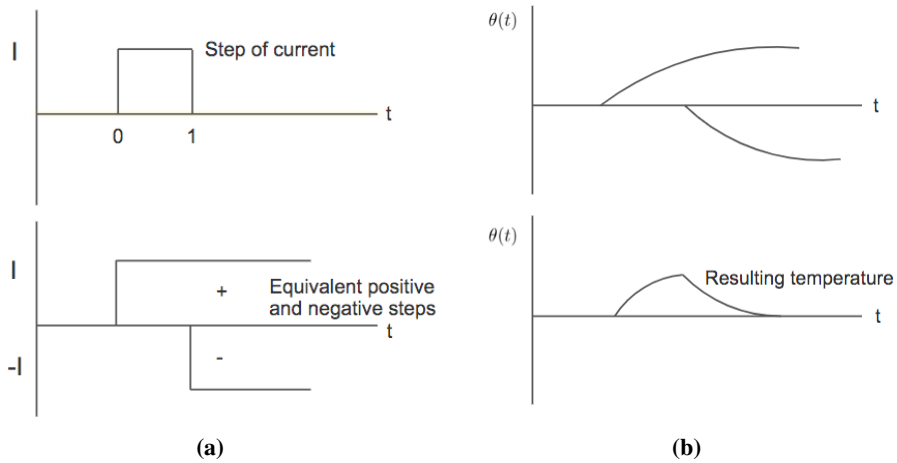


Figure 3.4: Temperature rise due to one step of current and applying of superposition principle.

Each of the equivalent positive and negative steps are moreover turned into separate transient-response curves for the heat sources, as can be seen in the upper part of Figure 3.4b. In the lower part of Figure 3.4b, the sum of the two responses representing one increase and one decrease is illustrated as the resulting temperature response of the system due to two heat sources.

Thermal Modelling - Calculation Methodology

This chapter is establishing a thermal ladder network. The network aims to determine an analytical solution using IEC standards for heat transfer from the conductor to the outer cable surface. The calculation method is used to establish a simulation in MATLAB that calculates the temperature response due to a specified current change.

First, the chapter presents the circuit theory for thermal modeling, including a discussion of the analogy between thermal and electrical relationships. Furthermore, a representation of heat sources that are causing cable losses is shown. Moreover, steady-state heat transfer theory is studied as it provides a basis for the transient representation that is furthermore presented. This includes the presentation of the equivalent thermal circuit and how to calculate the different parameters found in the network. The calculation method involves both calculations of cables located in free air and cables located in culverts. The calculation is accomplished to conduct comparisons with both the experimental method in Chapter 5 as well as studying the high voltage cable installation in Chapter 7.

4.1 Circuit theory for thermal modeling

The basis for the thermal model is utilizing the foundation of electric circuits. Aiming to establish a thermal equivalent, the relationship between electrical cur-

rent applied, and the temperature difference between the conductor and the surrounding medium is studied. This relationship is proven to be a common method investigating the thermal responses due to its flexibility [30]. Table 4.1 shows the relationships between thermal and electrical quantities.

Table 4.1: Analogy between thermal and electrical circuits including quantities, symbols and unit comparisons.

Electrical		Thermal	
Kirchoff's current law		Heat balance	
Electric potential	V	Temperature	T
Current	I [A]	Heat transfer rate	\dot{Q} [W]
Electric resistance	R [Ω]	Thermal resistance	R [$^{\circ}\text{C}/\text{W}$]
Electric capacitance	C [F]	Thermal capacitance	C [$\text{J}/^{\circ}\text{C}$]
Ohm's law	$I = \frac{\Delta V}{R}$	Steady heat conduction	$\dot{Q} = kA \frac{\Delta T}{x} = \frac{\Delta T}{R}$
Current through capacitor	$I = C \frac{dV}{dt}$	Heat flow rate	$\dot{Q} = C \frac{dT}{dt}$

From Table 4.1, one can see that electric resistance is analog to thermal resistance, while electric capacitance is analog to thermal capacitance. Thermal resistance is described as the material's ability to store heat, whereas thermal capacitance is the material's ability to resist heat flow [4]. Creating a thermal circuit considering the analogy between thermal and electrical parameters, the voltages from the electric circuit are concerned as temperatures in the thermal circuit. Furthermore, the heat represented in the thermal network is analogous to the charge concerning electric circuits; thus, Ohm's law corresponds to Fourier's law.

To simplify the calculations of the transient temperature, Anders [4] introduces a method by establishing a ladder network consisting of lumped parameters. The ladder network is considering the cable enhancing from the conductor and as far as to free air. The strategy for the lumped parameter representation is basically to represent elements of the power cable by adding up or lump as many elements in the construction as possible [30]. By creating this simplified network, one can easier solve the heat equations analytically, reducing the complexity related to the calculations. Hence, this is a popular and familiar method for cable constructions.

Thermal model reduction to a two-loop circuit involves calculations that are considered as very simplified. CIGRE and later IEC introduced computational procedures to build the two-loop circuit, aiming to ease the transient rating calculations

[4]. Although the two-loop representation appeared before the advanced computers occurred to the market, the method has turned into being pretty accurate compared to the newer methods involving computers. So it has also been adopted to international standards. The reduction to a two-loop circuit is utilized to calculate the transient temperature responses in this thesis.

4.1.1 Van Wormer coefficient

Thermal capacitances are involved when calculating the transient thermal response of a cable system. For these cases, the thermal capacitances of a cable layer need to be shared properly. First of all, one wants to establish an equivalent π -circuit that expresses the heat-transfer process taking place in such action [31]. Figure 4.1 illustrates this process regarding one specific layer in the cable system including the thermal capacitance, namely Q , as well as the thermal resistance, T . As the figure shows, the capacitance is divided into two different parts where p is a ratio of the capacitance portion-rule. The ratio is called the Van Wormer's coefficient [32].

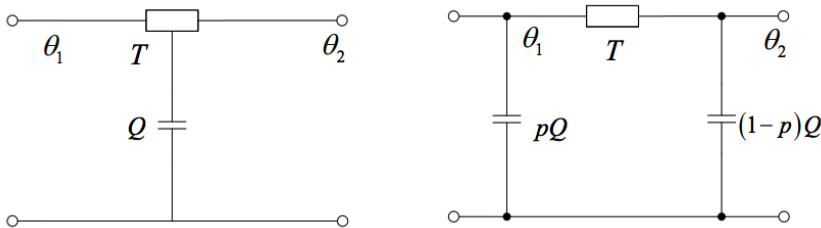


Figure 4.1: Model of the cable system before equivalence (left figure) and after equivalent π -circuit (right figure), including Van Wormer's coefficient [33].

Considering the insulation layer of a cable system, Van Wormer aimed to represent the total heat stored in the insulation by allocating the thermal capacity between the conductor and the screen using lumped parameters. The capacity is hence divided into a portion $p \cdot Q_{ins}$ at conductor and $(1 - p) \cdot Q_{ins}$ at the screen, illustrated in Figure 4.1 with a general approach. Van Wormer Coefficient is given in Equation (4.1). With a similar explanation, the Van Wormer Coefficient of the sheath layer is given in Equation (4.2).

$$p = \frac{1}{2\ln\left(\frac{D_i}{D_{cond}}\right)} - \frac{1}{\left(\frac{D_i}{D_{cond}}\right)^2 - 1} \quad (4.1)$$

$$p^* = \frac{1}{2\ln\left(\frac{D_e}{D_s}\right)} - \frac{1}{\left(\frac{D_e}{D_s}\right)^2 - 1} \quad (4.2)$$

Where:

D_e = external sheath diameter

D_s = internal sheath diameter

4.2 Heat sources causing cable losses

Power cable losses refer to the heat generated in conductor, sheath, and the cables insulating parts [34]. One often divide these losses into two types, namely current-dependent powers and voltage-dependent powers. While the current-dependent powers relate to the generated heat in the metallic cable components, the voltage-dependent powers correlate to the powers in the insulation, which is divided into dielectric powers and powers caused by a charging current [34].

Both power cable's internal and external heat sources are generating heat, which is creating losses in the cable installation. This thesis focuses on the effect of joule losses when it comes to internal heat sources. Joule losses, also called I^2R -losses, occur in the cable conductor when current is applied. The current produces conductor heat, causing the joule heating of the conductor. Heating of conductor is hence producing losses when the heat is leaking into the surrounding medium. Henceforth, the joule losses are representing the total internal losses.

Equation (4.3) shows the joule losses, where I denotes the conductor current, and the conductor ac resistance is R_{ac} . The ac resistance can be calculated by equation (4.4) [4].

$$W_t = I^2 \cdot R_{ac} \quad (4.3)$$

$$R_{ac} = R_{20} \cdot [1 + \alpha \cdot (\theta - 20)] = \frac{\rho_{20} \cdot L}{A} [1 + \alpha \cdot (\theta - 20)] \quad (4.4)$$

Where:

- R_θ = Temperature dependent conductor resistance [Ω]
- R_{20} = Conductor resistance at 20 °C [Ω]
- α = Temperature coefficient
- θ = Temperature of conductor [$^{\circ}\text{C}$]
- ρ_{20} = Specific resistivity of conductor at 20 °C [Km/W]
- L = Length [m]
- A = Conductor area [m^2]

Solar radiation from the sun is considered as an external heat source that is affecting the cable losses, indicated W_{sol} . However, solar radiation is neglected in the following calculations because non of the cable installations considered are exposed to the sun. The heat balance equation is obtained in Equation (4.5).

$$W_t + \sigma D_e H - \pi D_e h(\theta_e - \theta_{amb}) - \pi D_e \epsilon \sigma_B (\theta_e - \theta_{amb}) = 0 \quad (4.5)$$

Where:

- σ = Solar absorption coefficient
- H = Solar radiation intensity [W/m^2]
- σ_B = Stefan-Boltzmann coefficient
- ϵ = Cable external covering emissivity
- θ_{amb} = Ambient temperature [K]

4.3 Steady-state temperature: IEC 60287

In order to calculate the transient response of a cable system, the steady-state thermal equivalent circuit is demonstrated. Additionally, by considering the analogy between the electrical and thermal circuit as presented in Table 4.1, the thermal resistance can be determined, and the losses per unit length.

4.3.1 Thermal equivalent circuit

The thermal capacitances of the cable installation are neglected considering the steady-state thermal equivalent circuit, as it is assumed to be zero after a certain time. For transient calculations, on the other hand, the thermal capacitances play

an important role. Thus, the focus for steady-state conditions is the thermal resistances that exist for different layers. The following list is showing the thermal resistances and what they are representing:

- T_1 : Thermal resistance between conductor and sheath
- T_2 : Thermal resistance between sheath and armor
- T_3 : Thermal resistance of external covering
- T_4 : Thermal resistance of external cable environment

Figure 4.2 shows the thermal equivalent circuit constructed for a single power cable. The losses are indicated as constant current sources, while the ambient temperature is represented as a constant voltage.

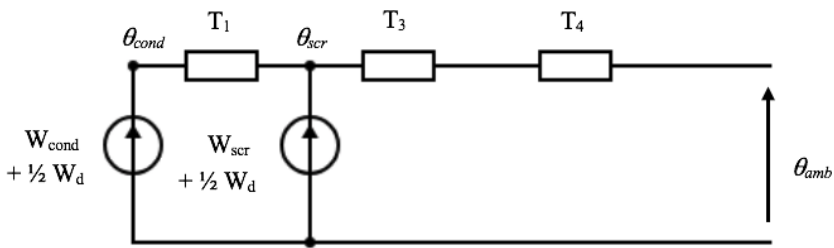


Figure 4.2: Thermal equivalent circuit for single power cable.

Where:

W_{cond} = Conductor losses per unit length [W/m]

W_{scr} = Screen losses per unit length [W/m]

W_d = Dielectric losses per unit length [W/m]

The thermal resistance T_4 is varying depending on the cable laying condition. For power cables located in ducts or culverts, the thermal resistance T_4 is a composed value consisting of three individual parts, explained in Section 4.3.2.

4.3.2 Thermal resistance

While the cable conductor is producing heat when the electric current is flowing through it, the nonconducting materials that surround the conductor will impede heat flow away from the cable. Consequently, a material's ability to resist heat flow is a widely discussed term considering cable rating.

Some assumptions have been made to simplify the mathematical relationships to calculate the thermal resistance of different layers. First of all, the thermal resistance of metallic layers with a thin thickness, such as the screen layer, has been neglected due to high thermal conductivity. Also, the swelling tape that is applicable for some cable installations is assumed to be a part of the insulation and should, therefore, be given an equally thermal resistance. Another assumption relevant tells that optical fibers installed in the system for temperature logging are supposed to have no thermal impact on any part of the system. The thermal resistances can be developed utilizing the analogy between thermal and electrical fields. For cylindrical layers such as the insulation layer and the conductor in the cable installation, the thermal resistance is shown in Equation (4.6) [4].

$$T_i = \frac{\rho_i}{2\pi} \cdot \ln\left(1 + \frac{2t_i}{D_i}\right) \quad (4.6)$$

Where:

- ρ_i = Thermal resistivity of material in layer i [$\frac{Km}{W}$]
- t_i = Thickness of layer i [mm]
- D_i = Diameter beneath layer i [mm]
- i = Layer i that are considered

External thermal resistance

Regarding the external thermal resistance, T_4 , the calculations are dependent on the surrounding medium of the cable installation. In the experiment carried out in this thesis, the cable is located in air in different forms. For the methodology of studying the data from Statnett, the cable investigated is located in a culvert as well.

Cable installations in air Cables installed in free air is commonly found in substations or at the connection point with overhead lines [35]. Equation (4.5) shows the heat balance equation for cables in free air. The standard IEC 60287 [36] allows for steady-state rating calculations regarding cables in free air. The standard presents some simple configurations that have been revealed from several tests on different cables in various configurations, performed in the 1930s in the United Kingdom. Whitehead and Hutchings [37] provided an equation for the total thermal dissipation from the cables surface when located in air, which is shown in Equation (4.7).

$$W_t = \pi D_{ext} h (\Delta\theta_s)^{5/4} \quad (4.7)$$

Where:

D_{ext} = Cable external diameter [m]

h = Heat transfer coefficient including convection, radiation and conduction

$\Delta\theta_s$ = Cable surface temperature rise above ambient

Whitehead and Hutchings [37] also provided a method to find the heat transfer coefficient, h , by making experimental attempts and obtaining curves as a function of the cable diameter. At a later point, the curves were used to achieve an analytical expression for the heat transfer coefficient. The expression is shown in Equation (4.8).

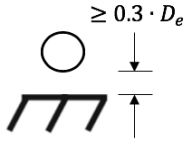

$$h = \frac{Z}{(D_{ext})^g} + E \quad (4.8)$$

Where Z , g and E are constants that is particular dependent on the installation mode of the cable. Table 4.2 shows the values for the constants regarding single cable installations with air as the surrounding medium. Table 4.2 includes both cases relevant for the experimental methodology for this thesis, respectively single cables located freely in air ($\geq 0.3 \cdot D_{ext}$) and cables positioned on ground surface surrounded by air.

The external thermal resistance when the cable is located in air can be obtained from Equation (4.7), and is shown in Equation (4.9).

$$T_4 = \frac{1}{\pi D_{ext} h (\Delta\theta_s)^{1/4}} \quad (4.9)$$

Table 4.2: Values for constants Z , E and g for cables in free air [4].

Installation	Z	E	g	Mode
Single cable	0.21	3.94	0.60	
Single cable	1.69	0.63	0.25	

As Equation (4.9) exposes, the external thermal resistance is dependent on $\Delta\theta_s$, which needs to be determined. The process of determining this parameter is shown in Appendix A.

Cable installations in culverts For cables located in ducts filled with air, the external thermal resistance consists of three different parts:

1. Thermal resistance between the cable surface and internal duct surface, $T_{4,1}$
2. Thermal resistance of the duct itself, $T_{4,2}$
3. External thermal resistance of the duct, $T_{4,3}$

The total value of thermal resistance T_4 is the sum of the three individual parts:

$$T_4 = T_{4,1} + T_{4,2} + T_{4,3}$$

$T_{4,1}$ can be found from a simplification given by Anders [4], as can be seen in Equation (4.10).

$$T_{4,1} = \frac{U}{1 + 0.1(V + Y\theta_m)D_e} \quad (4.10)$$

Where:

- U, V, Y = Material constants defined in Anders [4], Table 9.6
 θ_m = Mean temperature of the filling medium between cable and duct
 D_e = External diameter of the cable [m]

Furthermore, $T_{4,2}$ are found from Equation (4.11). Note that this equation is handling a circular duct, while the cables considered in this thesis are in a rectangular culvert. Thus, the rectangular shape of the duct must transform into a circular isotherm. The process of this conversion suggested by Karlstrand et al. [38] is shown in Appendix B.

$$T_{4,2} = \frac{\rho}{2\pi} \ln \frac{D_o}{D_d} \quad (4.11)$$

Where:

ρ = Thermal resistivity of the duct material [Km/W]

D_o = Outside diameter of duct [mm]

D_i = Inside diameter of duct [mm]

4.4 Transient temperature: IEC 60853

In order to calculate the transient temperature rise of a cable installation due to a change in the electric current applied to the system, one can use analytical approaches based on the standard IEC 60853.

4.4.1 Transient thermal equivalent circuit

A ladder thermal network, aiming to visualize the study of thermal behavior in power cables regarding both conductor and sheath layers, is presented [39]. Figure 9.2 in Appendix C shows the transient thermal equivalent for both cases of laying conditions, namely cable installations located in free air and ducts.

4.4.2 Thermal capacitance

Unlike the steady-state temperature calculations presented in Section 4.3, the transient temperature calculations involve thermal capacitances in addition to thermal resistance. The thermal capacitances illustrate the total heat stored in the different layers of the installation [40]. The heat capacitance is divided at each side of the thermal resistance, and is shared by using the Van Wormer coefficient as discussed in subsection 4.1.1.

The thermal capacitance of various layers of the cable installation in Figure 9.2 is found from the basis in Equation (4.12).

$$Q_i = V_b \cdot c_i \quad (4.12)$$

Where:

V_b = Volume of the body [m^3]

c_i = Specific heat of material i [J/Km^3]

From Equation (4.12), one can develop an equation for the case of a cylindrical layer, relevant for layers such as the insulation and sheath. The equation is utilizing the analogy as shown in Table 4.1. The heat capacitance for cylindrical layers is shown in Equation (4.13), where D_{ext} is representing the external diameter while D_{int} is the internal diameter of the given layer.

$$Q = \frac{\pi}{4} \cdot (D_{ext}^2 - D_{int}^2) \cdot c_i \quad (4.13)$$

4.4.3 Reduction to a two-loop circuit

The thermal equivalent circuits shown in Figure 9.2 can be reduced to two-loop circuits. The reduction is recommended by IEC 60853 part 1 and 2 who has chosen to implement this method of reduction for calculations involving transient responses [41]. The resulting thermal equivalent after the reduction to a two-loop circuit is shown in Figure 4.3.

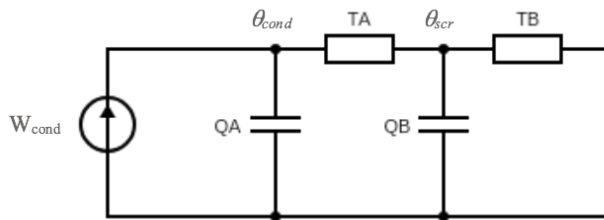


Figure 4.3: Reduction from ladder circuit to a two-loop thermal circuit.

The two-loop circuit in Figure 4.3 does apply for several different cable installations, depending on the thermal equivalent that covers the given installation.

Anders [4] presents relationships applicable to such transformations. For cables located in free air, the following relationship is valid:

$$\begin{aligned}
 T_A &= T_1 \\
 T_B &= \frac{1}{2}T_1 + (1 + \lambda_1)(T_3 + T_4) \\
 Q_A &= Q_{cond} + Q_i \cdot p \\
 Q_B &= Q_i \cdot (1 - p) + \frac{Q_{scr} + Q_{sh} \cdot p^*}{1 + \lambda_1}
 \end{aligned}$$

For cables located in a culvert, the following relationship is valid:

$$\begin{aligned}
 T_A &= T_1 \\
 T_B &= T_3 + (1 + \lambda_1)(T_{4,1} + T_{4,2}) \\
 Q_A &= Q_{cond} + Q_i \cdot p \\
 Q_B &= Q_i \cdot (1 - p) + \frac{Q_{scr} + Q_{sh} \cdot p^*}{1 + \lambda_1} + \left[\frac{(1 + \lambda_1)(T_{4,1} + T_{4,2})}{T_B} \right]^2 \left(\frac{(1 - p^*)Q_{sh}}{1 + \lambda_1} \right) \\
 &\quad + \left[\frac{(1 + \lambda_1)T_{4,2}}{T_B} \right]^2 \frac{Q_d}{1 + \lambda_1}
 \end{aligned}$$

In the above relationships, λ_1 is the screen loss caused by circulating currents and eddy currents. However, these are neglected in the calculations for this thesis.

As studied in the specialization project [39] as preparatory work to the current study, a direct buried cable installation was investigated. Buried laying method requires a separate response for the cable environment comprising an exponential integral. However, the exponential integral is not included in cases for cables with air as the surrounding medium. Thus, the formula of T_B for cable in air includes the external thermal resistance as well. The process of calculating the transient temperature rise of the internal cable parts and the surrounding medium is discussed further in the next subsection.

4.4.4 Transient temperature rise of cable installation

The theory regarding the temperature rise in the internal parts of the cable is similar to the material from the specialization project preceding this thesis, see reference [39]. Hence, the presentation from the project report is included in this subsection.

« For a linear network, such as the ones presented in Figure 9.2, a forcing function will cause a response function. This response function can be determined by using the network transfer function. For the specific case in this study, the response function is considered as the temperature rise while the forcing function is the conductor reviewed as the conductor heat loss [4]. The transfer function is the Fourier transform of the networks unit-impulse response. Laplace transform of the transfer function of the network is given by Equation (4.14), where $P(s)$ and $Q(s)$ is polynomials depending on the number of loops in the given network [4].

$$H(s) = \frac{P(s)}{Q(s)} \quad (4.14)$$

From the transfer function in Equation (4.14), the poles and zeroes are found by solving $P(s) = 0$ and $Q(s) = 0$. Furthermore, the time dependent response of different nodes in the network is given as in Equation (4.15).

$$\theta_{rise,i}(t) = W_t \sum_{j=1}^n T_{ij} \cdot (1 - e^{P_j t}) \quad (4.15)$$

Where:

- $\theta_i(t)$ = Temperature rise at node i at time t [°C]
- W_t = Conductor heat losses, [W/m]
- T_{ij} = Coefficient, °C, [m/W]
- P_{jt} = Chosen time constant, [s^{-1}]
- t = Starting time of the step, [s]
- n = Total number of loops in network
- j = Index from 1 to n

The parameters T_{ij} and P_j are both determined from the poles and zeros in equation (4.14). Furthermore, T_{ij} is given by Equation (4.16) [42].

$$T_{ij} = -\frac{a_{(n-1)i}}{b_n} \frac{\prod_{k=1}^{n-i} (Z_{ki} - P_j)}{P_j \prod_{k=1; k \neq j}^n (P_k - P_j)} \quad (4.16)$$

$a_{n-1}i$ = Numerator equation coefficient, transfer function

b_n = Denominator equation first coefficient, transfer function

Z_{ki} = Zeros of transfer function

P_j = Poles of transfer function

Calculations of the parameters T_{12} , T_{21} , T_{11} and T_{22} utilizing Equation (4.16) are shown in Appendix D, which are parameters used when calculating both conductor and sheath temperature rises. The resulting conductor temperature rise are shown in Equation (4.17) while the resulting sheath temperature rise are shown in Equation (4.18). The steps showing how to derive Equation (4.17) (4.18) are shown in Appendix D as well.

$$\theta_c(t) = W_t \cdot [T_{11}(1 - e^{P_1 t}) + T_{12}(1 - e^{P_2 t})] \quad (4.17)$$

$$\theta_{sheath}(t) = W_t \cdot [T_{21}(1 - e^{P_1 t}) + T_{22}(1 - e^{P_2 t})] \quad (4.18)$$

»

4.4.5 Calculating several load changes utilizing the principle of superposition

The principle of superposition is explained in detail in Chapter 3.3.2. Linear superposition in the case of transient temperature rises due to current applied to a power cable works likewise, as explained for the example in Figure 3.3. However, in the case of current applied in different steps of loads, the individual steps are representing separate temperature rises as heat sources, and the overall temperature rise is the summation of all the heat sources applied.

As an example, a load of 200 A will be considered as a single heat source producing one temperature rise. When a new current load of additionally 200 A is applied (total current of 400 A to the cable), it will be considered as a single heat

source that can be summarized with the first current load. The principle additionally holds for negative contributions or current decreases. Figure 3.4 illustrates this, showing the transient temperature rises due to one current step, and the resulting temperature response when utilizing the principle of superposition. Note that mutual heating effects from neighboring cables are not included.

Experimental methodology

The experimental methodology mainly intends to be used in comparative analysis with the results from the calculation method represented in Chapter 4. The experimental methodology includes a laboratory setup established at NTNU. However, due to the situation of Covid-19, the experiment was disturbed and terminated after the completion of two tests. Nevertheless, the conducted tests turned out to be considered sufficient and have given an adequate basis for the verification of the simulation from the calculation methodology as intended. The tests completed studies cases of temperature rises due to a load increase as well as temperature responses due to variable loads applied in order to study the effect of the superposition principle.

5.1 General explanation of the laboratory setup

The laboratory setup measures the temperature of a chosen cable installation and hence obtain an overview of the temperature response when applying an electric current. The setup contains a current transformer placed in a container, and the cable studied is connected in both ends to the transformer through a pair of cable lugs. The setup makes the cable itself laying in a loop formation on the floor. By using a current transformer, the current is produced as an alternating current in the transformer's secondary winding, which is proportional to the current measured in the primary winding [43]. Figure 5.1 shows the laboratory setup for the experimental methodology.

The cable is connected to the current transformer as a short circuit, meaning that the only voltage present will be the voltage drop due to current flowing in the cable, which is the reason why dielectric losses are neglected in this study.

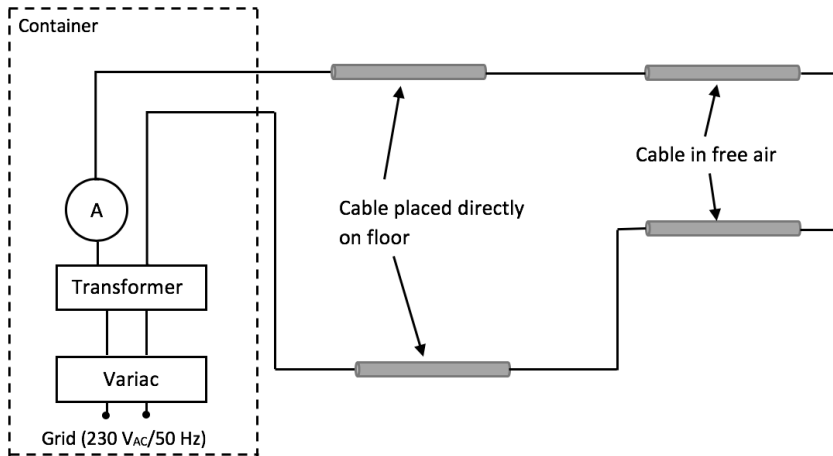


Figure 5.1: Overview of the laboratory setup. (Not drawn to scale)

5.1.1 Material list

The list of materials used in order to complete the laboratory setup:

- Noratel Current transformer
- Nexans TSLF 24 kV cable
- Copper-constantan thermocouples
- Cable lugs
- Fluke AC tang power meter
- Keysight Technologies data logger
- ACER computer to log the data

5.1.2 Cable installation

The power cable used for the laboratory experiment is a Nexans TSLF 24 kV with a round, stranded aluminum conductor. The conductor area is 50 mm^2 covered

with an intrinsic semiconductor to reduce the electric field strength of the cable. The chosen power cable has an extruded cross-linked polyethylene (XLPE) insulation covered with an outer semiconductor and a stranded copper wire screen. The screen is covered with aluminum tape for water protection in a radial direction and swelling tape to make sure that the cable is waterproof in a longitudinal direction. The outer covering of the power cable is a sheath made of polyethylene (PE) [44]. Figure 5.1 shows the power cable and additionally providing the relevant dimensions of the cable chosen.

Rated cable data	
Rated voltage	24 [kV]
Conductor area	50 [mm ²]
Screen area	16 [mm ²]
Conductor diameter	8.0 [mm]
Diameter over insulated conductor	19.3 [mm]
Thickness of insulation	5.5 [mm]
Thickness of sheath	2.1 [mm]
Cable outer diameter	27.0 [mm]



Figure 5.2: Rated cable data for 50/16 mm² cable (24 kV) and illustration of the power cable used for experimental method in laboratory [44].

5.1.3 Laying conditions of the laboratory setup

The laboratory setup enables to measure the cable temperature for two different laying conditions:

1. Cable placed on a concrete floor with air as surrounding medium
2. Cable lifted from the floor in free air

When testing the two laying methods, the comparison with the calculation method is considered strengthened. The parameters involving cables in free air are somewhat more complex and challenging to determine than other laying methods due to the uncertainties of the surrounding medium. The cable installation fastened to the floor, on the other hand, may be easier to determine as the medium of the floor contains less changing external parameters. Nevertheless, external parameters such as changing wind speed and ambient temperature changes, are not affecting the laboratory setup. Consequently, the two laying methods has the foundation to provide accurate results to complete a comparison.

5.2 Methods of measuring the relevant parameters of the experiment

5.2.1 Temperatures of different cable layers

Copper-constantan thermocouples are used to measure the temperature of the different parts of the cable. The thermocouples are placed at a total of four different places along the cable length to achieve two separate measurements for each laying condition. By doing this, one attains the ability to control results and double-check values. Additionally, any faults or irregularities may be detected when comparing the results for two different locations measuring the same and having equal prerequisites. The temperatures were logged every 20 seconds.

At each measurement point, the temperature is assessed with two temperature sensors at the cable's surface, one sensor located under the cable jacket measuring the sheath temperature, and one sensor placed at the conductor surface. An illustration of the total of four measurement points at a given location are shown in Figure 5.3.

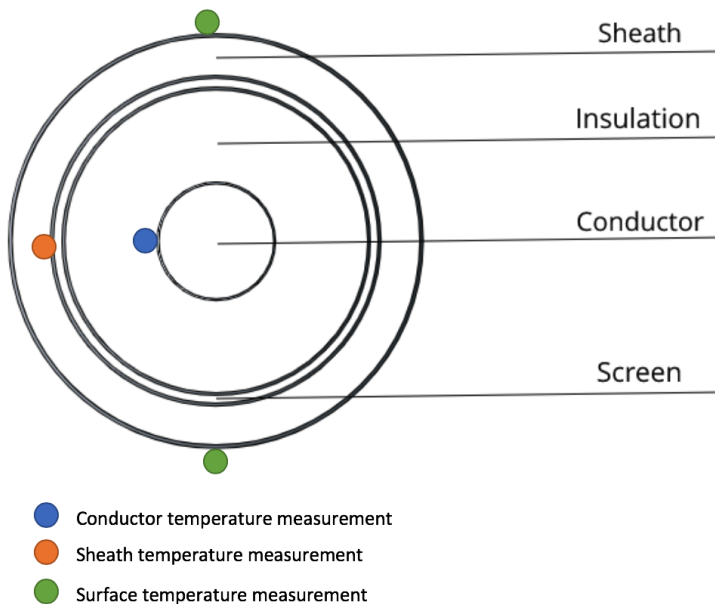


Figure 5.3: Overview of the measurement points on the cable construction.

The measurements under the cable jacket and on the conductor were carried out by drilling a small, obliquely hole into the cable at the chosen places of measurements. The losses related to the drilled hole has not been taken into account during the calculation.

5.2.2 Conductor current

The conductor current is logged with a data-logger every 20 seconds to achieve the same total of data-points as the temperature data logs. Attached to the cable is an AC tang power meter, assessing the conductor current. The AC current is produced by a $230V/7V - 640Amp$ current transformer with a $0 - 230V/20Amp$ variac. The current transformer has an effect of 4500 VA, and the frequency is 50 Hz.

5.2.3 Ambient temperature

The ambient temperature is detected utilizing the cable surface temperature shown in Figure 5.3 when the cable has been disconnected from the transformer for such time that the surface temperature has been stable for a while. By doing this, the surface temperature can be used as the ambient temperature.

Chapter 6

Results and Discussion

This chapter represents the results obtained from experimental methodology and calculation methodology explained in respectively Chapter 4 and Chapter 5. The results from the experimental methodology are mainly used to discuss the accuracy of the simulation made from the calculation methodology. Additionally, the calculation method is used to simulate cases considering the cable installation from the laboratory setup, aiming to study the effect of the superposition principle, overloading case examples, and the load history impact.

This chapter begins by presenting the results from the calculation method that are utilized for the simulation. Furthermore, a representation of the results from the experimental methodology carried out in the laboratory, as explained in Chapter 5, are shown. Two tests are completed, where a test of applying a current increase of 100 A is the first test and the second test handles a step current of 150 A. Furthermore, Section 6.3 compares the simulation from the calculation method with the results obtained in the lab for both conductor and sheath temperature. Moreover, studying the principle of superposition completed in Section 6.4 by using the simulation for cables in free air. Finally, an overload case example for the cable installation and a discussion on the load history impact on the system is completed in respectively Section 6.5 and Section 6.6.

6.1 Analytical modeling based on IEC standards for cable installation utilized in the laboratory setup

All the results shown in this section, are determined from the equations and calculations from Chapter 4. Parameters that are used for the calculations are shown in Table 6.1. Moreover, the thermal resistances are shown in Table 6.2, while the thermal capacitance are revealed in Table 6.3. In the two-loop circuit that was established for the calculation, the simplified parameters involved in the resulting thermal circuit are given in Table 6.4 and Table 6.5.

In addition, aluminum conductor temperature coefficient, α_{al} , is chosen to be 0.0043 [1/K] and the conductor resistance, R_{20} , is found to be $5.3 \cdot 10^{-4}$ [m]. The Van Wormer coefficients are found to be $p = 0.3603$ and $p^* = 0.4445$.

Table 6.1: Cable parameters for cable installation in the experiment.

Cable information	
Thermal resistivity of conductor, $\rho_{cond,20}$	$2.65 \cdot 10^{-8} [\frac{Km}{W}]$
Thermal resistivity of XLPE insulation, ρ_{ins}	$3.5 [\frac{Km}{W}]$
Thermal resistivity of lead sheath, ρ_{sheath}	$3.5 [\frac{Km}{W}]$
Specific heat of conductor, c_{cond}	$2.5 \cdot 10^6 [\frac{J}{m^3K}]$
Specific heat of XLPE insulation, c_{ins}	$2.4 \cdot 10^6 [\frac{J}{m^3K}]$
Specific heat of sheath, c_{sheath}	$2.4 \cdot 10^6 [\frac{J}{m^3K}]$
Specific heat of metallic screen, c_{screen}	$3.45 \cdot 10^6 [\frac{J}{m^3K}]$

Table 6.2: Thermal resistances calculated for both laying conditions.

Cable in free air	Thermal resistance $[\frac{m}{W}]$	Cable placed on the floor	Thermal resistance $[\frac{m}{W}]$
T_1	0.4818	T_1	0.4818
T_3	0.1870	T_3	0.1870
T_4	0.9109	T_4	1.0776
T_A	0.4818	T_A	0.4818
T_B	1.3608	T_B	1.5308

6.1 Analytical modeling based on IEC standards for cable installation utilized in the laboratory setup

Table 6.3: Thermal capacitance calculated for both laying conditions.

Cable for laying conditions	Thermal capacitance [$\frac{J}{Km}$]
Q_{cond}	125.00
Q_{ins}	581.49
Q_{scr}	470.69
Q_{sh}	672.01
Q_A	334.51
Q_B	670.66

Table 6.4: Parameters P_1 , P_2 , N_0 and M_0 obtained from the two-loop network for both laying conditions.

	Cable in free air	Cable placed on the floor
$-P_1$	0.0096	0.0097
$-P_2$	0.0006	0.0007
M_0	849	764
N_0	165470	147100

Table 6.5: Thermal resistance of the conductor temperature rise and sheath temperature rise for both cable laying methods.

Cable in free air	Thermal resistance [$\frac{m}{W}$]	Cable placed on the floor	Thermal resistance [$\frac{m}{W}$]
T_{11}	0.1887	T_{11}	0.1916
T_{12}	1.6539	T_{12}	1.8210
T_{21}	0.0511	T_{21}	0.0512
T_{22}	0.7068	T_{22}	0.7888

6.2 Results from the experimental methodology carried out in the lab

Figure 5.1 illustrates the chosen experiment provided in the laboratory setup, showing that Position 1 and Position 4 is located on the floor with the surrounding medium air. In contrast, Position 2 and Position 3 handles power cables located in free air (not placed on the floor). The experiment that carried out consists of the following two tests:

- Test 1: Current increase of 100 A applied for 1.6 hours investigating the temperature rise of the conductor, sheath, and the surface layer.
- Test 2: Step current of 150 A applied for 0.5 hours before switched off investigating the temperature response of conductor, sheath, and the surface layer, aiming to study the effect of the superposition principle.

Tests 1 and 2 were running while temperatures were measured for the four measuring points, completed for a total of four different locations on the cable length. The current path obtained from respectively Test 1 and Test 2 are shown in Figure 6.1 and Figure 6.2.

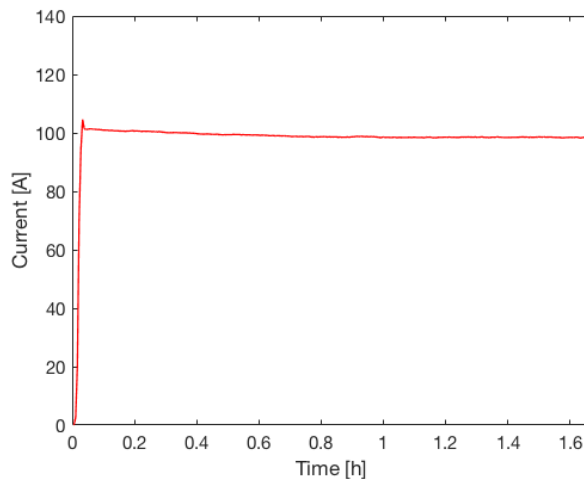


Figure 6.1: The current pattern for Test 1 performed in experimental methodology.

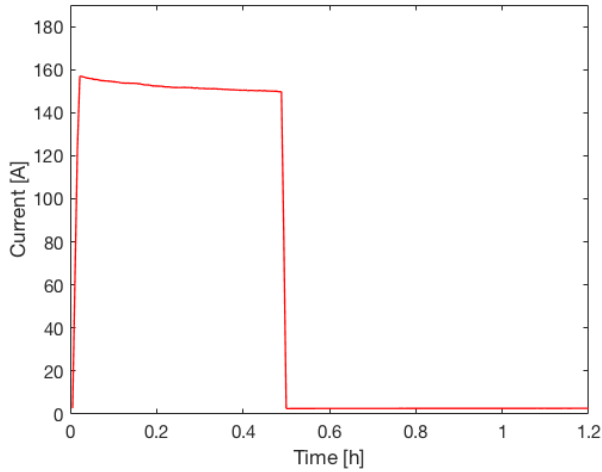


Figure 6.2: The current pattern for Test 2 performed in experimental methodology.

Section 6.2.1 and 6.2.2 are presenting the results from Test 1 and Test 2, respectively. In the following subsections, the results are presented as four results together in grid-formation, revealing results from the positions in the laboratory setup. This presentation aims to display the results in a way that makes it easy to compare the different positions with each other. However, for larger scaled figures, it is referred to Figure 9.3-9.26 in Appendix E. Additionally, note that the surface temperatures measured only are used to predict the ambient temperature for the calculation method.

6.2.1 Test 1: 100 A current increase

Figure 6.1 presents the current step that was applied for 1.6 hours for Test 1. As the figure reveals, the load is switched on at $t=0$ and not switched off until the test is completed. Figure 6.3 shows an overview of results obtained from Position 1 – 4 discovered from the current applied.

A positive correlation was found between the two positions located in free air: Position 2 and 3. As the two positions have equally laying conditions, it is to expect the results to be approximately similar. As the figures reveal, the transient temperature rise for both conductor and sheath layers for the two positions seems to match each-other well as they both are approaching a steady-state temperature of 26.2 °C. Similarly, the sheath temperatures approach the same temperature of

24.8 °C for both cable installations in free air. The surface temperatures are approximately equal as well, as they roughly approach 24 – 25 °C. Additionally, the shape of the transient temperature responses for all measuring points turns out to have similar forms of when the cable temperature rises and becomes stable.

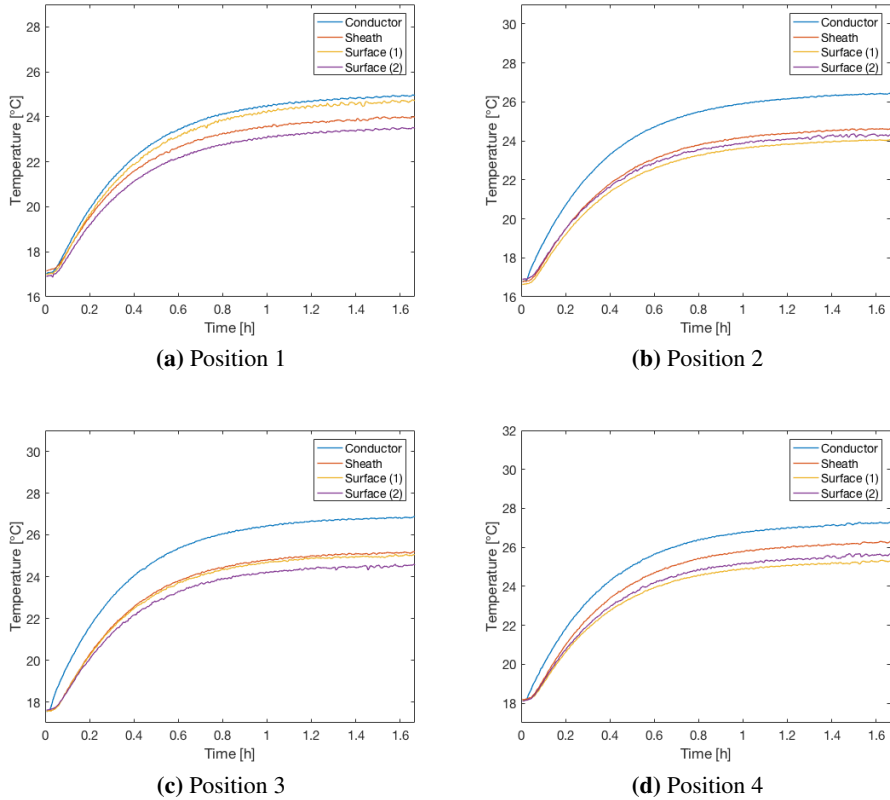


Figure 6.3: Temperature responses for the four measurements applying a current of 100 A for Position 1 – 4.

For Position 2 and 3, the temperature of the sheath layer and one of the surface measurements are very similar. The similarity may be a consequence of the thin thickness of the insulation or due to the effective heat transfer mechanism present for the cable installation in free air. It can also indicate an error for the placement of the thermocouples measuring one of the surface temperatures.

Position 1 reveals a rather surprising outcome when it comes to the sheath temperature rise. While Position 2 – 4 has sheath temperatures that are higher than the surface temperatures, Position 1 shows that one of the detected surface temperatures is higher than the sheath temperature. This may indicate an error for the placement of the thermocouples of either sheath or surface measurements for Position 1. The possible error found for Position 1 leads to a significant difference for Position 1 and 4 with identical laying conditions, which makes it challenging to conclude yet whether or not the measurements are precise as we are not able to verify the results. However, Position 4 is showing a result that is correct when it comes to the order of the temperatures for different layers, which may indicate that Position 4 is the most accurate one.

Due to a somewhat slower heat transfer of the cable placed on the floor compared to the cable located in free air, the steady-state temperatures of the different layers in Position 4 are slightly higher than the same layers for Position 2 and 3.

Another observation is that the starting temperature of Position 1 and 2 are slightly different from what is seen in Position 3 and 4. The difference observed probably relates to the location along the cable route rather than the laying condition. A reason for the difference may be that Position 3 and 4 is closer to the computer logging the temperature and the current load, which may emit heat both from the computer and the computer charger.

6.2.2 Test 2: A current step of 150 A

Figure 6.2 shows the step current that was applied for Test 2. As the figure reveals, a current of 150 A was applied at time $t = 0$ and switched off after 0.5 hours. Figure 6.4 shows the results when applying the step current of 150 A for the four positions.

Similar to Test 1, Figure 6.4a reveals that one of the surface temperature measurements is as high as the conductor temperature, which is unlikely to be correct. Besides, the abnormally high surface temperature indicated 'Surface (1)' seems to fluctuate during the cooling process from 0.8 – 1.2 hours, which also indicates that an error is present in the laboratory setup. The positions investigating the cable located in free air shown in Figure 6.4b-6.4c displays that the measurements are approximately equal, as expected.

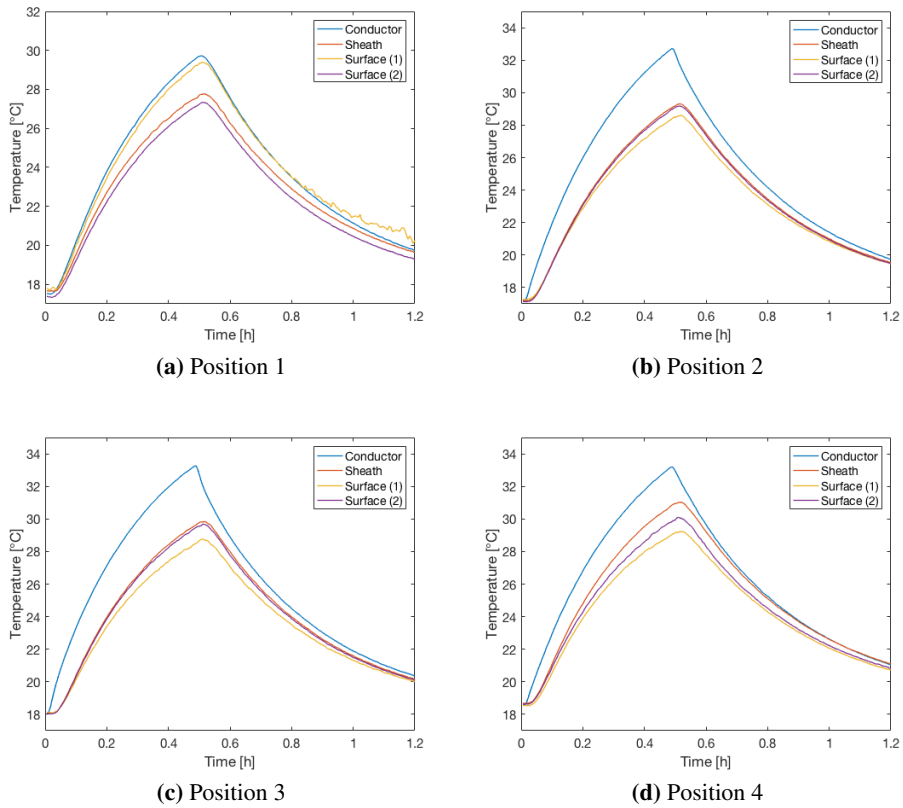


Figure 6.4: Temperatures for the four measurements applying a step current of 150 A for Position 1 - 4.

The current is switched off after 0.5 hours. The first observation is that the conductor temperature is decreasing fast just after the current is off, and has a relatively steep temperature fall for the first half-hour after the switch. The sheath temperature has a relatively steep temperature fall as well, indicating that the insulation of the cable installation is narrow.

The surface temperature indicated 'Surface(2)' is almost similar to the sheath temperature for Position 2 and 3, which was the case in Test 1 as well; however, a greater similarity is observed for Test 2. One possible reason for this result may be that there has been applied a higher current load for the second test, which means that the cable experiences a larger temperature difference. Because of the small thickness between the sheath and surface layer, this can lead to a greater and faster

heat transfer between the layers.

For the cable on the floor in Figure 6.4d, the conductor temperature and the sheath temperature are approaching the same value after a short time. For the cables in free air displayed in Figure 6.4b-6.4c, the conductor temperature and sheath temperature uses slightly longer time to reach the equal temperature, which can be explained by the fact that there is a more considerable gap between the two heats at the vertex.

6.3 Verification of calculation methodology through comparison with experimental methodology

The calculation method and the experimental method are comparable as both methods determine the temperature response at the conductor and sheath layer. By performing a comparison, one can decide whether the simulation can be used for further temperature analysis and identifying the weaknesses so that these are known when completing the calculations. The comparison is made for both Test 1 and Test 2 consisting results introduced respectively in Section 6.2.1 and Section 6.2.2. The simulation in MATLAB for the tests is presented in Appendix H.

6.3.1 Comparison of Test 1 from the experiment with the calculation methodology

Conductor temperature

The results obtained from the conductor temperature is shown in Figure 6.5. Figure 6.5a confirms the suspicion of an error in the conductor temperature measurements for Position 1. The correlation between the simulated model and the experimental methodology is different for Position 1 than for the other positions, while the calculation methodology remains the same for all the positions. There can be different reasons for the error observed for Position 1. Most likely, it is a logical error, such as faults due to the sensors and connections. These errors may, for instance, arise due to incorrect positioning of the sensors, calibration of amplifier inputs, or other factors that one initially thought were insignificant when establishing the set up that nevertheless turned out to be significant. These faults could probably be detected and fixed under normal circumstances; however, due to the situation of Covid-19, there were not given priority to study and detect these faults.

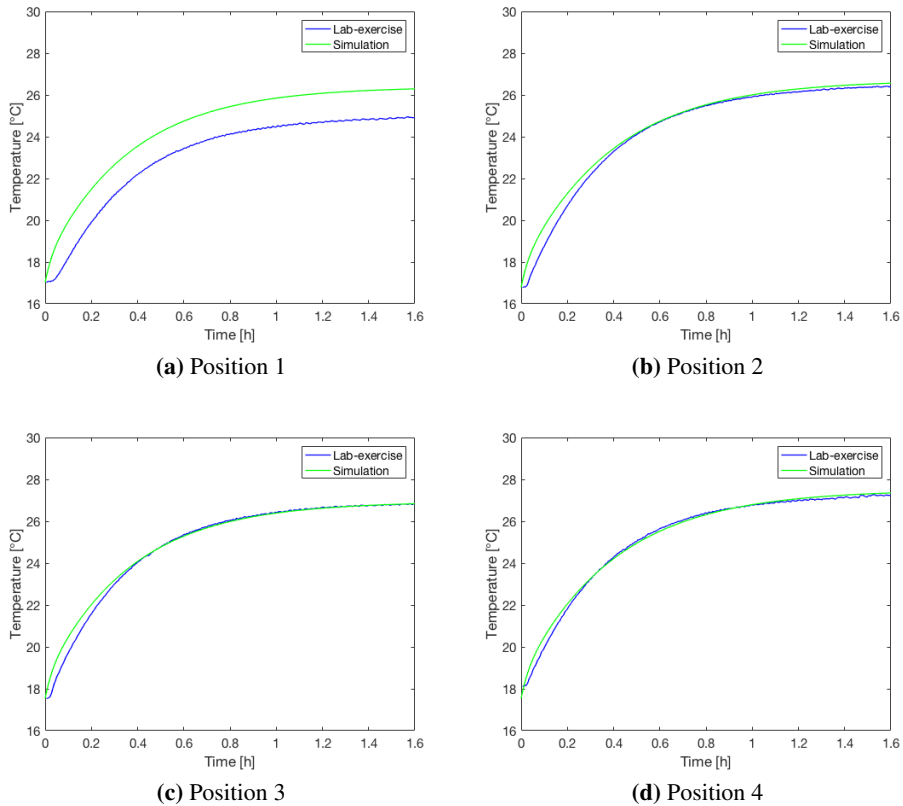


Figure 6.5: Comparison between conductor temperature obtained from laboratory setup and simulation provided in MATLAB for the four positions with an applied current of 100 A.

For the three remaining positions (2,3 and 4) that can be seen in Figures 6.5b-6.5d, on the other hand, the results are comparable. At first glance, the simulation and lab-exercise give remarkably similar results. However, by studying the results more closely, some weaknesses can be observed that are relevant to highlight.

One observation is that the simulation has a steeper growth at the beginning of the graphs than the results from the lab-exercise reveals. This is illustrated in Figure 6.6 by investigating Position 2. By comparing the slope of the graphs, ratio $a = dy/dx$ can be used as a reference.

6.3 Verification of calculation methodology through comparison with experimental methodology

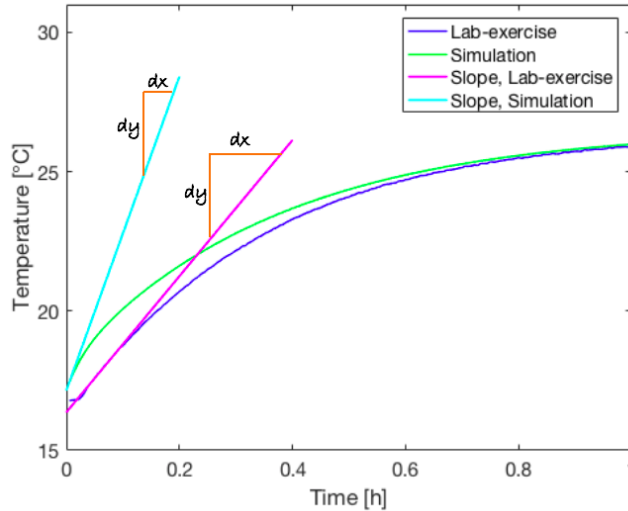


Figure 6.6: Comparison of conductor temperature in Position 2 for lab-exercise and simulation with corresponding slopes illustrating the steep of the starting temperature.

Table 6.6 exhibits the result determining the relationship of $a = dy/dx$ for Position 2, 3 and 4. The simulation for Position 4 reveals the most accurate calculations, while the difference of the ratios for Position 2 and 3 are approximately similar. Thus, the cable installation in free air turns out to be most accurate regarding the temperature rise for the first hour of current applied to the system.

Table 6.6: Comparison of the ratio dy/dx for conductor temperature simulation and lab-exercise for Position 2-4.

Position	dy/dx , simulation	dy/dx , lab-exercise	Difference
2	30	15	15
3	30	16	14
4	24	26	2

To study the temperature rise when approaching steady-state, Figure 6.7 shows the result when zooming in the temperatures from 1.5 – 1.6 hours.

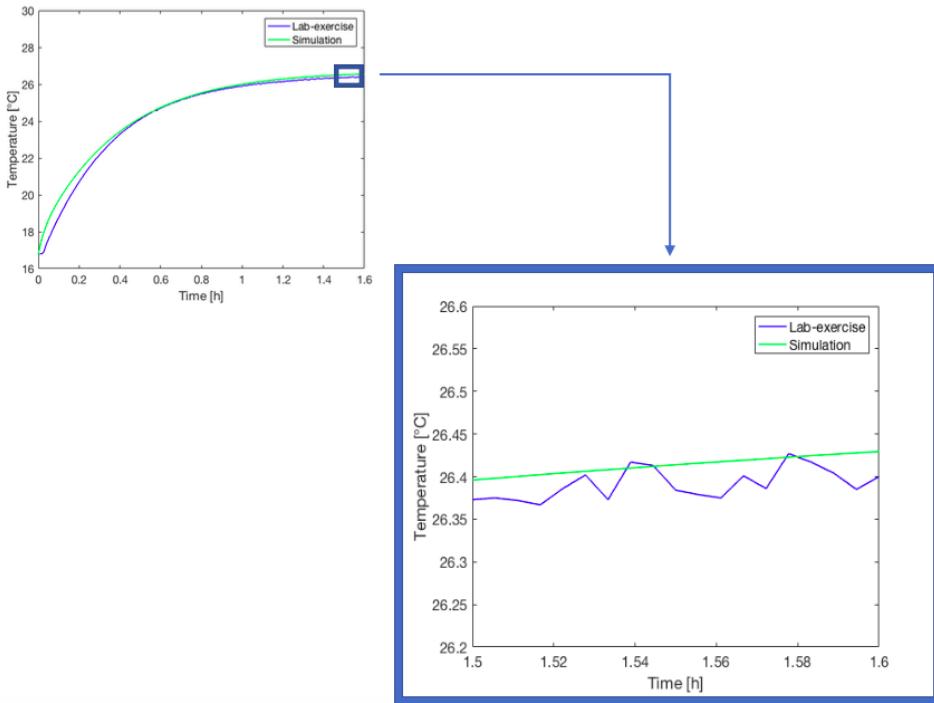


Figure 6.7: Zoomed in figure of the conductor temperature for Position 2 showing only the time span of 1.5 – 1.6 hours.

Figure 6.7 reveals that after merely 0.5 hours the graphs seems to be very similar. As can be seen, the simulation produces temperature results that are only 0.025 – 0.05 °C from the results obtained from lab-exercise. Additionally, the results for Position 3 and 4 revealed a difference of only 0.025–0.05 °C. Thus, the simulation code provided is sufficiently good to give an accurate result of the temperature approaching steady-state.

Sheath temperature

The results obtained for the sheath-temperature are summarised in Figure 6.8.

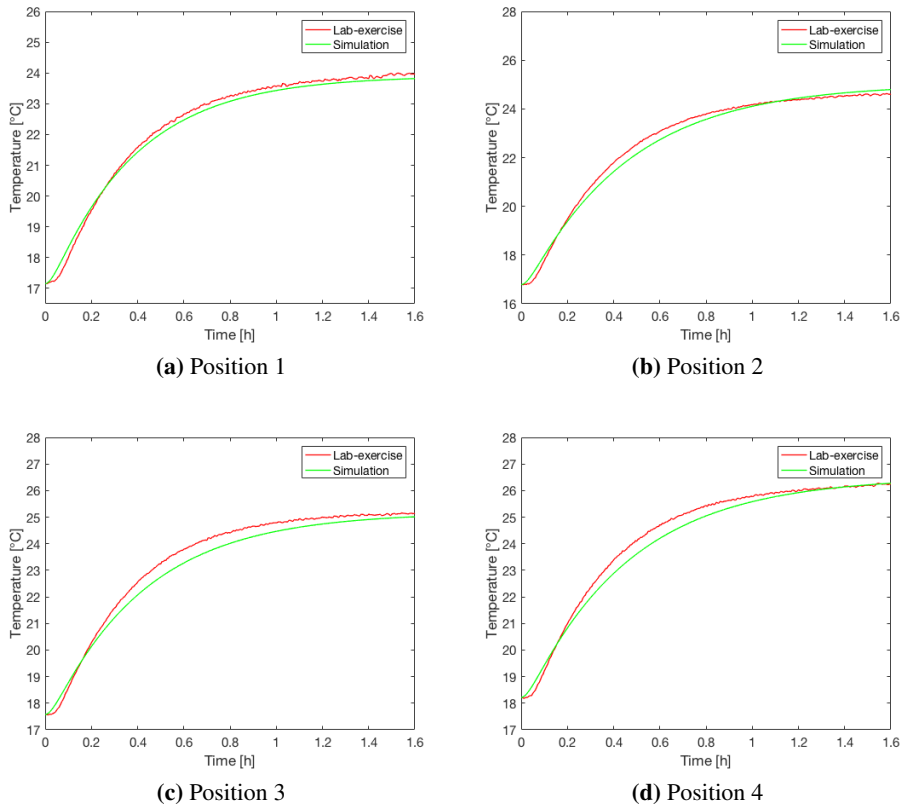


Figure 6.8: Comparison between sheath temperature obtained from laboratory setup and simulation provided in MATLAB for all four positions with an applied current of 100 A.

Unlike the conductor temperature measurements, Position 1 seems to be proper for the sheath measurement. Hence, the error is present for the thermocouples measuring the conductor temperature at Position 1 while the measurements for sheath temperature appears to be correct. Furthermore, the simulation provides a good estimate of the temperature response that is measured from the laboratory setup. Table 6.7 shows the ratio $a = dy/dx$ for the sheath temperature. The table tells that regarding the first period of the current applied, Position 1 and 4 reveals the

smallest difference of the slope at the start of the testing period. From this, one can see that the simulation for cable installations in the air is slightly more uncertain for sheath temperature calculations than the cables attached to the floor.

One observation from the figures is that the cable installation located in air (Position 2 and 3) has a somewhat lower temperature than for the cable installation placed on the floor. This result is as expected because heat dissipation for cables on the floor is more difficult than the cable located in free air.

Table 6.7: Comparison of the ratio dy/dx for sheath temperature simulation and lab-exercise for Position 1 – 4.

Position	dy/dx , simulation	dy/dx , lab-exercise	Difference
1	14.3	15.1	0.8
2	13.2	16	2.8
3	13.3	16.7	3.4
4	14.5	15.9	1.4

Additionally, Figure 6.9 shows that the simulation and results from the lab correspond well when approaching a steady-state. The sheath temperature from the simulation turns out to vary with only 0.1–0.15 °C compared to the experiment.

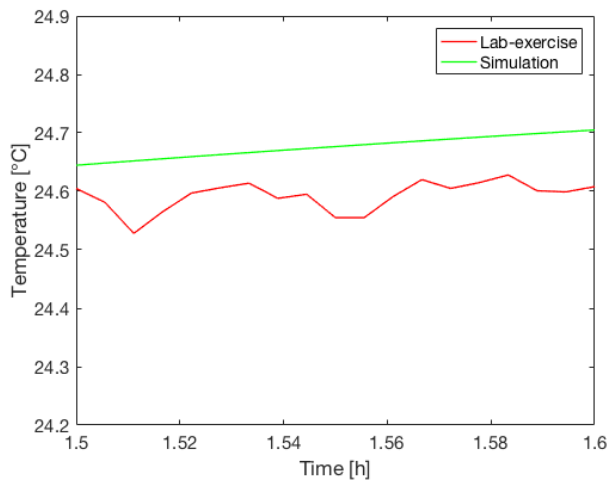


Figure 6.9: Zoomed in figure of the sheath temperature for Position 2 showing only the time span of 1.5 – 1.6 hours.

6.3.2 Comparison of Test 2 from the experiment with the calculation methodology

Conductor temperature

The results from the comparison between simulation and the experiment are shown in Figure 6.10.

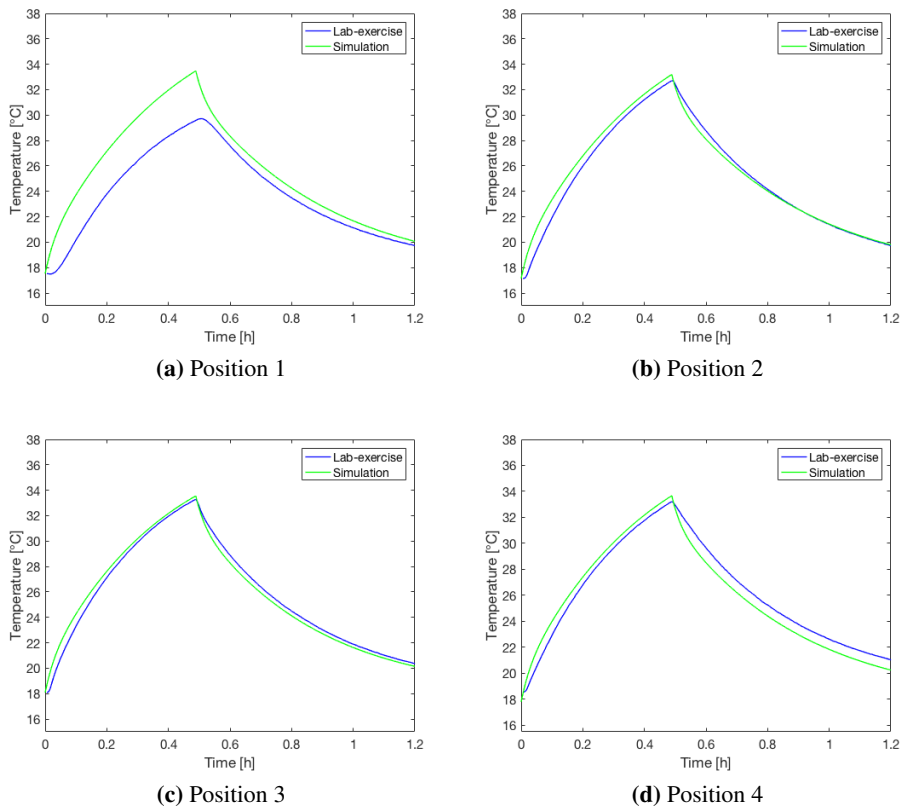


Figure 6.10: Comparison between conductor temperature obtained from laboratory setup and simulation provided in MATLAB for the four positions with an applied step current of 150 A.

The focus for the following comparison is Position 2–4. The reasoning completed for Test 1 is still valid for the temperature rises for Position 2 – 4 until the load is turned off after 0.5 hours. Because of this, the main focus in this section is to

study the cable installation in the cooling process.

Figure 6.11 illustrates the difference comparing Position 2 located in free air and Position 4 placed on floor by zooming in the results between 1.15 – 1.2 hours time span. The cooling effect as a result of a switched off current resembles to be better fitted regarding the cable located in free air. The calculations that include heat transfer phenomena for cable installations in free air is known to be complex due to the incorporation of several uncertain parameters concerning the process [4]. Among the heat energy balance equations required for such calculations, the heat transfer coefficient at the cable surface is considered as the most unpredictable element in light of influence from air velocity, ambient temperature, and flow angle of the air.

One reason for the error displayed in Figure 6.11b can be that the chosen method does not take into account the medium of the floor. Furthermore, the cable was not clipped to the floor, so it cannot be guaranteed that the cable was touching the floor the entire time of the experiment.

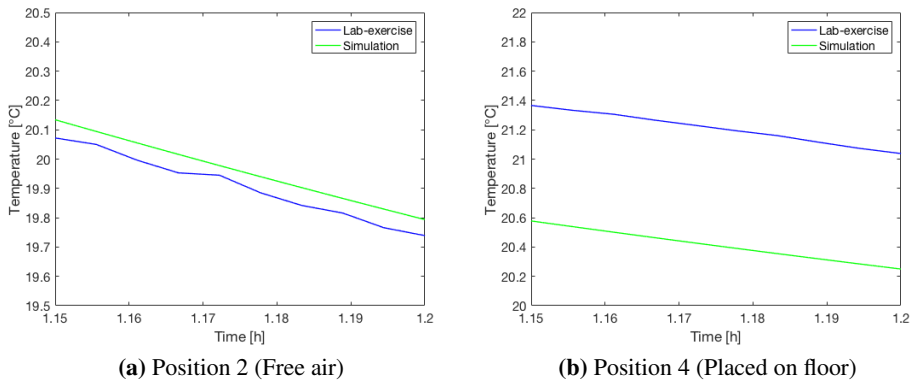


Figure 6.11: Comparison between the conductor temperature simulated and the one obtained from lab-experiment.

Sheath temperature

Figure 6.12 compares an overview of the simulation and the experiment for the sheath temperature calculations.

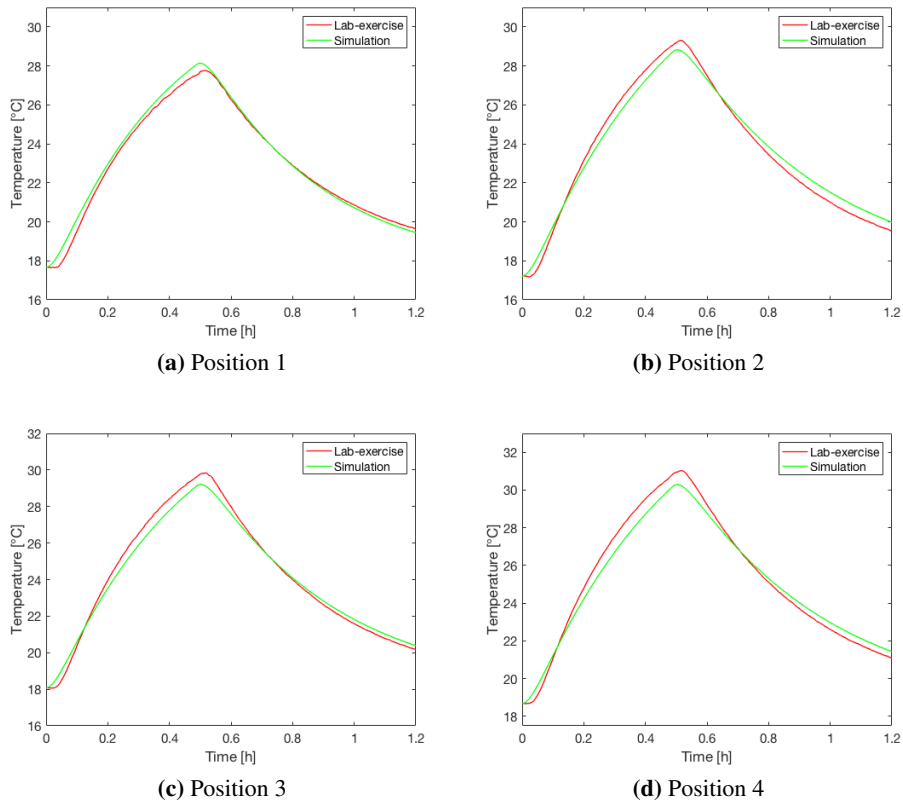


Figure 6.12: Comparison between sheath temperature obtained from laboratory setup and simulation provided in MATLAB for the four positions with an applied step current of 150 A.

A slight difference can be spotted comparing Position 1 to the other positions as Position 1 is the only position where the simulation has a higher vertex than the results from the experiment. This may be due to small errors in thermocouples placement for Position 1, or only due to a natural deviation present.

Investigating the point where the current goes off, the simulation provides results

somewhat lower than experiment results for Position 2 – 4. One possible reason for this discrepancy is that the current applied is slightly higher at the start of the test. As Figure 6.2 indicates, the current appears to have a minor decrease in the period of 0 to 0.5 hours. However, the simulation turns out to be accurate and thus suitable comparing them to the experiment results. The cooling process simulated from time $t = 0.5$ hours provides reassuring precise results to indicate the temperature response.

6.4 Studying the effect of superposition principle considering the cable installation from laboratory setup

As Section 6.3 verified the simulation for currents loads of 100 A and 150 A, this section will take a look at several higher current loads applied including studying the effect of the superposition principle. According to the previous sections, the cable was not approaching the maximum allowed conductor temperature, and therefore the cable is considered to be underutilized.

For XLPE cables as focused on in this thesis, the thermal limit of the conductor is set to 90 °C under normal operation, 105 °C for emergency loading during, for instance, a fault in the grid and 250 °C for short circuits [3]. Table 6.8 presents the overview of these three operation types including an explanation of the operation.

Table 6.8: Overview of type of operation with maximum permissible conductor temperature including an explanation of the operation [3].

	Max permissible cond. temp. [°C]	Comment
Normal operation	90	Can be maintained through a given period of time everyday or continuously, without effecting the operation
Emergency operation	105	Can be maintained for a short period of time under the condition of system breakdown or under state of excessively loaded operation, without causing a defect
Short circuit	250	Causes no defect of the cable when an irregular current flows for short time due to shorting or earthing

6.4 Studying the effect of superposition principle considering the cable installation from laboratory setup

The first simulation conducted in this section is considering the cable located in free air attached to the floor and is shown in Figure 6.13. In this case, several current loads are applied to the cable system every second hour as described in Table 6.9. The highest current reached is 300 A as a consequence of several currents applied. The ambient temperature is 17 °C.

Table 6.9: Overview of current applied and time of current changed investigating the principle of superposition.

Current [A]	150	300	200	300	150	0
Time elapsed from $t = 0$ [h]	0	2	4	6	8	10

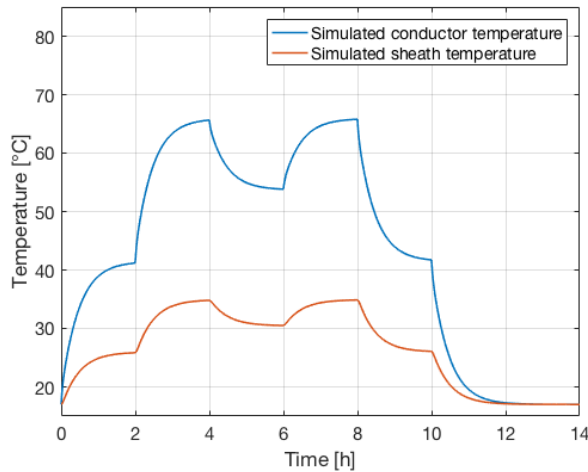


Figure 6.13: Several current loads applied every second hour to the cable located in free air.

One remark from the above figure is that the conductor and sheath temperatures approach steady-state after 2 hours as the curves are leveled off at this point. When the difference between the sheath temperature and the conductor temperature is stable, the sheath temperature can be used to predict the conductor temperature. For the above example, the relationship becomes stable after approximately 1.75 hours. In a practical situation, this result may be helpful for the system owners as they have the opportunity to predict the conductor temperature from the known sheath temperature (for instance, logged with a DTS-system) after the current has been applied for 1.75 hours.

One interesting finding is that the highest conductor temperature in Figure 6.13 reaches about 65 °C. It is therefore clear that the situation in Figure 6.13 does not reach the maximum allowed temperature of such installation for any of the three operations. Further, the sheath temperature approaches 35 °C at the maximum point of applying a current load of 300 A.

Moreover, Figure 6.14 studies the same current applied as in Table 6.9, however with the current applied every hour instead of every two hour. In this case, the temperature will not have reached a steady-state before a current change is applied.

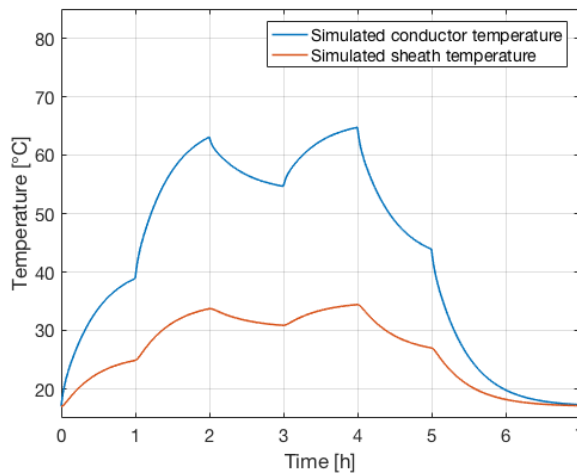


Figure 6.14: Several current load applied every hour to the cable in free air.

As the above figure indicates, the maximum conductor temperature is slightly lower than the one observed for Figure 6.13, which was expected as the temperature did not reach its maximum value before the current change. The time of one hour between the changes in Figure 6.14 additionally shows that the correlation between the sheath and conductor does not reach a stable relationship before it is changed. This result highlights the importance of accurate transient temperature analysis when the current changes rapidly.

Aiming to study the superposition principle on a more complex example, Table 6.10 shows a situation where the current is changed 10 times during a short time period. The result of utilizing the simulation code is shown in Figure 6.15.

6.4 Studying the effect of superposition principle considering the cable installation from laboratory setup

Table 6.10: Overview of current applied and time of current changed in a short time period.

Current [A]	100	50	250	350	250	400	500	400	300	200
Time elapsed from $t = 0$ [h]	0	1	2	4	4.5	6	7	10	10.5	12

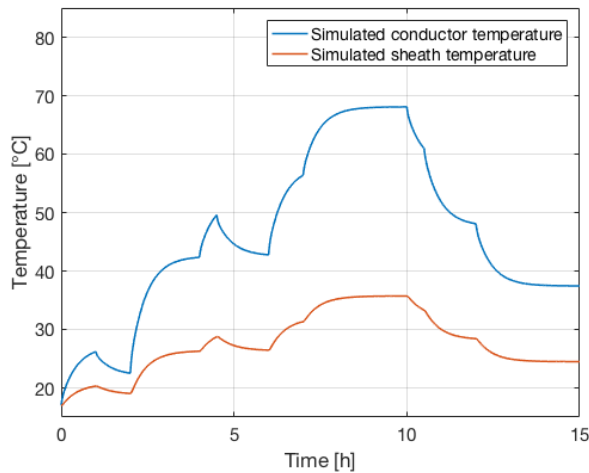


Figure 6.15: Conductor and sheath temperature of a complex example consisting of several different current changes during a short time period.

Studying Figure 6.15 reveals that although the maximum current reaches a value of 500 A, the maximum conductor temperature is not reaching more than almost 70°C. Applying a single current of 500 A, on the other hand, would, according to the simulation, reach a maximum conductor temperature of 165°C, and a maximum sheath temperature of 73°C. Thus, this implies that several of the current increases described in Table 6.10 do not result in a maximum temperature rise before the next current increase is applied. This result emphasizes the effect of superposition that applies to such situations in the power grid. Because of this, the example above also shows the importance of transient temperature calculations during short periods of current loads used.

6.5 Overloading case example of cable installation from laboratory setup

This section provides a study of overloading the cable installation in the experimental methodology, including analyzing how long time the overloading can take place. The cable installation is assumed to be attached to the floor with air as the surrounding medium.

For the chosen cable installation used in the laboratory setup, the permissible load in air at 25°C for a flat laying condition are 225 A [44]. These parameters were used for the simulation code to verify the maximum permissible load of this cable installation. The result are shown in Figure 6.16.

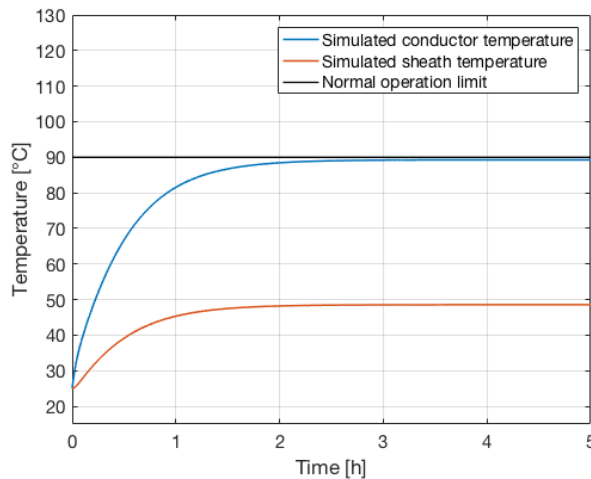


Figure 6.16: Simulated conductor and sheath temperature in order to verify the permissible load of the cable system.

The result found from the simulation confirms the maximum permissible conductor temperature of 25°C with a current load of 225 A, and are considered as a highly positive result that verifies the accuracy of the calculation methodology. The results from the overloading case example is presented in Table 6.11, considering an ambient temperature of 25°C as well.

Table 6.11: Results from overloading the cable installation from experimental methodology in air.

Applied current [A]	Time to reach 90°C [h]	Time to reach 105°C [h]
230	1.40	-
250	0.75	1.25
270	0.50	0.70
290	0.40	0.50
310	0.25	0.30

Although the maximum permissible load for this cable is 225 A, the result from Table 6.11 tells that the cable can handle higher loads for several minutes or hours without exceeding the thermal limit. According to the simulation, the power cable can handle a load of 230 A for 1 hour and 24 minutes under normal operation and with no time limit considering emergency operations. Furthermore, a current load of 310 is handled for 15 minutes during normal operation and 18 minutes during emergency operation. The results show that the faster it takes for the cable to reach the thermal limits, the steeper the temperature growth is, which means that the time to reach respectively 90°C and 105°C is approaching the same value. Having the ability to overload the cable for some time can contribute to better utilization of the cable capacity for the system owners.

6.6 Load history impact on power cable systems in air

In order to study the effect of load history, a test was performed aiming to determine how much time the temperature needs to reach ambient temperature after the current goes to 0 A. The test was conducted with an ambient temperature of 17 °C. Table 6.12 shows the results from this test.

Note that the results in Table 6.12 are considering that the ambient temperature are reached with a margin of 0.05 °C. As the table indicates, the conductor and sheath temperature needs more time to reach ambient temperature, the higher the current is. According to the simulation, the conductor needs 2 hours and 20 minutes to reach the reference temperature when the current applied is 100 A. The sheath temperature only needs 1 hour and 57 minutes before it reaches ambient temperature. This comparison presents a difference of 23 minutes between conductor and sheath temperature approaching ambient temperature. Additionally,

current loads of 150 A and 200 A have a difference of 22 – 23 minutes between the conductor and sheath temperature. When the current load applied is 250 A, on the contrary, the difference is found to be 36.

Table 6.12: Time for conductor and sheath to reach ambient temperature after the current is switched to 0 A. Assuming temperature margin of 0.05 °C.

Current [A]	Steady state conductor temp. [°C]	Time to reach ambient temp. after switching the current to 0 A [h]	
		Conductor	Sheath
100	27	2.34	1.96
150	42	2.74	2.37
200	65	3.09	2.70
250	102	3.41	3.01

If the margin set for the test in Table 6.12 of 0.05 °C is changed to 0.01 °C, longer times to reach ambient temperature are found for the conductor. However, the time for the sheath temperature to reach ambient temperature is equal to the discussion above. For the conductor temperature considering a temperature margin of 0.01 °C, the results in Table 6.13 are valid.

Table 6.13: Time for conductor to reach ambient temperature after the current is switched to 0 A. Assuming temperature margin of 0.01 °C.

Current applied [A]	Time to reach conductor steady state temp. [h]
100	3.05
150	3.46
200	3.80
250	4.12

The above table indicates that for all the different currents loads (100 A, 150 A, 200 A and 250 A), the conductor needs 43 – 44 minutes more before it has reached ambient temperature if considering a temperature margin of 0.01 °C instead of 0.05

°C. This result shows that although the conductor temperature falls relatively fast when the current is switched off, the temperature needs a long time before actually reaching the temperature reference. The results reveal that the cable in free air will need about 3 hours when the current load applied is 100 A before the load history does not longer affect the temperature measurements. For the current applied of 250 A for such cable installation, the cable will be affected by the load history for shortly 4 hours.

Chapter 7

Case-Study Utilizing Data Provided by Statnett

This chapter utilizes data provided by Statnett in order to complete a practical example of using the calculation methodology that was established in Chapter 4. A visit to Statnett in Oslo was arranged at the end of February 2020 as a part of the study. The visit included a trip to observe the sub-sea cable installation that runs from Brenntangen to Solbergstøa, which are the relevant route investigated in this chapter. The visit aimed to visualize the power cable relevant.

This chapter consists of a general explanation of the cable installation, followed by a comparison between the calculation method simulating the sheath temperature and the logged sheath temperature. This is done to verify the calculation for a high-voltage cable installation. Moreover, a case-study has been completed, including the following four cases aiming to predict the conductor temperature:

1. Temperature rise due to one current increase
2. Temperature response due to several current changes discussing the effect of the superposition principle
3. Overloading example of the cable installation
4. Seasonal changes impact on conductor temperature response

The sub-sea cable relevant proved to undergo most variations as well as being most prone to changes in ambient temperature on the distances located on land. Hence this chapter is focusing on calculating the temperatures at the land area.

7.1 General explanation of the cable installation

The cable used for the study is a real cable installation owned by Statnett that runs from Brenntangen to Solbergstøa, crossing the Oslofjord's. The cable studied has an installed DTS system that provides data regarding the sheath temperature. Additionally, the load is measured. The sheath temperature and loads are logged for the year 2019.

Detailed information on the cable installation is not provided in this thesis as it is confidential data. However, a simplified illustration of the cable installation studied can be seen in Figure 7.1. Fiber optic sensors are installed between the inner semiconducting sheath and the cable bedding in order to measure the sheath temperature. The cable installation from Brenntangen to Solbergstøa consists of a total of seven parallel cables. However, this thesis focuses on one cable installation and is not considering the impact of the neighboring cables.

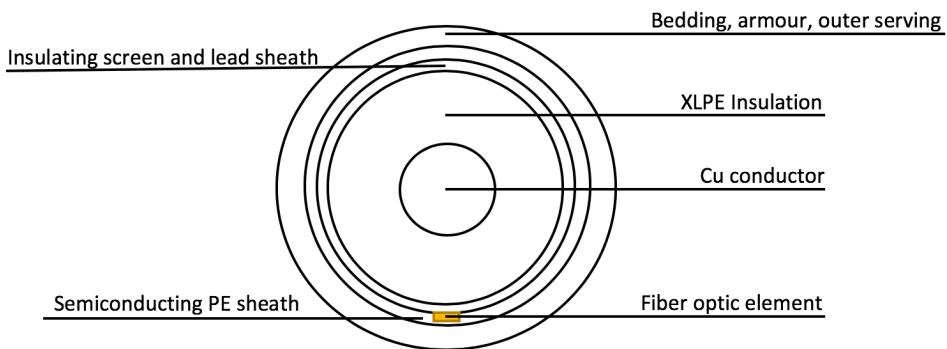


Figure 7.1: Simplified illustration of cable construction. Not drawn to scale.

The cables are transformed from overhead power lines to high voltage power cables at Brenntangen, as can be seen in Figure 7.2 that shows a picture taken during the visit. After the transition, the cables are entering a culvert that is eventually leading the cable to the sea.

In order to compare the calculation and the data received from Statnett, some assumptions and simplifications are made. The assumptions involve adding layers in the complex cable system and hence consider the layers with equal thermal resistances. The added layers are illustrated in Figure 7.1. For instance, such sim-

plification is done for the insulating screen and the lead sheath. The simplifications may lead to somewhat uncertain parameters with a present error rate. However, the use of IEC standards for the simulation would be too complex with the including of several changes in thermal resistance in the outer layers of the cable installation.



Figure 7.2: Transition between the overhead power lines and the cables that are entering the culverts.

7.1.1 Laying conditions

When the cable installation transforms from the overhead line to power cable installation, the cable runs into a culvert that is leading the cable into the sea. When the cable is reaching Solbersøra, it is entering a culvert, just like the one at Brenntangen. Earlier studies have shown that the bottleneck of such installation is, in most cases, found before the cable enters the sea. The reason for this is that when the cable is undersea, it holds a relatively stable temperature.

Figure 7.3 shows the plot of the average, maximum and minimum temperature of the cable installation from Brenntangen to Solbergstøa for May 2019. As can be seen, the temperature is relatively stable when located below the sea (from

1000 – 2500 meters). The temperature found before and after the cable is located in the sea, on the other hand, varies more. Figure 7.4 shows the standard deviation of maximum and minimum temperature, which also confirms the location of the bottleneck. Thus, the interesting study is the cable installation in free air and in the culvert.

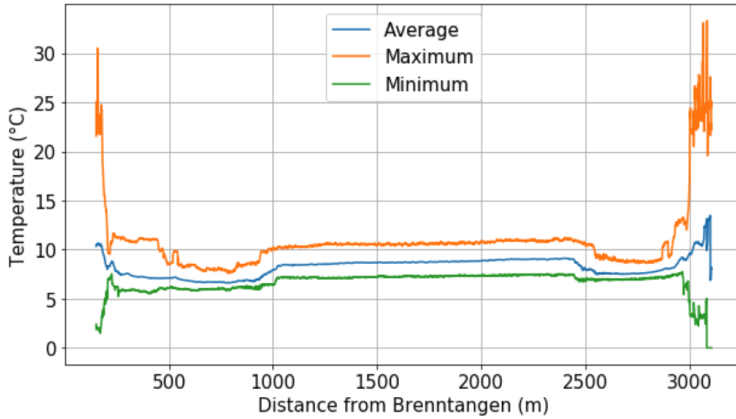


Figure 7.3: Average, maximum and minimum sheath temperature of the cable route from Brenntangen to Solbergstøa.

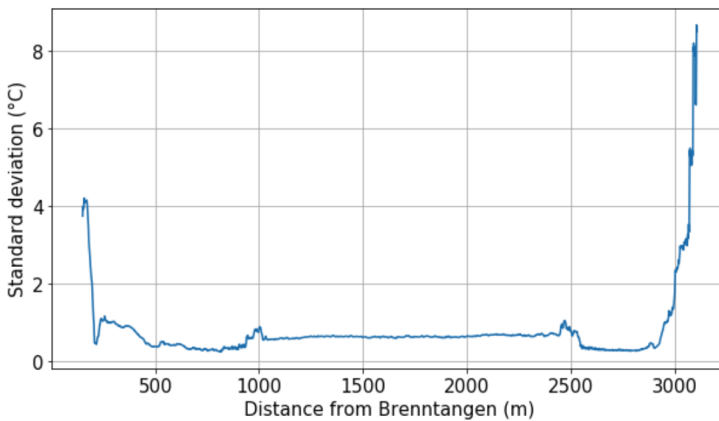


Figure 7.4: Standard deviation of maximum and minimum temperature difference on the route from Brenntangen to Solbergstøa.

7.1.2 Method for measuring values

In order to accomplish a comparison, data gathering of respectively load and temperature was needed from Statnett.

The temperature-data is detected by a fiber-optic (FO) sensor installed under the jacket of the cable, at the outer sheath layer, which is shown in Figure 7.1. The FO sensor is measuring and logging the temperature for every half meter of the cable route. Before the FO sensor cable is entering the high voltage cable carrying the current, it is coiled up on the wall of the culvert inlet. The FO logged temperature at that location is used as the ambient temperature. However, one should notice that this ambient temperature is valid for calculations of the cable located at the start of the culvert. Thus, calculations of the culvert cable assume a somewhat different temperature than logged by the FO sensor at the inlet.

The load-data provided consists of information regarding the applicable route, including load data with time and date at the different locations on the whole distance. The load data has been logged every hour for the entire cable installation.

7.2 A comparison between the simulated sheath temperature and the logged sheath temperature

Aiming to compare the result from the simulation with actual logged temperature from Statnett, this section studies a current step. There will be interesting to take a look at a period where the current has been relatively stable for a while before it is increasing considerably. In such a situation, the load history will have the least impact on temperature rises analyzed. Additionally, the case will attempt to look at a period where the ambient temperature is relatively stable.

The current and temperature relationship studied for this section is found in April 2019. The load varying with time for April 2019 is shown in Figure 7.5. Furthermore, Figure 7.6 shows the ambient temperature for the same period. At first sight, the period from April 23rd to April 26th seems like a suitable period for the testing. However, it turned out to be a difficult period to analyze due to the ongoing increase in the ambient temperature, which can be seen in Figure 7.6.

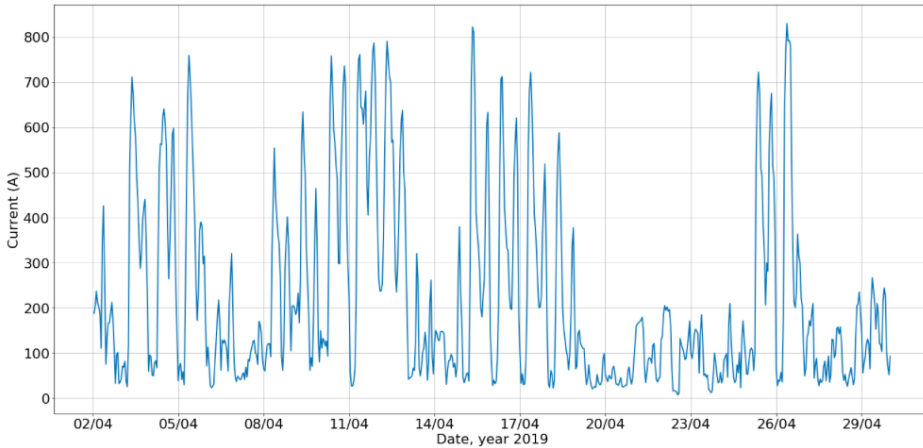


Figure 7.5: Current loads of April 2019

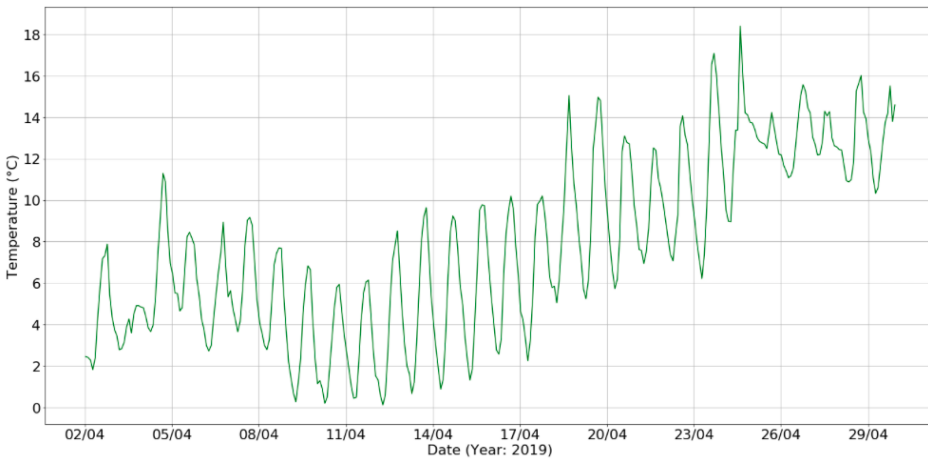


Figure 7.6: Ambient temperature detected by the DTS-system logging the temperature of the FO-cable before entering the HV-cable.

Because the ambient temperature experiences relatively large variations in the previous days before April 23rd, the cable is more complicated to study. Nevertheless, Figure 7.5 and 7.6 reveals that the period from April 14th to April 16th is a situation that may be a relevant to study. The period has a low and stable current over several hours before applying a considerably higher load. Besides, this period has a stable ambient temperature concerning both day and night temperatures. From

7.2 A comparison between the simulated sheath temperature and the logged sheath temperature

April 14th to April 16th, the ambient temperature is fluctuating from day till night. An average ambient temperature of 4.9 °C is used when simulating the sheath temperature.

The zoomed-in current load for the chosen period are shown in Figure 7.7. The current step utilized for the simulation assumes as a rectangular-shaped step marked in yellow. The simulation considers no load-history and a stable ambient temperature during the test.

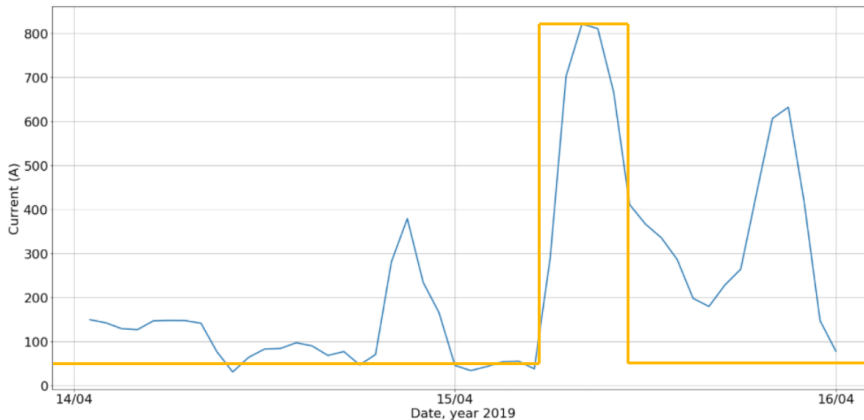


Figure 7.7: Current step logged from April 14th to April 16th.

7.2.1 Cable in free air

This subsection handles the cable installation in free air before entering the culvert. Both simulated and logged sheath temperatures can be seen in Figure 7.8, which shows the comparison between the methods. Figure 7.9 shows the zoomed-in figure for the relevant time span investigated.

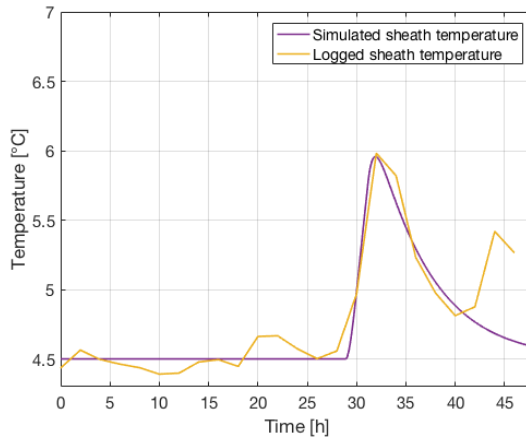


Figure 7.8: Comparison of simulated and logged sheath temperature for cable in free air from April 14th to April 16th.

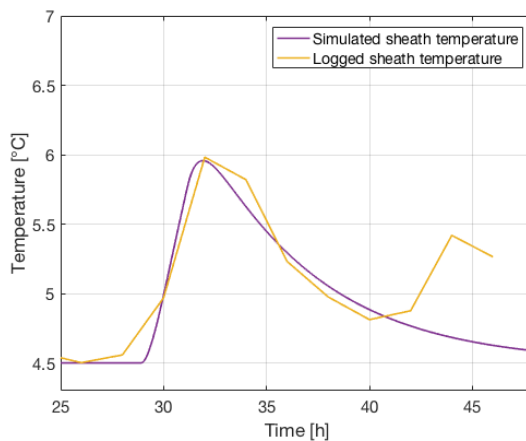


Figure 7.9: Comparison of simulated and logged sheath temperature for cable in free air from April 15th to April 16th.

7.2 A comparison between the simulated sheath temperature and the logged sheath temperature

Figure 7.8 and 7.9 reveals that the simulated sheath correlates with the actual sheath temperature. However, some errors are observed. One reason can be due to significant uncertainties associated with the temperature starting conditions. Besides, the load-history in advance of the tested area is not taken into account, which will impact the sheath temperature, as can be seen from the fluctuating temperature in Figure 7.8 from 0 – 25 hours.

One important factor for the power system owners is to predict the maximum temperature when loads are applied. Comparing the temperatures in Figure 7.8 shows that the maximum temperature only differs with 0.04 °C. The steepness of the curves are relatively correlated; however, some errors are observed for both the heating and cooling processes. Seen from the perspective of power system owners, the course of the temperature rise and temperature drop is not as important as predicting the correct maximum temperature.

7.2.2 Cable in culvert

Figure 7.10 and 7.11 compares the simulated and logged sheath temperature of the situation when the cable has entered the culvert.

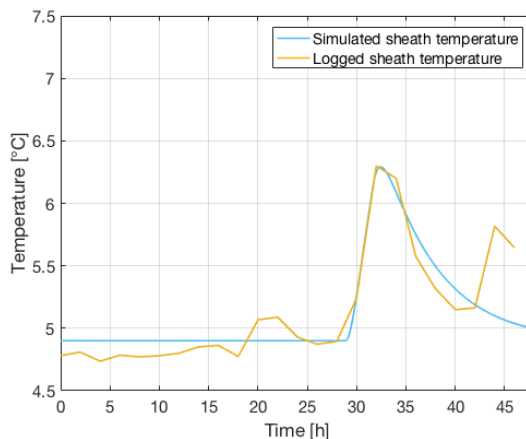


Figure 7.10: Comparison of simulated and logged sheath temperature for cable in free air from April 14th to April 16th.

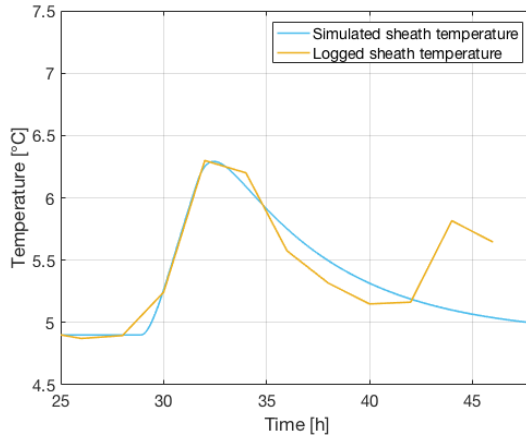


Figure 7.11: Comparison of simulated and logged sheath temperature for cable in free air from April 15th to April 16th.

One observation is that the sheath temperature of the cable in culvert is somewhat higher than the logged sheath temperature in free air seen in Figure 7.8. The discrepancy may be due to higher ambient temperature in the culvert than in free air. This can be a consequence of the heating process that takes place in a culvert with a heating cable.

The maximum temperature in the graph's vertex shows that the simulation is approximately equal to the maximum temperatures, as it only varies with about 0.001 °C. Moreover, the simulated temperature rise has found to be satisfactory alike the actual logged temperature. However, regarding the temperature response due to the current switch-off, the simulation shows a cooling process that is less steep than the logged temperature cooling. One reason for the deviation may be that the parameters that account for the culvert size involve uncertain parameters in the calculations. The calculations are assuming a circular duct or tunnel, but the case of the installation studied is dealing with a rectangular shape. The mathematical calculations thus need to convert an oval duct geometry to an equivalent circular diameter, as explained in Appendix A [45]. This convention is introducing uncertainty, which is not to be avoided.

7.3 Case-study predicting conductor temperatures

The case-study that follows in this section is utilizing the simulation created for cables located in culverts and in free air to estimate the conductor temperature for the cable installation owned by Statnett.

7.3.1 Case 1: Temperature rise due to a current increase

Case 1 determines the temperature response due to the current step that is explained in Section 7.2. By considering an ambient temperature of 10 °C, the conductor temperature and the sheath temperature is simulated for both laying conditions (in free air and culvert) and are shown in Figure 7.12.

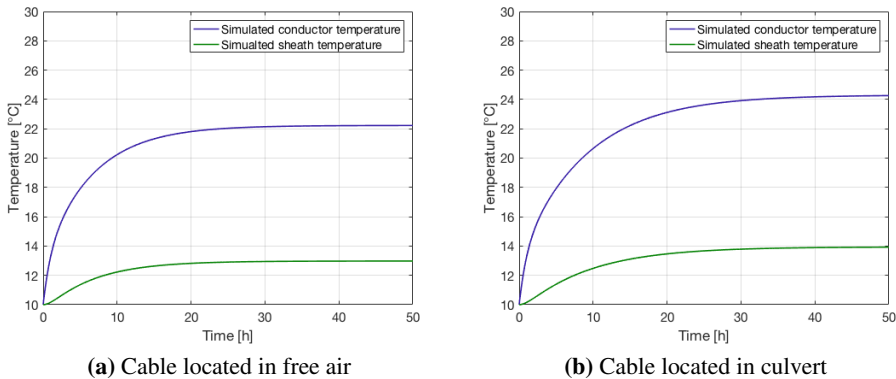


Figure 7.12: Simulated conductor and sheath temperature from April 14th to April 16th applying a current increase of 750 A.

As the above figure reveals, the conductor temperature when applying a current increase of 750 A is approaching the value of 23 °C and 24 °C for respectively the cable in free air and the cable in a culvert. Regarding the sheath temperature, the cable in free air is approaching 13 °C, while the cable in the culvert is reaching 14 °C. These results confirm that the cable located in a culvert has a higher conductor- and sheath temperature due to a less effective cooling in a closed condition. However, in a practical situation, the ambient temperature of a culvert installation can be lower than the ambient temperature of a cable in free air so that the comparison should account for this.

What is surprising from the results is that the simulated conductor temperature is not nearby the maximum temperature that such cable installation can handle. This result thus uncovers that a cable optimization is possible by allowing higher loads applied to the installation for periods.

7.3.2 Case 2: Temperature response due to several current changes discussing the effect of superposition principle

Case 2 aims to investigate the conductor temperature due to several current changes. Figure 7.13 illustrates the logged current from May 23th to May 25th as the basis for Case 2.

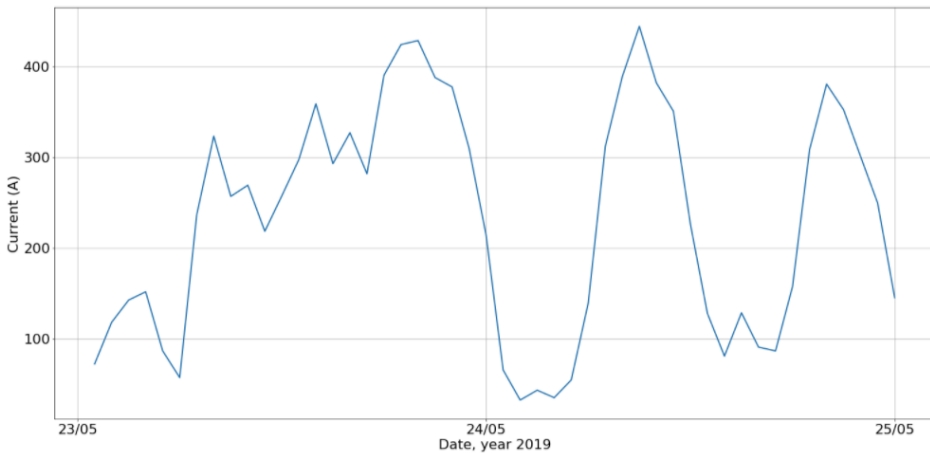


Figure 7.13: Logged current loads from May 23th to May 25th.

In order to simulate the conductor temperature, it is relevant to make an overview showing the current increases and decreases, and at what time the change occurs. This is illustrated in Table 7.1.

Table 7.1: Overview of current applied and time elapsed from 23/05.

Current [A]	0	300	350	420	0	450	100	380	150
Time elapsed [h]	0	10	13	15	20	26	33	41	45

The simulation completed provides the temperature response for both the conductor and the sheath layer. The result is shown in Figure 7.14. As the graphs indicate, the sheath temperature has a minor temperature change when the current shifts rapidly. Additionally, the increasing loads applied appears to result in a continuous growing temperature affected by its history of loads applied. In other words, the results present a clear correlation between load history and temperature response.

What is surprising from the results in Figure 7.14 is that the conductor temperature seems to be considerably small. However, the current is only applied for a minor period before switched off or changed, which means that the temperature does not get time to affect much before the switch-off. As the steepness of the graphs shows, the temperature is far from reaching steady-state temperature. Additionally, the maximum current observed during the days studied in this case was only 450 A, which is notably beneath the maximum current allowed for such cable installations. Consequently, the cable is exposed to minimal stress compared to what it can handle.

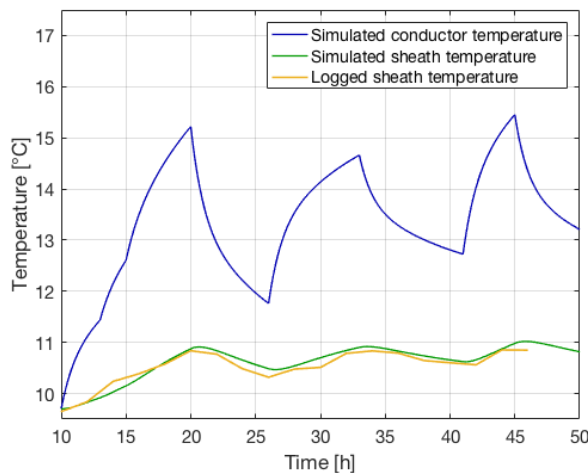


Figure 7.14: Simulated conductor and sheath temperature for the time period from May 23th to May 25th.

In order to analyze the impact of load history, a test was carried out. The test is simulating different cases of loads applied to the system to determine the conductor and sheath temperature, focusing on the cooling effect and the time to reach ambient temperature after a switch-off. Table 7.2 presents the results from the test

where one current increase of 1000 A is applied to the system. Table 7.3 shows the results when applying two individual current increases of 500 A.

Table 7.2: Results for testing the superposition principle through one current increase of 1000 A.

Explanation of current applied	Time to reach ambient temperature after current is switched off [h]
One current of 1000 A switched off after 5 hours	40.44
One current of 1000 A switched off after 15 hours	46.06
One current increase of 1000 A switched off after reaching steady state condition	53.8

Table 7.3: Results for testing the superposition principle through two current increases of 500 A.

Explanation of current applied	Time to reach ambient temperature after current is switched off [h]
Two current increases of 500 A applied every 2.5 hours before switching the current off after 5 hours	30.67
Two current increases of 500 A applied every 7.5 hours before switching the current off after 15 hours	36.99
Two current increases of 500 A where both individual current is applied until steady state reaches steady state condition	53.8

Table 7.2 and 7.3 reveals that applying one current of 1000 A and switching it off after respectively 5 and 15 hours is not comparable to applying two currents of 500 A. The reason why it is not comparable is due to a too small time span for the temperatures to reach a steady state.

Figure 7.15 illustrates the two cases where the current is switched off after 15 hours. While the load of 1000 A in Figure 7.15a reaches a maximum temperature of 22.5 °C, the two individual increases of 500 A merely reaches a maximum temperature of 9.3 °C. Hence, the first increase does not get time to grow enough before a new current is applied. A comparison of the results from Table 7.2 and Ta-

ble 7.3 exposes a difference of approximately 10 hours before reaching steady-state after current switch-off for the situations where steady-state is not reached.

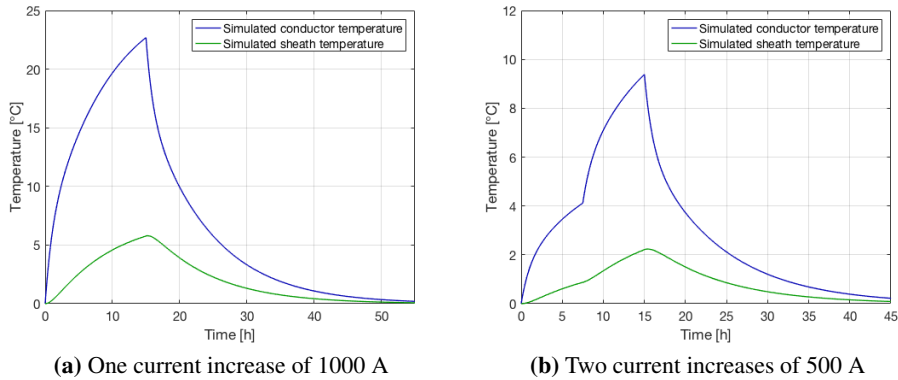


Figure 7.15: Overview of two cases applying where current is switched off after 15 hours.

7.3.3 Case 3: Overloading example of the cable installation

As the previous cases have shown, the conductor temperature is far beneath the maximum permitted temperature of such cable installation. Case 3 is, therefore, analyzing the temperature rise due to an overloaded case to highlight the cable capacity and the situation of an underutilized cable system. Table 6.8 flaunts an overview of the three operation types and their thermal limit valid for this case-study. The ambient temperature considered for the following tests is 10 °C.

Table 7.4 presents an overview of the results that were found when simulating the conductor temperatures for both laying conditions. Figures illustrating the test can be seen in Appendix F. An important observation to emerge from the table was that currents of 2000 A or higher, both laying conditions reach the limits for normal operation and emergency operation at the same time. This is a rather significant outcome as it asserts that the temperature rise is similar for roughly the first 8 – 10 hours from load applied. The table also unveils that the cable located in a culvert can handle a current of 1600 A for the entire 25 hours before reaching the normal operation limit. During emergency operation, no limit was reached. According to the simulation, 1800 A can be handled for 12 hours before reaching 90°C and for 40 hours before reaching 105°C. Moreover, a current of 1600 A can

be applied without reaching the limits for cables in free air. However, the cable in the culvert is reaching the normal operation limit after about 25 hours.

Given the maximum current for April 2019 of 800 A, a current of 2400 A will correspond to a 200 % increase. The study found that the cable can be overloaded this much for 2.5 hours before reaching the normal operation temperature and 3.5 hours before approaching the emergency operation temperature for both laying conditions.

Table 7.4: Overview of applied currents and time before reaching normal operation limit and emergency operation limit for both laying conditions considering ambient temperature of 10 °C.

Current [A]	Cable in free air		Cable in culvert	
	Time to reach 90 °C [h]	Time to reach 105 °C [h]	Time to reach 90 °C [h]	Time to reach 105 °C [h]
1600	-	-	25	-
1800	12	40	10	15
2000	6	8	6	8
2200	4	5	4	5
2400	2.5	3.5	2.5	3.5
2600	2	2.5	2	2.5
2800	1.5	1.9	1.5	1.9
3000	1.2	1.3	1.2	1.3

A test was furthermore carried out to determine the time when the current is reaching the short circuit thermal limit of 250°C. The results from this simulation is shown in Table 7.5. The simulation tested currents from 2200 A to 4000 A where the current was increased by 100 A for every testing interval. Table 7.5 shows the overview for a testing interval of 200 A. Moreover, Table 9.1 in Appendix G shows the entire simulation results.

The results obtained further supports the idea of identically temperature behavior for the laying conditions before reaching the time of 8 hours. A current of 2200 A can be applied for cables in free air without exceeding the short circuit limit. However, if it is located in a culvert, it reaches 250°C after 60 hours.

Table 7.5: Overview of applied currents and time before reaching short circuit limit for both laying conditions considering ambient temperature of 10 °C.

Applied current	Cable in free air	Cable in culvert
	Time to reach 250 °C [h]	Time to reach 250 °C [h]
2200	-	60
2400	22	14
2600	9	8
2800	6	6
3000	4.5	4.5
3200	3.25	3.25
3400	2.5	2.5
3600	2.1	2.1
3800	1.8	1.8
4000	1.3	1.3

It should be kept in mind that the results in this section handle an ambient temperature of 10°C. Section 7.3.4 is referred to for the study of seasonal changes, including several ambient temperature's impacts on the results.

7.3.4 Case 4: Seasonal changes impact on conductor temperature response

Considering a year, the ambient temperature for the cable installation varies. Because of this, the question regarding how much the cable can be loaded will change as well. Case 4 studies the temperature variations of one week in a winter month (January) and one week in a summer month (June). The logged ambient temperatures for the two months are shown in Figure 7.16 and Figure 7.17.

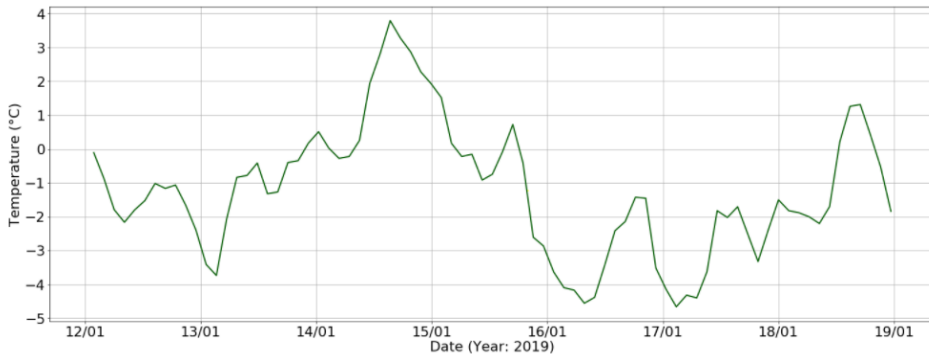


Figure 7.16: Logged ambient temperature during a week in January 2019.

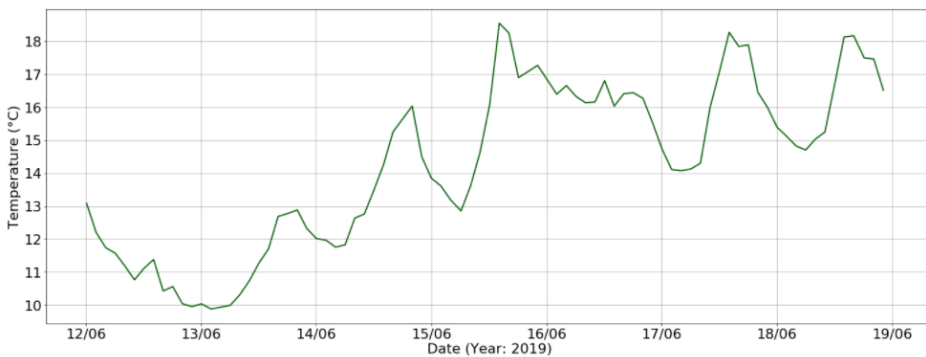


Figure 7.17: Logged ambient temperature during a week in June 2019.

Comparing the figures above shows that there are relatively significant differences in ambient temperature that surrounds the cable installation. While the ambient temperature of January varies from -4°C to 4°C , the ambient temperature of June

varies from 10°C to 18.5°C. These results highlight that the dynamic rating should be varied with the seasonal changes. When the ambient temperature is low, such as the case for January, the cable can have a higher current than the case for June. The difference is visualized in Figure 7.18, which shows the simulated conductor temperature due to a load of 1550 A. In the test, the average ambient temperatures were used which was 0°C for the chosen week in January and 14.25°C for the week in June.

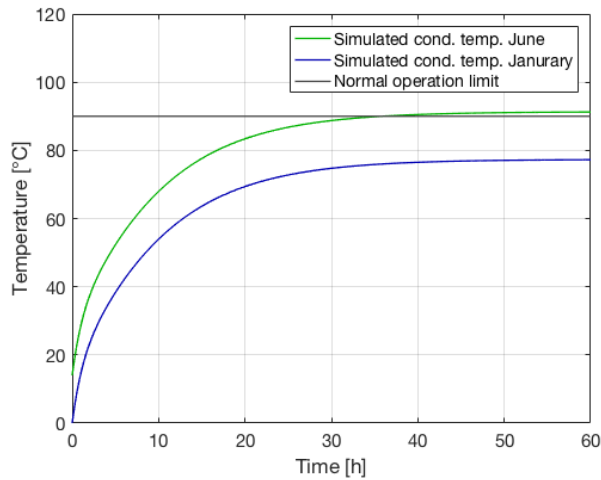


Figure 7.18: Simulated conductor temperature of a week of respectively January and June 2019 including the normal operation limit for cable installation in culvert.

Observing the above figure, one can see that when applying a similar load to the two cases, the system reaches the normal operation thermal limit of 90°C for the summer month. In contrast, it reaches steady-state temperature before the normal operation limit for the winter month. This result is rather expected as higher ambient temperatures lead to a higher temperature rise of the conductor. Furthermore, Table 7.6 and 7.7 shows the outcomes for respectively cable installation in culverts and in free air when comparing the two weeks. The results show how long time the various loads can be applied before reaching the limits for normal operation and emergency operation.

Table 7.6: Overview of the results comparing overloading cases for cable installation in culverts for a week in respectively January and June.

Applied current [A]	Time to reach 90°C [h]		Time to reach 105°C [h]	
	January	June	January	June
1600	-	20	-	-
1700	21	12	-	22
1800	13	9	20	14
1900	9	7	13	9
2000	7	6	9	7
2100	5.5	4.5	7.5	6
2200	4.5	3.5	6	4.5

Table 7.7: Overview of the results comparing overloading cases for cable installations in free air for a week in respectively January and June.

Applied current [A]	Time to reach 90°C [h]		Time to reach 105°C [h]	
	January	June	January	June
1600	-	-	-	-
1700	-	18	-	-
1800	18.5	10	-	19
1900	11	7	18	12
2000	7	6	11	7
2100	5	5.5	7.5	6
2200	3.5	4.5	6	4.5

By comparing the results from Table 7.6 and 7.7, the first observation is that the cable installation in free air can handle the different loads between 1600 – 1900 A for a longer time than the cable in the culvert. Still, for loads of 2000 A and higher, the results show that the two laying conditions can handle the load for roughly the same time.

Regarding seasonal changes, the week in January is found to handle the load for a relatively long time compared to the week in June for both cases of laying conditions. The cable in culvert in Table 7.6 found that the normal operating limit is

reached only for the cable installation in June for a load of 1600 A. The cable can, however, handle the load for several hours for both months in case of an emergency operation. Further, several hours longer are observed for loading the cable without exceeding the limits for January than June. For instance, a load of 1800 A can be applied for 13 hours during normal operation for the case in January. However, the same load can only be applied for 9 hours, considering a week in June. As the results indicate, seasonal changes do have a significant influence on the maximum load allowed. These results additionally highlight the importance of dynamic cable rating during a year due to the higher capacity in the cold winter months.

Table 7.7 focuses on the cable installation in free air shows more considerable differences than the culvert cable installation between January and June. The discrepancy may be due to a more consequential effect of seasonal changes for the cable in free air as the ambient temperature fluctuate more on the installation. Moreover, the correlation between time to reach thermal limits for loading in January and June seems to vary with 100 A consistently. For instance, time to reach normal operation limit is almost equal for January with 1900 A as for June with 1800 A. This applies for both cable-laying methods.

Conclusion

In this thesis, multiple simulations have been completed with the basis of a calculation method established according to IEC standards. The key findings for the thesis are:

- The laboratory setup concludes to provide realistic results for both tests: Test 1 that applied a current increase and Test 2 that applied a step current. However, an error was discovered in Position 1 for the cable installation placed on the floor of the setup.
- The simulation established with the basis of the calculation methodology had a positive correlation with the cable installation from the experimental test. The correlation applies for both laying conditions: in free air and for cable placed on the floor. Both simulated sheath and conductor temperature interact with the logged temperatures from the laboratory setup. Especially the simulated steady-state temperature has been found to be similar to the logged temperature for both sheath and conductor.
- Utilizing the superposition principle in order to determine the temperature response has turned out to give results that correspond with the logged temperatures. The simulation has highlighted the importance of utilizing the principle of superposition when the temperature does not reach a steady-state before a new current is applied.
- An overloading example was simulated for the cable installation from the laboratory setup. The results show, among others, that an overload of 30% above maximum permissible current can be applied for 24 minutes.

- Simulating the load history impact on the power cable from the experiment has found that after switching off a 150 A load, the reference ambient temperature was reached after 2 hours and 45 minutes assuming a temperature margin of 0.05°C.
- The simulated sheath temperature for a high voltage cable tuned out to correspond well with the sheath temperature logged from the high voltage cable owned by Statnett.
- A case-study has revealed results considering the potential of the underutilized capacity of the high voltage cable installation. For instance, in April 2019, the cable could be overloaded with 150% more than it did for 6 hours under normal operation and 8 hours under emergency operation for the high voltage cable in free air as well as in a culvert. Furthermore, an overload of 150% to the cable installation in culvert may be applied for 1 hours longer under normal operation and 2 hours under emergency operation for a week in January than a week in June. The seasonal changes is found to have a great impact on the potential of dynamic cable rating.

Further Work

Based on the research completed in this thesis, the following suggestions are given for further work:

- More tests could be done in the laboratory setup to verify the calculation method even further. This was, however, not possible due to the situation of Covid-19 in the current study.
- The parameters utilized in the calculation methodology could be tested more detailed by changing different parameters and observing the results obtained. This would verify the method even more than it is done in this thesis, as it may highlight the importance of the different parameters utilized.
- Studying the high voltage cable installation, the calculations could also determine the temperature responses for the cable located in the seabed. The current study focused only on the bottlenecks that were assumed to be located on land.
- Applying the calculation method on other laying conditions, such as directly buried cable installations.

Bibliography

- [1] C. J. Wallnerström et al. “Potential of dynamic rating in Sweden”. In: (July 2014), pp. 1–6. DOI: 10.1109/PMAPS.2014.6960605.
- [2] V. Lackovic. “Practical Power Cable Ampacity Analysis”. In: *Continuing Education and Development, Inc.* ().
- [3] LS EHV Cable System. “66 - 500 kV XLPE Cable Accessories”. In: ().
- [4] G. J. Anders. *Rating of Electric Power Cables. Ampacity Computations for Transmission, Distribution, and Industrial Applications*. McGraw-Hill Professional; 1 edition, 1997.
- [5] G. J. Anders and M. A. El-Kady. “Transient ratings of buried power cables. I. Historical perspective and mathematical model”. In: *IEEE Transactions on Power Delivery* 7.4 (Oct. 1992), pp. 1724–1734. ISSN: 1937-4208. DOI: 10.1109/61.156972.
- [6] C. J. Wallnerström, P. Westerlund, and P. Hilber. “Using power system temperature sensors for more uses than originally intended - Exemplified by investigating dynamic rating possibilities”. In: Sept. 2014. DOI: 10.13140/2.1.1563.0723.
- [7] S. Huang, W. Lee, and M. Kuo. “An Online Dynamic Cable Rating System for an Industrial Power Plant in the Restructured Electric Market”. In: *IEEE Transactions on Industry Applications* 43.6 (Nov. 2007), pp. 1449–1458. ISSN: 1939-9367. DOI: 10.1109/TIA.2007.908206.
- [8] R. Adapa and D. Douglass. “Dynamic thermal ratings: Monitors and calculation methods”. In: (Aug. 2005), pp. 163–167. DOI: 10.1109/PESAFR.2005.1611807.

-
- [9] M. Miura et al. “Application of dynamic rating to increase the available transfer capability”. In: (Mar. 2009), pp. 40–47. DOI: 10.1002/eej.20537.
- [10] G. Kariniotakis. “Renewable Energy Forecasting: From Models to Applications”. In: *Renewable Energy Forecasting: From Models to Applications* (June 2017).
- [11] R. Hemparuva et al. “Geographic information system and weather based dynamic line rating for generation scheduling”. In: *Engineering Science and Technology, an International Journal* 21 (June 2018). DOI: 10.1016/j.jestch.2018.05.011.
- [12] K. Morozovska. “Dynamic Rating with Applications to Renewable Energy”. In: *KTH School of Electrical Engineering and Computer Science* (Jan. 2020).
- [13] B. Hennuy et al. “Thermal monitoring of cable circuits and grid operators’ use of dynamic rating systems”. In: *Cigre: B1 Insulated cables, Ref: 756* (Feb. 2019).
- [14] G. J. Anders and S. Cherukupalli. *Distributed Fiber Sensing and Dynamic Rating of Power Cables*. John Wiley Sons; 1 edition, 2019.
- [15] H. J. Li, K. C. Tan, and Qi S. “Assessment of underground cable ratings based on distributed temperature sensing”. In: *IEEE Transactions on Power Delivery* 21.4 (Oct. 2006), pp. 1763–1769. DOI: 10.1109/TPWRD.2006.874668.
- [16] K. T. Yoon and D. S. A. Teo. “Controlling and monitoring Singapore’s underground grid”. In: *IEEE Computer Applications in Power* 12.4 (Oct. 1999), pp. 23–29. DOI: 10.1109/67.795134.
- [17] J. Hanania et al. “Heat transfer mechanisms”. In: (Jan. 2017).
- [18] F. P. Incropera et al. *Fundamentals of Heat and Mass Transfer*. John Wiley Sons, 2006.
- [19] E. Ildstad. “TET4160 Insulating Materials for High Voltage Applications”. In: (Aug. 2018).
- [20] E. Ildstad. *TET4195 High Voltage Equipment - Compendium*. NTNU, 2019.
- [21] B. M. Galitseyskiy. “Fundamentals of the heat transfer theory”. In: (2009), pp. 1–9.
- [22] *Definition of Ampacity*. <https://www.merriam-webster.com/dictionary/ampacity>. Accessed: 2020-02-02.
-

-
- [23] S. Kahourzade et al. "Ampacity calculation of the underground power cables in voluntary conditions by finite element method". In: (May 2011), pp. 657–660. ISSN: null. DOI: 10.1109/ECTICON.2011.5947925.
- [24] D. Nishanthi and U. Abhisek. "Cable Ampacity Calculation and Analysis for Power Flow Optimization". In: (Oct. 2016). DOI: 10.1109/ACEPT.2016.7811535.
- [25] A. Bernath, D. B. Olfe, and J. F. Martin. "Short-Term Transient Temperature Calculations and Measurements for Underground Power Cables". In: *IEEE Transactions on Power Delivery* 1.3 (July 1986), pp. 22–27. ISSN: 1937-4208. DOI: 10.1109/TPWRD.1986.4307970.
- [26] J. H. Neher and M. H. McGrath. "The calculation of the temperature rise and load capability of cable systems". In: *Transactions of the American Institute of Electrical Engineers. Part III: Power Apparatus and Systems* 76.3 (Apr. 1957), pp. 752–764. ISSN: 2379-6766. DOI: 10.1109/AIEEPAS.1957.4499653.
- [27] R. J. Millar. "A comprehensive approach to real time power cable temperature prediction and rating in thermally unstable environments". In: *Helsinki University of Technology* (Nov. 2006).
- [28] R. Stout. "Part two: Linear superposition speeds thermal modeling". In: 33 (Feb. 2007), pp. 28–33.
- [29] R. Stout. "Part one: Linear superposition speeds thermal modeling". In: 33 (Jan. 2007).
- [30] G. Parnis. "Building Thermal Modelling Using Electric Circuit Simulation". In: *School of Photovoltaic and Renewable Energy Engineering University of New South Wales* (July 2012).
- [31] A. Hoshmeh et al. "A single-phase cable model based on lumped-parameters for transient calculations in the time domain". In: (June 2015), pp. 731–736. ISSN: null. DOI: 10.1109/EEEIC.2015.7165255.
- [32] F. C. V. Wormer. "An Improved Approximate Technique for Calculating Cable Temperature Transients [includes discussion]". In: *Transactions of the American Institute of Electrical Engineers. Part III: Power Apparatus and Systems* 74.3 (Jan. 1955), pp. 277–281. DOI: 10.1109/AIEEPAS.1955.4499079.
- [33] L. Yang et al. "Comparison of Conductor-Temperature Calculations Based on Different Radial-Position-Temperature Detections for High-Voltage Power Cable". In: *Electric Power Research Institute, China* (Jan. 2018).
-

-
- [34] I. Sarajcevic, M. Majstrovic, and Ivan Medic. "Calculation of losses in electric power cables as the base for cable temperature analysis". In: *Journal of Advanced Computational Methods in Heat Transfer* 4 (Jan. 2000).
- [35] A. Sedaghat and F. de León. "Thermal Analysis of Power Cables in Free Air: Evaluation and Improvement of the IEC Standard Ampacity Calculations". In: *IEEE Transactions on Power Delivery* 29.5 (Oct. 2014), pp. 2306–2314. ISSN: 1937-4208. DOI: 10.1109/TPWRD.2013.2296912.
- [36] "IEC 60287. Electric cables. Calculation of the current rating - part 1-1: Current rating equations (100 % load factor) and calculation of losses - general". In: *IEC Standard 60287* (2006).
- [37] S. Whitehead and E. E. Hutchings. "Current rating of cables for transmission and distribution". In: *Journal of the Institution of Electrical Engineers* 83.502 (Oct. 1938), pp. 517–557. ISSN: null. DOI: 10.1049/jiee-1.1938.0170.
- [38] J. Karlstrand and G. Henning. "Modern FEM tools - An example of cables installed in duct-banks". In: ().
- [39] R. Skjoldli. "Transient temperature calculations for dynamic cable rating". In: *Master of science in electric power engineering* (Dec. 2019).
- [40] P. Wang et al. "Dynamic Thermal Analysis of High-Voltage Power Cable Insulation for Cable Dynamic Thermal Rating". In: *IEEE Access* 7 (2019), pp. 56095–56106. ISSN: 2169-3536. DOI: 10.1109/ACCESS.2019.2913704.
- [41] C. Gianoulis. "Investigate the use of thermal protection for underground cables in Ergon Engery's electricity network". In: (Nov. 2006).
- [42] G. J. Anders. "Review of Power Cable Standard Rating Methods". In: (2005), pp. 1–75. ISSN: null. DOI: 10.1109/9780471718741.ch1. URL: <https://ieeexplore.ieee.org/document/5444124>.
- [43] *The Current Transformer*. <https://www.electronics-tutorials.ws/transformer/current-transformer.html>. Accessed: 2020-03-03.
- [44] *TSLF 24 kV 1x50A*. https://www.nexans.no/eservice/Norway-no_NO/navigateproduct_540395461/TSLF_24_kV_1x50A.html. Accessed: 2020-02-17.
- [45] *Equivalent Diameter*. https://www.engineeringtoolbox.com/equivalent-diameter-d_205.html. Accessed: 2020-05-05.
-

-
- [46] V. T. Morgan. “Effect of surface-temperature rise on external thermal resistance of single-core and multi-core bundled cables in still air”. In: *IEE Proceedings - Generation, Transmission and Distribution* 141.3 (May 1994), pp. 215–218. ISSN: 1350-2360. DOI: 10.1049/ip-gtd:19949939.
- [47] “Calculation of the Current Rating – Part 2: Thermal Resistance – Section 1: Calculation of the Thermal Resistance”. In: *IEC Standard 60287-2-1* (Dec. 1994).

Appendix A

Determining $\Delta\theta_s$ for cable installations in free air

As Equation (4.9) exposes, the external thermal resistance is dependent on $\Delta\theta_s$, which needs to be determined. Morgan [46] studied the effect of the surface temperature rise of the external thermal resistance, and reveals that an increase in cable surface temperature rise leads to a greater velocity of the air. Consequently, the heat transfer on the cable surface will increase, meaning the value of h increases as well. Thus, both exponent ($\frac{1}{4}$) and the heat transfer coefficient (h) varies with the temperature rise of the cable surface. The IEC Standard IEC-60287-2-1 [47] suggests a mathematical method to obtain a reasonable value for $\Delta\theta_s$, which is demonstrated in the following.

$$(\Delta\theta_s)^{1/4} = \left[\frac{\Delta\theta + \Delta\theta_d}{1 + K_A(\Delta\theta_s)^{1/4}} \right]^{1/4} \quad (9.1)$$

Where:

$$K_A = \frac{\pi D_e h T_{int}}{1 + \lambda_1 + \lambda_2}$$

Where λ_1 and λ_2 is the sheath and armour loss factors, respectively. $\Delta\theta$ is the conductor temperature rise allowed above ambient temperature, hence $\Delta\theta = \theta_{cond} - \theta_{amb}$, while the temperature representing dielectric losses can be neglected, $\Delta\theta_d = 0$. Furthermore, T_{int} is representing the internal thermal resistance of the cable installation, hence in cases where the thermal resistance between sheath and armour, T_2 , is neglected:

$$T_{int} = T_1 + (1 + \lambda_1 + \lambda_2)T_3$$

The IEC Standard IEC-60287-2-1 [47] suggests an iterative process that can be implemented in order to determine the value of $(\Delta\theta_s)^{1/4}$ from Equation (9.1). This is done by considering the heat balance equation at the cable surface, which can be seen in Equation (9.2) for cables protected for direct solar radiation, and when neglecting the temperature rises due to dielectric losses.

$$\theta_{cond} - \theta_{amb} - \Delta\theta_s = \frac{\pi D_e h (\Delta\theta)^{5/4} T_{int}}{1 + \lambda_1 + \lambda_2} \quad (9.2)$$

The iterative process suggested is shown in Equation (9.3). To obtain the proper value of $(\Delta\theta_s)^{1/4}$, the iteration that is constructed from Equation (9.3) is recommended to have an initial value of 2, and the iteration should be repeated until $(\Delta\theta_s)_{n+1}^{1/4} - (\Delta\theta_s)_n^{1/4} \leq 0.001$.

$$(\Delta\theta_s)_{n+1}^{1/4} = \left[\frac{\Delta\theta + \Delta\theta_d}{1 + K_A(\Delta\theta_s)_n^{1/4}} \right]^{1/4} \quad (9.3)$$

Cables with a jacket or other nonmetallic surfaces should be considered to have a black surface. The value h should be 80 % of the value for a cable with black surface.

Appendix B

Conversion between circular and rectangular duct

As the formulas related to cable installations in ducts are applicable for circular shapes, the diameter utilized in the equations needs to be converted in order to fit into a rectangular culvert. The process of this conversion is suggested by Karlstrand et al. [38]. The diameter of the new transformed shape is shown in Equation (9.4).

$$D_b = x \left(1 + \left(\frac{y}{x} \right)^2 \right)^{\frac{x}{2y} \left(\frac{4}{\pi} - \frac{x}{y} \right)} = x f \left(\frac{y}{x} \right) \quad (9.4)$$

Where:

x = Length of the shortest side in the rectangular-shaped culvert

y = Length of the longest side in the rectangular-shaped culvert

f = Function that is used to determine the ratio

The function f in Equation (9.4) can be determined by studying the relationship introduced in Figure 9.1. The arrow pointing upwards in the figure tells that if the ratio y/x is greater than 3, the method described should not be used with IEC standards. For the calculations accomplished in this thesis, the value of the ratio was below 1.5.

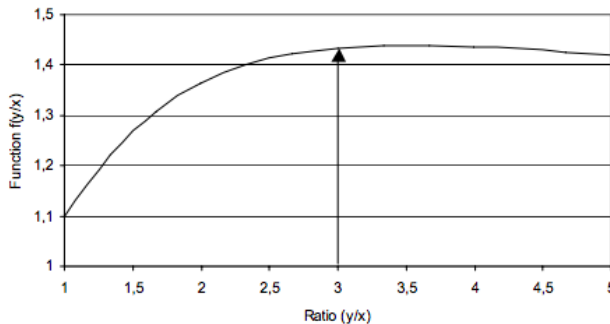


Figure 9.1: Relationship between ratio of y/x and the function f

Appendix C

Ladder network for thermal model

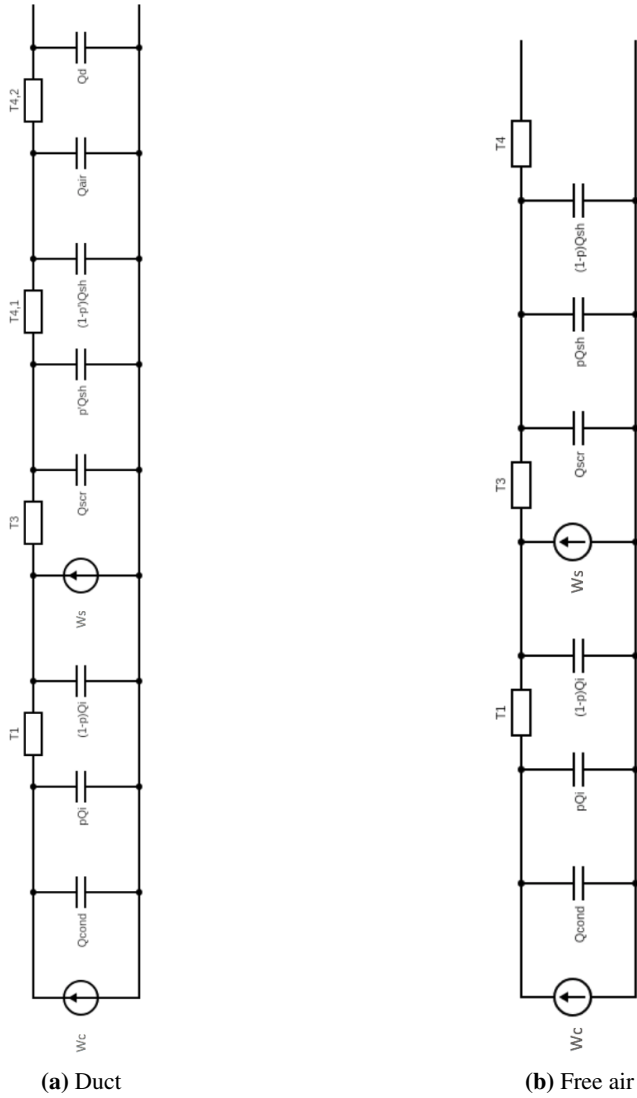


Figure 9.2: Ladder network for thermal model

Appendix D

The basis for the calculations of both conductor and sheath temperature rises are found from Anders [4].

Conductor transient temperature rise

The transfer function from the thermal network in Figure 9.2 can be found by utilizing Equation (4.14). The transfer function is the same for both laying conditions (in free air and in duct), and is shown in Equation (9.5).

$$H_{cond} = \frac{\theta_c}{W_c} = Z_{tot} \quad (9.5)$$

Where Z_{tot} is the total impedance of the network:

$$Z_{tot} = \frac{1}{sQ_A + \frac{1}{T_A + \frac{1}{sQ_B + \frac{1}{T_B}}}}$$

Now it is possible to calculate equation (9.5) for the conductor and can be seen in equation (9.6).

$$H_{cond}(s) = \frac{(T_A + T_B) + sT_A T_B Q_B}{1 + s(T_A Q_A + T_B Q_B + T_B Q_A) + s^2 T_A Q_A T_B Q_B} \quad (9.6)$$

Furthermore, we are interested in determining the parameters for T_{ij} in equation (4.15). When calculating the conductor temperature response, we consider $i = 1$ and $j = 1, 2$ regarding equation (4.15). For the conductor temperature calculations, the following relationships are used:

$$-P_1 = \frac{M_0 + \sqrt{M_0^2 - N_0}}{N_0}$$

$$-P_2 = \frac{M_0 - \sqrt{M_0^2 - N_0}}{N_0}$$

Where:

$$M_0 = \frac{1}{2}(T_1Q_1 + T_3Q_2 + T_3Q_1)$$

$$N_0 = T_1Q_1T_3Q_2$$

The transfer functions zeros and poles are given by:

$$Z_{11} = \frac{T_1 + T_3}{T_1T_3Q_2}$$

The following is found from Equation (9.6):

$$a_{(2-1),1} = T_1T_3Q_2$$

$$b_2 = T_1T_3Q_1Q_2$$

It is referred to 'Appendix B: An Algorithm to Calculate the Coefficients of the Transfer Function Equation' from Anders [4] for an explanation of the procedure related to the parameters calculations. Furthermore, one finds that:

$$\frac{a_{11}}{b_2} = \frac{1}{Q_1}$$

From Equation (4.16), the following is further obtained:

$$T_{11} = -\frac{1}{Q_1} \frac{1 - \frac{T_1+T_3}{T_1T_3Q_2} - P_1}{P_1(P_2 - P_1)} = \frac{1}{P_2 - P_1} \left(\frac{1}{Q_1} - \frac{T_1 + T_3}{-P_1T_1T_3Q_1Q_2} \right) \quad (9.7)$$

However,

$$P_1P_2 = \frac{1}{T_1T_3Q_1Q_2}$$

And because of this, we get Equation (9.8) and Equation (9.9) as the final results for T_{ij} .

$$T_{11} = \frac{1}{P_2 - P_1} \left[\frac{1}{Q_1} + P_2(T_1 + T_3) \right] \quad (9.8)$$

$$T_{12} = T_1 + T_3 - T_{11} \quad (9.9)$$

By using Equation (4.15) with the values obtained in Equation (9.8) and (9.9), Equation (9.10) is obtained that illustrates the conductor temperature as a function of time for both laying conditions investigated.

$$\theta_c(t) = W_c[T_{11}(1 - e^{P_1 t}) + T_{12}(1 - e^{P_2 t})] \quad (9.10)$$

Sheath transient temperature rise

In order to calculate the sheath temperature rise, one has to consider $i = 2$ and $j = 1, 2$. From the two-loop circuit, the transfer function when considering the sheath node can be written with basis from Equation (9.5). Z_{tot} in this case is given:

$$Z_{tot} = \frac{1}{sQ_B + \frac{1}{T_B}}$$

Solving the transfer function in Equation (9.5), gives the solution shown in Equation (9.11). Note that the denominator is equal as the transfer function found for the conductor temperature rise; however, the numerator is different.

$$H_{sheath}(s) = \frac{T_B}{1 + s(T_A Q_A + T_B Q_A + T_B Q_B) + s^2 T_A T_B Q_A Q_B} \quad (9.11)$$

Note that also for the sheath temperature rise calculations the following relationships are valid:

$$\begin{aligned} -P_1 &= \frac{M_0 + \sqrt{M_0^2 - N_0}}{N_0} \\ -P_2 &= \frac{M_0 - \sqrt{M_0^2 - N_0}}{N_0} \\ M_0 &= \frac{1}{2}(T_1 Q_1 + T_3 Q_2 + T_3 Q_1) \\ N_0 &= T_1 Q_1 T_3 Q_2 \end{aligned}$$

Considering Equation (4.16), the parameters valid is found and are given as follows:

$$a_{(2-2),2} = T_B T_A$$

$$b_2 = T_A T_B Q_A Q_B$$

The resulting results from Equation (4.16) when considering the parameters found, can be seen in Equation (9.12) and (9.13).

$$T_{21} = \frac{T_A T_B}{T_A T_B Q_A Q_B} \cdot \frac{1}{P_1 P_2 - P_1^2} \quad (9.12)$$

$$T_{22} = \frac{T_A T_B}{T_A T_B Q_A Q_B} \cdot \frac{1}{P_1 P_2 - P_2^2} \quad (9.13)$$

Finally, by inserting the values found for T_{21} and T_{22} and inserting them into Equation (4.15), one get the resulting sheath temperature rise shown in Equation (9.14).

$$\theta_{sheath}(t) = W_c [T_{21}(1 - e^{P_1 t}) + T_{22}(1 - e^{P_2 t})] \quad (9.14)$$

Appendix E

Large scaled figures of the results from Chapter 6.

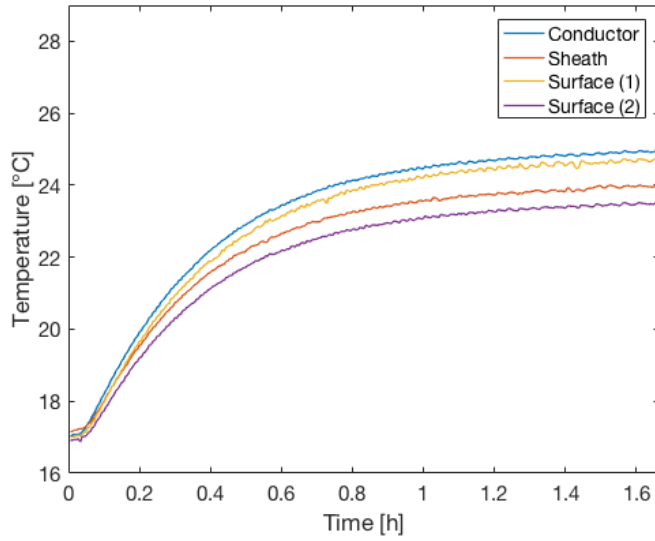


Figure 9.3: Temperature responses for the four measurements applying a current of 100 A for Position 1.

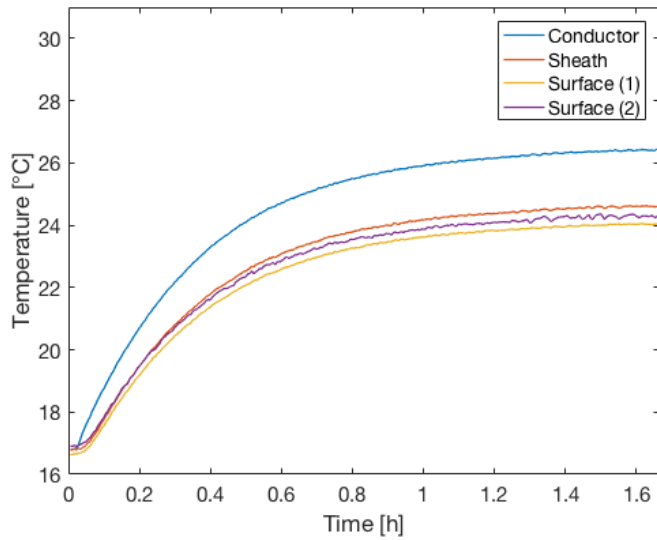


Figure 9.4: Temperature responses for the four measurements applying a current of 100 A for Position 2.

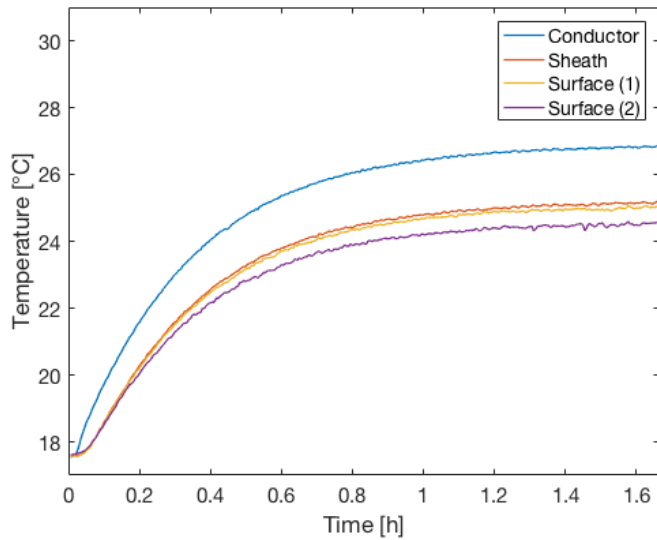


Figure 9.5: Temperature responses for the four measurements applying a current of 100 A for Position 3.

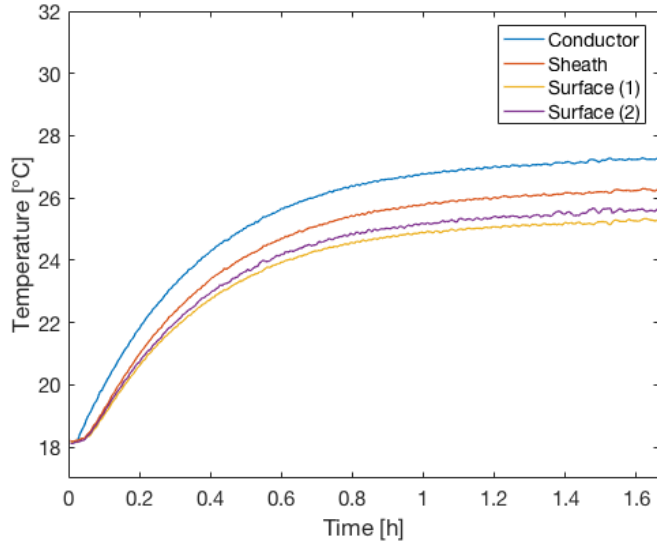


Figure 9.6: Temperature responses for the four measurements applying a current of 100 A for Position 4.

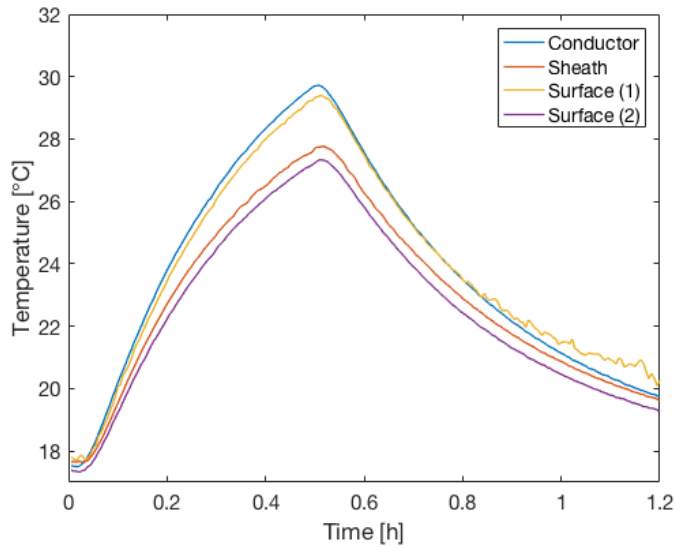


Figure 9.7: Temperatures for the four measurements applying a step current of 150 A for position 1.

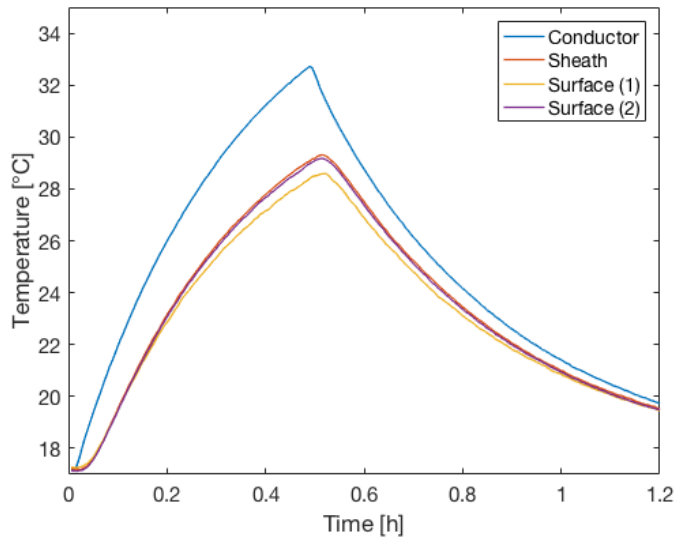


Figure 9.8: Temperatures for the four measurements applying a step current of 150 A for position 2.

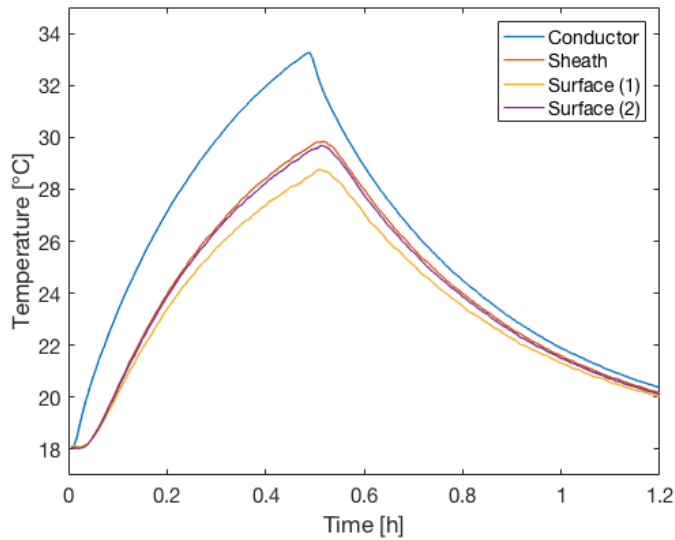


Figure 9.9: Temperatures for the four measurements applying a step current of 150 A for position 3.

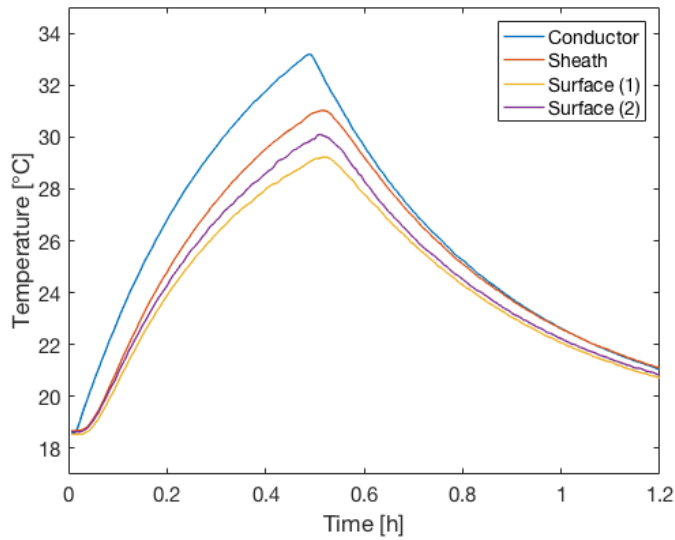


Figure 9.10: Temperatures for the four measurements applying a step current of 150 A for position 4.

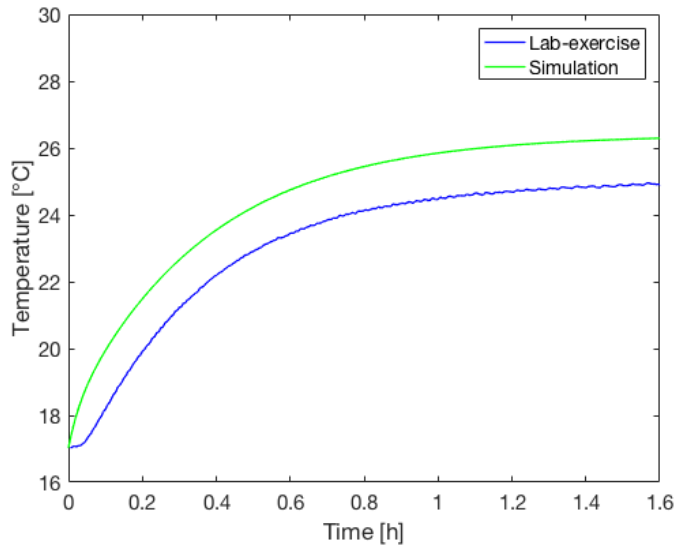


Figure 9.11: Comparison between conductor temperature from laboratory setup and simulation for Position 1 with a load of 100 A.

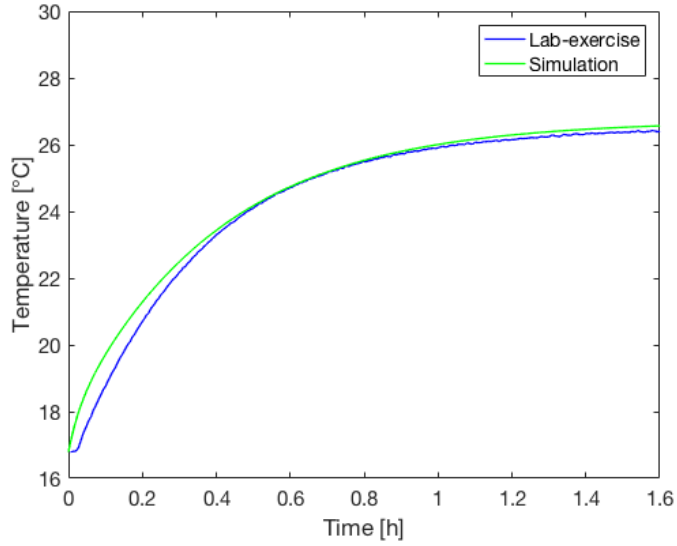


Figure 9.12: Comparison between conductor temperature from laboratory setup and simulation for Position 2 with a load of 100 A.

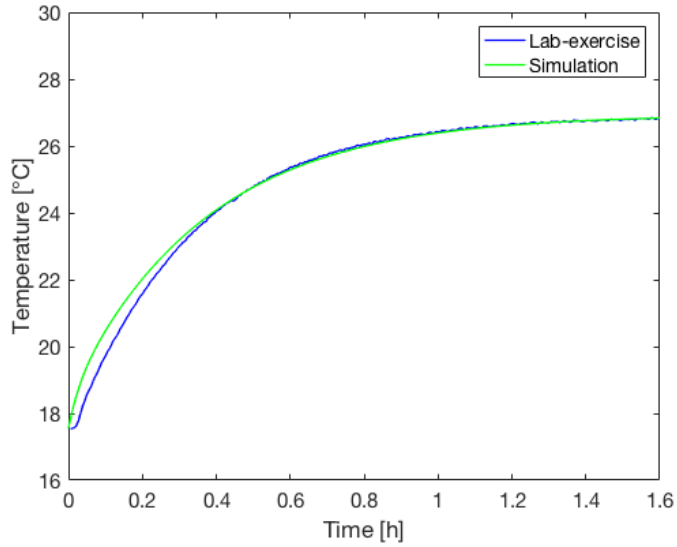


Figure 9.13: Comparison between conductor temperature from laboratory setup and simulation for Position 3 with a load of 100 A.

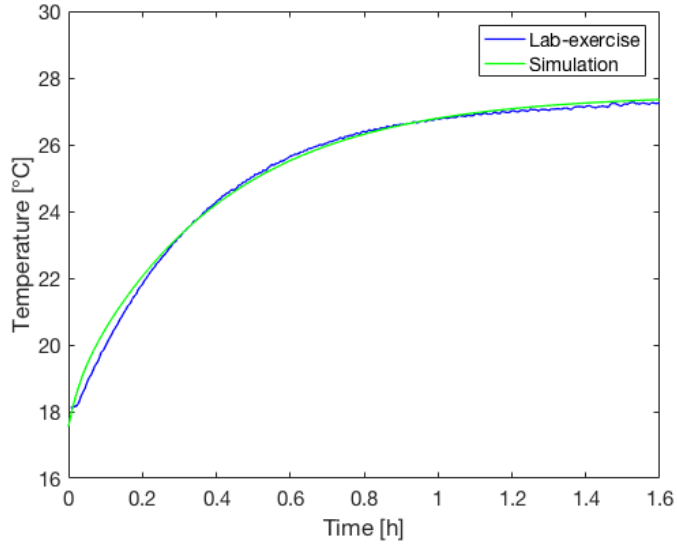


Figure 9.14: Comparison between conductor temperature from laboratory setup and simulation for Position 4 with a load of 100 A.

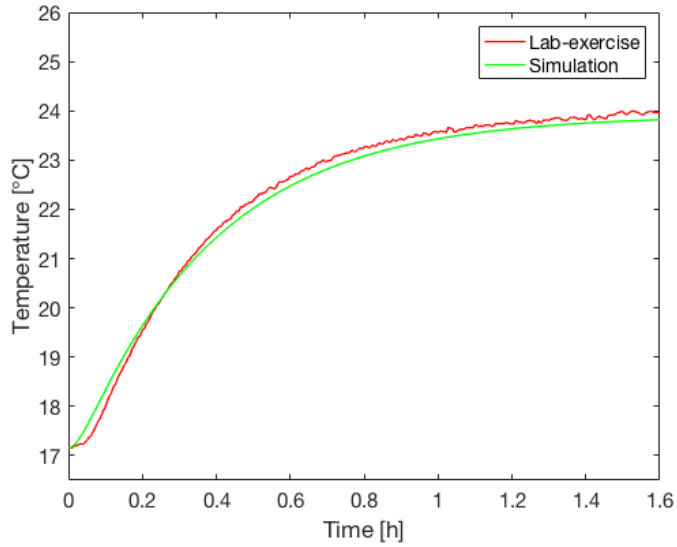


Figure 9.15: Comparison between sheath temperature obtained from laboratory setup and simulation for Position 1 with a load of 100 A.

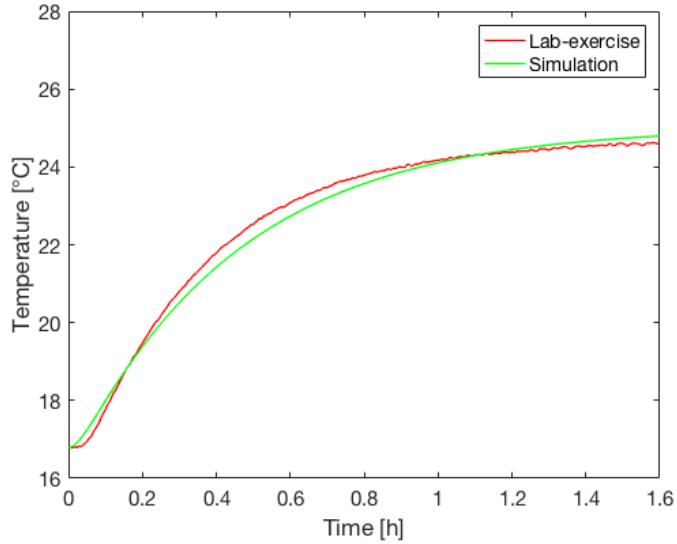


Figure 9.16: Comparison between sheath temperature obtained from laboratory setup and simulation for Position 2 with a load of 100 A.

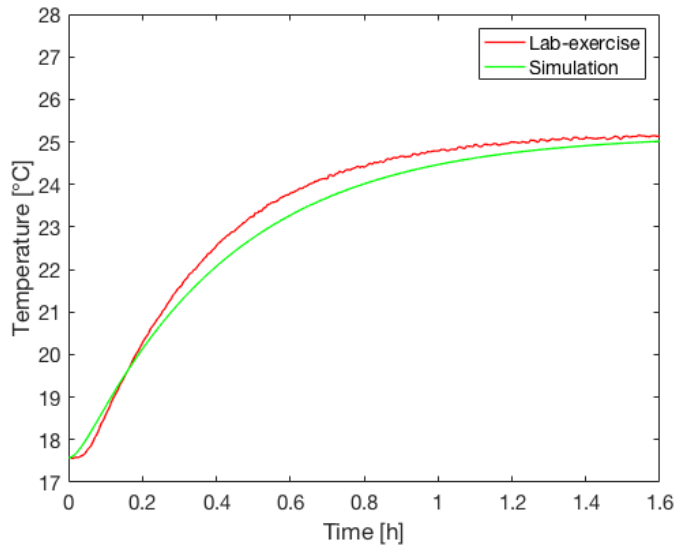


Figure 9.17: Comparison between sheath temperature obtained from laboratory setup and simulation for Position 3 with a load of 100 A.

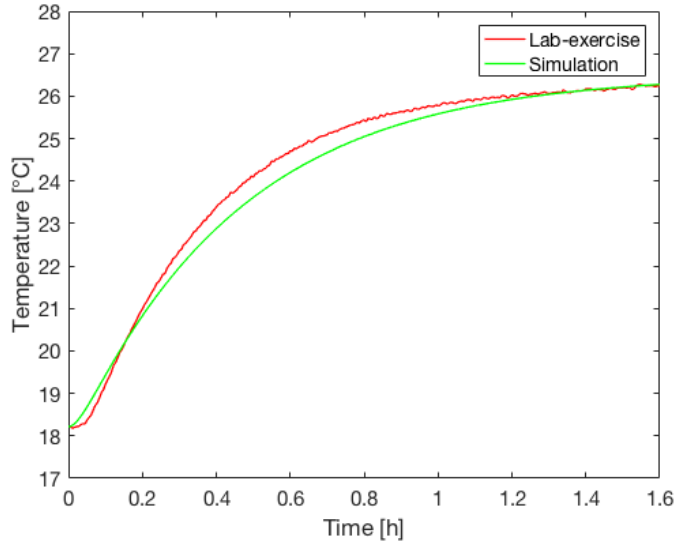


Figure 9.18: Comparison between sheath temperature obtained from laboratory setup and simulation for Position 4 with a load of 100 A.

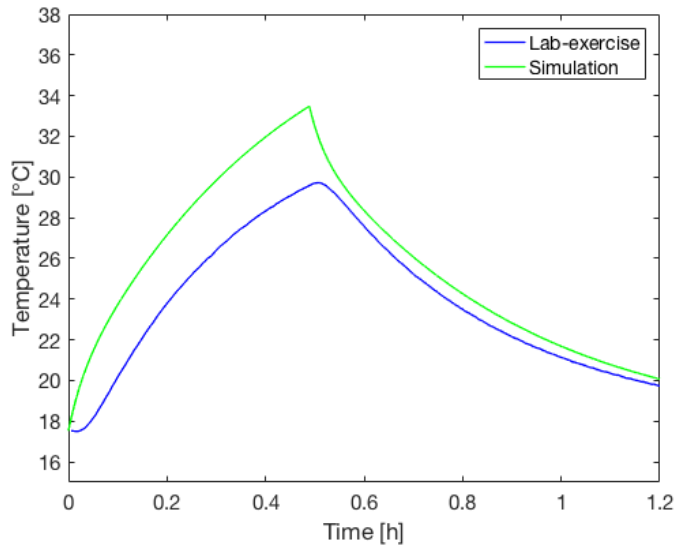


Figure 9.19: Comparison between conductor temperature from laboratory setup and simulation for Position 1 with a step current of 150 A.

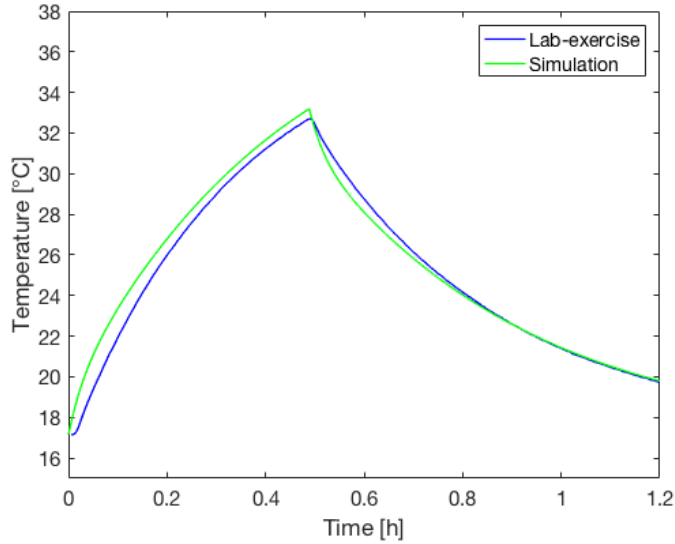


Figure 9.20: Comparison between conductor temperature from laboratory setup and simulation for Position 2 with a step current of 150 A.

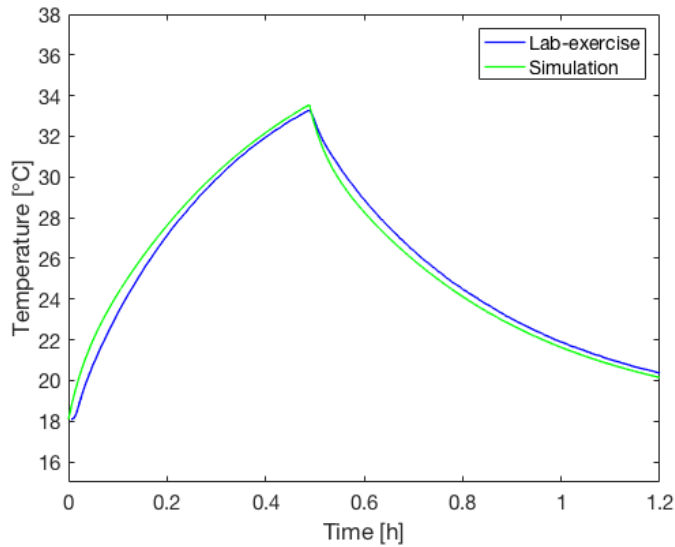


Figure 9.21: Comparison between conductor temperature from laboratory setup and simulation for Position 3 with a step current of 150 A.

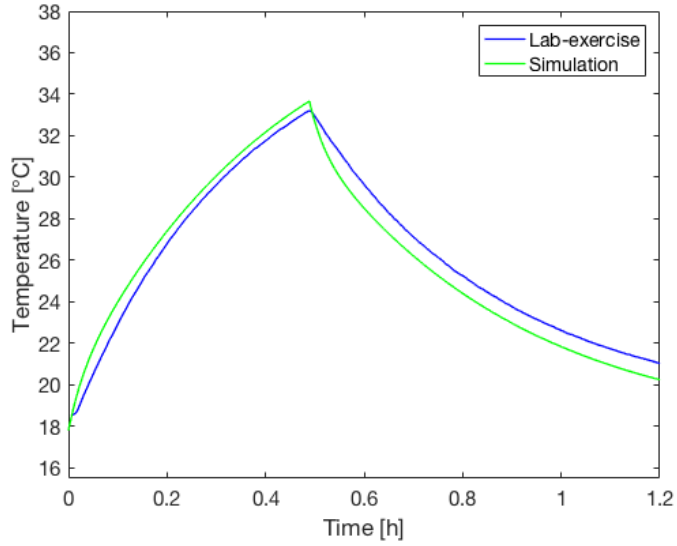


Figure 9.22: Comparison between conductor temperature from laboratory setup and simulation for Position 4 with a step current of 150 A.

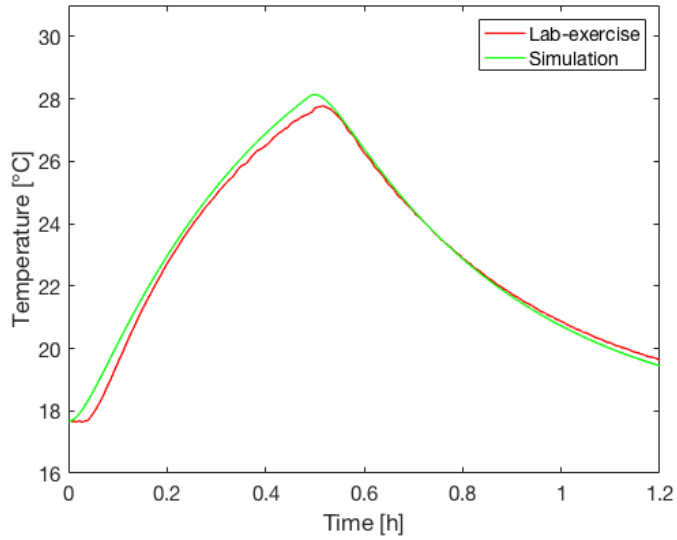


Figure 9.23: Comparison between sheath temperature from laboratory setup and simulation for Position 1 with a step current of 150 A.

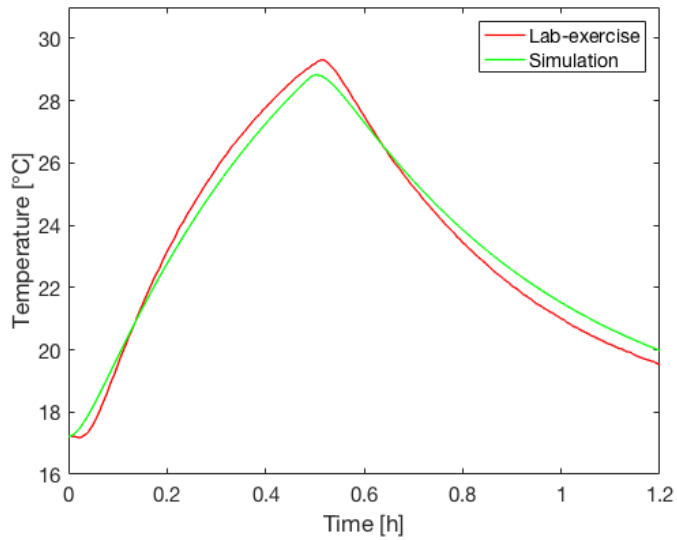


Figure 9.24: Comparison between sheath temperature from laboratory setup and simulation for Position 2 with a step current of 150 A.

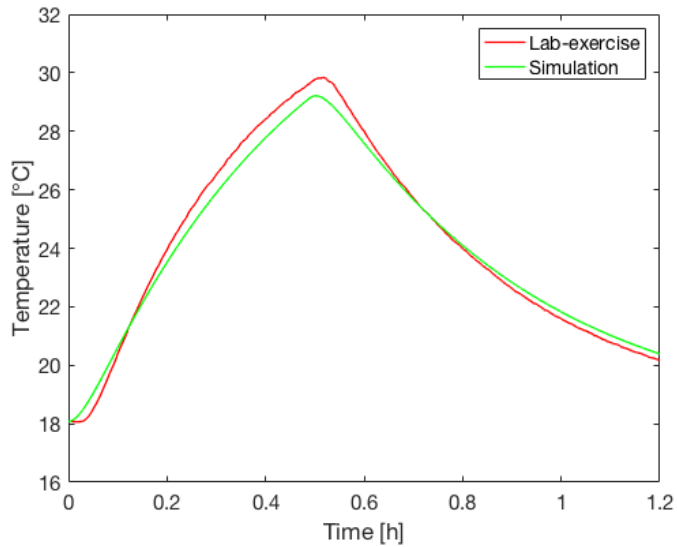


Figure 9.25: Comparison between sheath temperature from laboratory setup and simulation for Position 3 with a step current of 150 A.

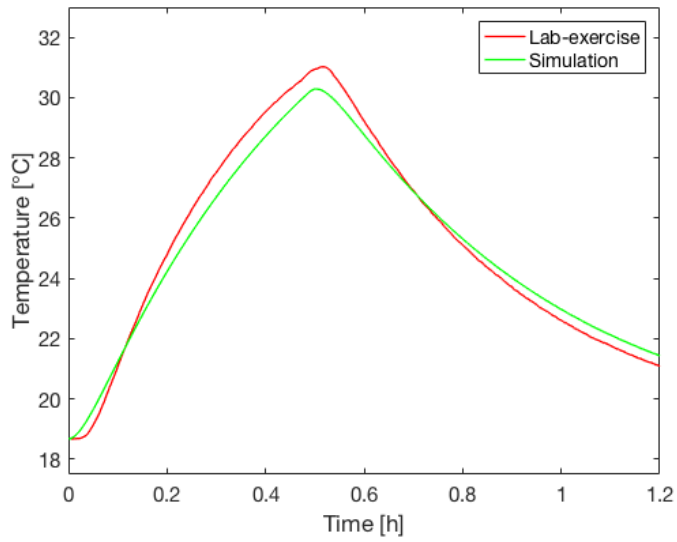
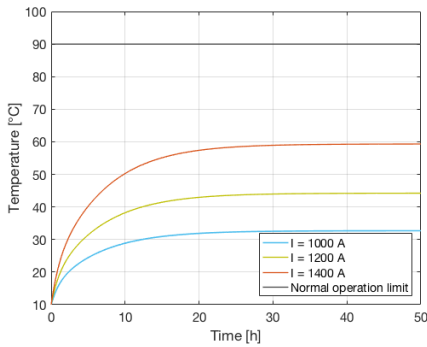


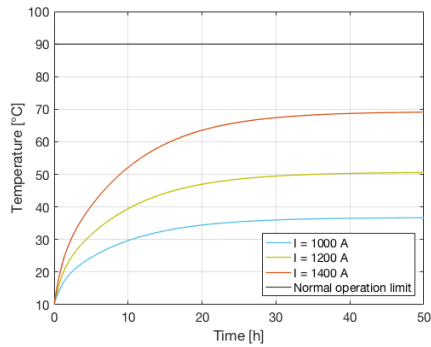
Figure 9.26: Comparison between sheath temperature from laboratory setup and simulation for Position 4 with a step current of 150 A.

Appendix F

Figures illustrating the overloading case for Statnett cable

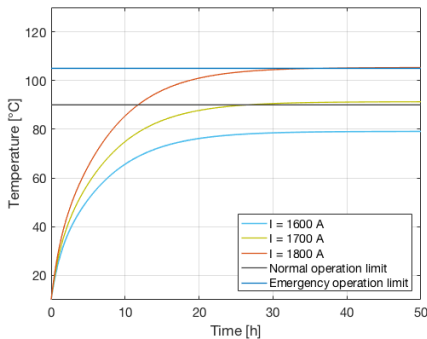


(a) Cable located in free air

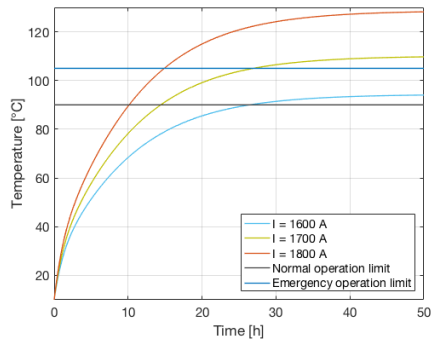


(b) Cable located in culvert

Figure 9.27: Simulated conductor temperature due to overloading currents of 1000 A, 1200 A and 1400 A.

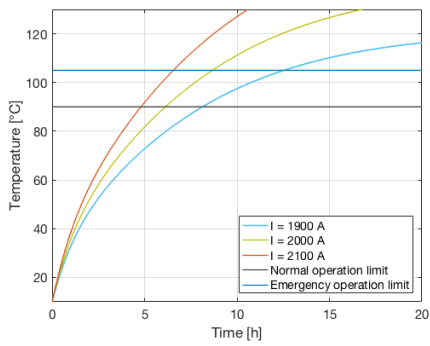


(a) Cable located in free air

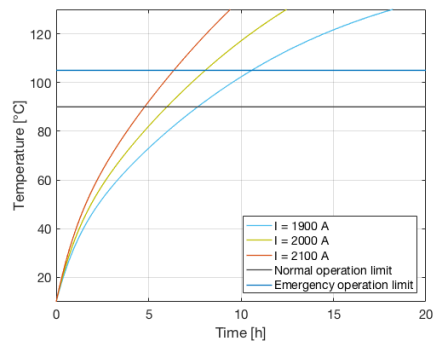


(b) Cable located in culvert

Figure 9.28: Simulated conductor temperature due to overloading currents of 1600 A, 1700 A and 1800 A.



(a) Cable located in free air



(b) Cable located in culvert

Figure 9.29: Simulated conductor temperature due to overloading currents of 1900 A, 2000 A and 2100 A.

Appendix G

Results from detailed simulation regarding overloading cable installation

Table 9.1: Overview of applied currents and time before reaching normal operation limit and emergency operation limit for both laying conditions.

Applied current	Cable in free air	Cable in culvert
	Time to reach 250 °C [h]	Time to reach 250 °C [h]
2200	-	60
2300	-	19
2400	22	14
2500	13	11
2600	9	8
2700	7.5	7.5
2800	6	6
2900	5	5
3000	4.5	4.5
3100	3.5	3.5
3200	3.25	3.25
3300	2.75	2.75
3400	2.5	2.5
3500	2.25	2.25
3600	2.1	2.1
3700	1.9	1.9
3800	1.8	1.8
3900	1.6	1.6
4000	1.3	1.3

Appendix H

Simulation codes utilized for predicting the temperature responses

Conductor temperature rise

```
function [TotalTempRise_Amb, Wc] = temp_rise_func(Wsh, t,
    Dcab, h, Wc, T11, T12, T21, T22, a, b, TB, TA, R20, I,
    alpha_al, tetha_ref, tetha_amb)
%% Conductor temperature rise

TR_Cond = Wc*(T11*(1-exp(-a*t))+T12*(1-exp(-b*t)));

TotalTCond_Amb = TR_Cond + tetha_amb;

TotalTempRise_Amb= TotalTCond_Amb;

%% Updating the losses

Wc = I^2*R20*(1+alpha_al*(TotalTCond_Amb-tetha_ref));

end
```

Sheath temperature rise

```
function [TotalTempRise_Amb, Wc] =
    temp_rise_sheath_func_air_test(t, Dcab, h, Wc, T21, T22,
    a, b, TB, TA, R20, I, alpha_al, tetha_ref, tetha_amb)

%% Sheath Temperature rise

TR_sh = Wc*(T21*(1-exp(-a*t))+T22*(1-exp(-b*t)));

TotalTSh_Amb = TR_sh+ tetha_amb;

TotalTempRise_Amb= TotalTSh_Amb;

end
```

Calculating the conductor and sheath temperature response for laboratory setup cable installation

In the below simulation code, both conductor temperature and sheath temperature responses are calculated and plotted. As the code indicates, it utilized the functions described in the two previous subsections. The code can handle different load variations using the principle of superposition.

```
%% Cable data from experimental methodology
A = 50*10(-6); %Conductor cross section/conductor area
t_i = 5.5*10(-3); %Tickness of insulation
t_sh = 3.85*10(-3); %Tickness of sheath
Dcond = 8*10(-3); %Diameter of conductor
Dcab = 27*10(-3); %Diameter of the whole cable
Di = 19.3*10(-3); %Diameter of the insulation

%% Rho-variables
rho_cond_20 = 2.65*10(-8); %Thermal resistivity , aluminium
    conductor
rho_i = 3.5; %Thermal resistivity , XLPE insulation
rho_sh = 3.5; %Thermal resistivity , PE lead sheath

%% Various parameters
I = 300; %Current load into the cable (variable)
alpha_al = 0.0043; %Temperature coefficient for aluminium
R20 = (rho_cond_20)/A; %Conductor resistance

%% Temperature variables
tetha_amb = 0; %Ambient temperature (variable)
tetha_ref = 20; %Ref temperature

%% Specific heat of different cable parts
c_cond = 2.5*10(6); %Specific heat of the al-conductor [J/
    Km3]
c_i = 2.4*10(6); %Specific heat of XLPE insulation [J/Km
    3]
c_sh = 2.4*10(6); %Specific heat of the sheath (outer
    covering) [J/Km3]
c_scr = 3.45*10(6); %Specific heat of the screen [J/Km3]

%% Van Wormer Coefficients
p1 = (1/(2*log(Di/Dcond))) - (1/(((Di/Dcond)2 - 1)));
p2 = (1/(2*log(Dcab/(Dcab-2*t_sh)))) - (1/(((Dcab/(Dcab-2*
    t_sh))2 - 1)));
```

```

%% Parameters for cable in air
%Comment out the one laying method that are not relevant
%Parameters for cable played in free air
%Z = 0.21;
%E = 3.94;
%g = 0.6;
%Parameters for cable placed on floor in air
Z = 1.69;
E = 0.63;
g = 0.25;

%% Thermal resistance calculations
T1 = rho_i/(2*pi)*log(1+2*t_i/Dcond); %Thermal resistance
    of the conductor
T3 = rho_sh/(2*pi)*log(1+2*t_sh/(Dcab-2*t_sh)); %Thermal
    resistance of the sheath
T_int = T1+T3; %Internal thermal resistance of cable
h = 0.88*((Z/(Dcab^g))+E); %Coefficient for calculations.
    0.88 due to black surface
k = (pi*Dcab*h*T_int)/(1); % k er bare en parameter for
    finne deltaS

%% Iteration to find Delta_s
delta_s_14 = 2; %Starting value
delta_new = 0;
diff = abs(delta_s_14 - delta_new);
target_diff = 0.001;
iteration_count = 0;

while (diff > target_diff)
    delta_new = ((90 - 17)/(1 + (k * delta_s_14)))^(1/4);
    diff = abs(delta_s_14 - delta_new);
    delta_s_14 = delta_new;
    iteration_count = iteration_count + 1;
end

DeltaS = delta_s_14^4;
T4_air = 1/(pi*Dcab*h*delta_s_14); %Thermal resistance of
    cables in air

%% Wc calculations
Wc = I^2*R20*(1+alpha_al*(tetha_amb-tetha_ref)); %
    Conductor-loss
Wsh = pi*Dcab*h*(DeltaS); %Surface-loss

```

```

%% Heat capacitance/Thermal capacitance calculations
Qcond = A * c_cond; %Thermal capacitance of conductor
Qi = pi/4*(Di^2-Dcond^2)*c_i; %Thermal capacitance of
    insulation
Qscr = pi/4*((Dcab-2*t_sh)^2-Di^2)*c_scr; %Thermal
    capacitance of screen
Qsh = pi/4*(Dcab^2-(Dcab-2*t_sh)^2)*c_sh; %Thermal
    capacitance of sheath

%% Establishing 2-loop network
TA = T1;
TB = 0.5*T1 + ((1+0.02)*(T3+T4_air)); %T3+T4_air; %In air ,
    side 75 i Anders-bok: 0.5*T1 + (1+0.02)*(T3+T4_air)
QA = Qcond + p1*Qi;
QB = (1-p1)*Qi + Qscr + p2*Qsh ;

Mo=0.5*(TA*QA + TB*QB + TB*QA);
No=TA*QA*TB*QB;
a = (Mo + sqrt(Mo^2-No))/No;
b = (Mo - sqrt(Mo^2-No))/No;

T11 = 1/(a-b)*(1/QA-b*(TA+TB)); %Conductor
T12 = TA + TB - T11; %Conductor
T21 = (TB*TA/(TA*TB*QA*QB))*(1/(a*b-a^2)); %T22 = (TB*a^2)
    /(a-b^2); %Sheath %
T22 = (TB*TA/(TA*TB*QA*QB))*(1/(a*b-b^2)); %T21 = (TB*a*b)
    /(a-b); %Sheath

%% Temperature rise for conductor and sheath layer
test = true;
index = 1;

%% Put in values of when the current are about to change
t_switch = [0, 100*3600, 20*3600, 40*3600, 450*3600,
    60*3600, 70*3600, 100*3600, 105*3600, 120*3600];
%% Wc_switch needs to have as many elements as t_switch
Wc_switch = [Wc, Wc, Wc, Wc, Wc, Wc, Wc, Wc, Wc, Wc];

dt = 0.1;
time = 0:dt:15*3600;

plot_matrix = zeros(length(t_switch)+1, length(time));
plot_matrix_sheath = zeros(length(t_switch)+1, length(time)
    );

```

```

for t = time

    for i = 1:length(t_switch)
        if(t >= t_switch(i))
            [plot_matrix(i, index), Wc_switch(i)] =
                temp_rise_func_air(Wsh, t-t_switch(i), Dcab,
                    h, Wc_switch(i), T11, T12, T21, T22, a, b,
                    TB, TA, R20, I, alpha_al, tetha_ref,
                    tetha_amb) ;
            [plot_matrix_sheath(i, index), Wc_switch(i)] =
                temp_rise_sheath_func_air(Wsh, t-t_switch(i)
                    , Dcab, h, Wc_switch(i), T11, T12, T21, T22,
                    a, b, TB, TA, R20, I, alpha_al, tetha_ref,
                    tetha_amb) ;

        end
    end

    %% Choose below if the currents are positive or
    %% negative contributions. Needs to be as many elements
    %% as t_switch. The functions can be multiplied or
    %% divided with whatever value in order to handle
    %% current loads with changing values.
    plot_matrix(length(t_switch)+1, index) = plot_matrix(1,
        index) - plot_matrix(2,index) + plot_matrix(3,index)
        + plot_matrix(4,index) - plot_matrix(5,index) +
        plot_matrix(6,index) + plot_matrix(7,index) -
        plot_matrix(8,index) - plot_matrix(9,index) -
        plot_matrix(10,index);
    plot_matrix_sheath(length(t_switch)+1, index) =
        plot_matrix_sheath(1,index) - plot_matrix_sheath(2,
            index) + plot_matrix_sheath(3,index) +
        plot_matrix_sheath(4,index) - plot_matrix_sheath(5,
            index) + plot_matrix_sheath(6,index) +
        plot_matrix_sheath(7,index) - plot_matrix_sheath(8,
            index) - plot_matrix_sheath(9,index) -
        plot_matrix_sheath(10,index);

    %% Testing when the value of the conductor temperature
    %% reaches the ambient temperature
    if ( test )
        if ( plot_matrix(length(t_switch)+1, index) < 0.01
            && t > 3600)
            fprintf('COND%20.2f', t/3600);
        end
    end
end

```

```
        test = false;
    end
end

    index = index + 1;

end

%% Plotting the conductor temperature response
plot(time/3600, plot_matrix(11, :)+25, 'LineWidth', 1.5);
hold on
%% Plotting the sheath temperature response
plot(time/3600, plot_matrix_sheath(11, :)+25, 'LineWidth',
    1.5);
hold on
%% Plotting the thermal limits of normal operation and
    emergency operation
plot(time/3600, 105*ones(size(time/3600)), 'LineWidth', 1.3,
    'color', 'g')
hold on
plot(time/3600, 90*ones(size(time/3600)), 'LineWidth', 1.3, '
    color', 'k')
```

Calculating the conductor and sheath temperature response for high voltage cable installation

The code that follows in this subsection handles the high voltage cable from Statnett. However, several values are not written here due to numbers that are sensitive. Parts of the calculations are similar to the case of the laboratory set up cable, however, the below code does account for the cable located in a culvert. For high voltage cables in free air, one has to use the parameters for the HV cable and use the algorithm explained in the previous subsection for cables in free air.

%% Parameters of high voltage cable

```
A = ; %Conductor cross section
t_i = ; %Tickness of insulation
t_sh = ; %Tickness of sheath
Dcond = ; %Diameter of conductor
Dcab = ; %Diameter of the whole cable
Di = ; %Diameter of the insulation
D_out_duct = ; %Duct outer diameter
D_in_duct = ; %Duct inner diameter
```

%% Rho-variables

```
rho_cond_20 = 2.65*10^(-8); %Thermal resistivity , aluminium
    conductor
rho_i = 3.5; %Thermal resistivity , XLPE insulation
rho_sh = 3.5; %Thermal resistivity , PE lead sheath
rho_duct = ;
```

%% Various parameters

```
I = 1000; %Current load into the cable
alpha_al = 0.0043; %Temperature coefficient for aluminium
R20 = (rho_cond_20)/A; %Conductor resistance
```

%% Temperature variables

```
tetha_amb = 0; %Ambient temperature
tetha_ref = 10; %Ref temperature
```

%% Specific heat of different parts

```
c_cond = 2.5*10^(6); %Specific heat of the al-conductor [J/
    Km^3]
c_i = 2.4*10^(6); %Specific heat of XLPE insulation [J/Km
    ^3]
c_sh = 2.4*10^(6); %Specific heat of the sheath (outer
    covering) [J/Km^3]
```

$c_{scr} = 3.45 \times 10^6$; %Specific heat of the screen [J/Km³]

%% Van Wormer Coefficients

$p1 = (1/(2 * \log(Di/Dcond))) - (1/(((Di/Dcond)^2) - 1));$
 $p2 = (1/(2 * \log(Dcab/(Dcab - 2 * t_sh)))) - (1/(((Dcab/(Dcab - 2 * t_sh))^2) - 1));$

%% Thermal resistance calculations

$T1 = \rho_i / (2 * \pi) * \log(1 + 2 * t_i / Dcond);$ %Thermal resistance of the conductor
 $T3 = \rho_{sh} / (2 * \pi) * \log(1 + 2 * t_{sh} / (Dcab - 2 * t_{sh}));$ %Thermal resistance of the sheath

%% Parameters used for calculations of cable in duct/ culvert

$U = 5.2;$
 $V = 0.91;$
 $Y = 0.01;$
 $\delta_m = 20 + 273;$
 $T4_1 = U / (1 + 0.1 * (V + (Y * \delta_m) * Dcab * 10^3));$
 $T4_2 = (\rho_{duct} / (2 * \pi)) * \log(D_{out_duct} / D_{in_duct});$ %
Transforming from circular duct to rectangular shaped culvert.

%% Wc calculations

$Wc = I^2 * R20 * (1 + \alpha_{al} * (t_{etha_amb} - t_{etha_ref}));$ %
Conductor-loss

%% Heat capacitance/Thermal capacitance calculations

$Q_{cond} = A * c_{cond};$ %Thermal capacitance of conductor
 $Q_i = \pi / 4 * (Di^2 - Dcond^2) * c_i;$ %Thermal capacitance of insulation
 $Q_{scr} = \pi / 4 * ((Dcab - 2 * t_{sh})^2 - Di^2) * c_{scr};$ %Thermal capacitance of screen
 $Q_{sh} = \pi / 4 * (Dcab^2 - (Dcab - 2 * t_{sh})^2) * c_{sh};$ %Thermal capacitance of sheath
 $Q_d = ;$ %Thermal capacitance of duct

%% 2-loop network

$TA = T1;$
 $TB = T3 + (T4_1 + T4_2);$
 $QA = Q_{cond} + p1 * Qi;$
 $QB = (1 - p1) * Qi + Q_{scr} + p2 * Q_{sh} + ((T4_1 + T4_2) / TB)^2 * ((1 - p2) * Q_{sh}) + ((T4_2 / TB)^2) * Q_d ;$

```

Mo=0.5*(TA*QA + TB*QB + TB*QA);
No=TA*QA*TB*QB;
a = (Mo + sqrt(Mo^2-No))/No;
b = (Mo - sqrt(Mo^2-No))/No;

T11 = 1/(a-b)*(1/QA-b*(TA+TB)); %Conductor
T12 = TA + TB - T11; %Conductor
T21 = (TB*TA/(TA*TB*QA*QB))*(1/(a*b-a^2)); %Sheath
T22 = (TB*TA/(TA*TB*QA*QB))*(1/(a*b-b^2)); %Sheath

%% Temperature rise for conductor and sheath layer
amb=14;
I = 2200;

test = true;
index = 1;

%% Put in values of when the current are about to change
t_switch = [0, 100*3600, 20*3600, 40*3600, 450*3600,
            60*3600, 70*3600, 100*3600, 105*3600, 120*3600];
%% Wc_switch needs to have as many elements as t_switch
Wc_switch = [Wc, Wc, Wc, Wc, Wc, Wc, Wc, Wc, Wc, Wc];

dt = 0.1;
time = 0:dt:200*3600;

plot_matrix = zeros(length(t_switch)+1, length(time));
plot_matrix_sheath = zeros(length(t_switch)+1, length(time)
);

for t = time

    for i = 1:length(t_switch)
        if(t >= t_switch(i))
            [plot_matrix(i, index), Wc_switch(i)] =
                temp_rise_func_test(t-t_switch(i), Dcab, h,
                Wc_switch(i), T11, T12, a, b, TB, TA, R20, I
                , alpha_al, tetha_ref, tetha_amb) ;
            [plot_matrix_sheath(i, index), Wc_switch(i)] =
                temp_rise_sheath_func_air_test(t-t_switch(i)
                , Dcab, h, Wc_switch(i), T21, T22, a, b, TB,
                TA, R20, I, alpha_al, tetha_ref, tetha_amb)
            ;
        end
    end
end

```

```

end
plot_matrix(length(t_switch)+1, index) = plot_matrix(1,
    index)+amb + plot_matrix(2,index) - 2*plot_matrix(3,
    index) - plot_matrix(4,index) + plot_matrix(5,index)
    - plot_matrix(6,index) + plot_matrix(7,index) -
    plot_matrix(8,index);
plot_matrix_sheath(length(t_switch)+1, index) =
    plot_matrix_sheath(1,index)+amb + plot_matrix_sheath
    (2,index) - 2*plot_matrix_sheath(3,index) -
    plot_matrix_sheath(4,index) + plot_matrix_sheath(5,
    index) - plot_matrix_sheath(6,index) +
    plot_matrix_sheath(7,index) - plot_matrix_sheath(8,
    index);

if ( test )
    if ( plot_matrix(length(t_switch)+1, index) < 0.1
        && t > 3600)
        fprintf( '%20.2f ', t/3600);
        test = false;
    end
end

index = index + 1;

end

plot(time/3600, plot_matrix(9,:), 'LineWidth',1.3, 'color',
    '[0, 0.7, 0]');
hold on
plot(time/3600, plot_matrix_sheath(9,:), 'LineWidth',1.3, '
    color', '[0, 0.6, 0]');

```

